

Spore size evolution in nivicolous myxomycetes

A study about trait adaptation in the morphospecies *Physarum albescens*
with respect to cryptic speciation and species distribution

INAUGURALDISSERTATION

Zur

Erlangung des akademischen Grades eines

Doctor rerum naturalium

(Dr. rer. nat.)

an der Mathematisch-Naturwissenschaftlichen Fakultät

der

Universität Greifswald

vorgelegt von:

Jan Woyzichovski

Greifswald, 22 February 2022

Dekan*in: Prof. Dr. Gerald Kerth

1. Gutachter*in: Prof. Dr. Martin Schnittler

2. Gutachter*in: Prof. Dr. Claus Bässler

Tag der Promotion: 14.06.2022

List of publications included in this dissertation

Accepted in peer-reviewed journals

- Shchepin ON; Novozhilov Y; Woyzichovski J; Bog M; Prikhodko I; Fedorova N et al. (2021): Genetic structure of the protist *Physarum albescens* (Amoebozoa) revealed by multiple markers and genotyping by sequencing. *Molecular Ecology*. DOI: 10.1111/mec.16239.
- Dagamac NHA; Bauer B; Woyzichovski J; Shchepin ON.; Novozhilov YK; Schnittler M (2021): Where do niviculous myxomycetes occur? – Modeling the potential worldwide distribution of *Physarum albescens*. *Fungal Ecology* 53, p. 101079. DOI: 10.1016/j.funeco.2021.101079.
- Woyzichovski J; Shchepin ON; Dagamac NH; Schnittler M (2021): A workflow for low-cost automated image analysis of myxomycete spore numbers, size and shape. *PeerJ* 9, e12471. DOI: 10.7717/peerj.12471.

Manuscripts submitted for peer review

- Woyzichovski J; Shchepin ON; Schnittler M. (2022): High environmental induced plasticity in spore size and numbers of nuclei per spore in *Physarum albescens* (Myxomycetes). *Protist*

Contents

Contents

List of publications included in this dissertation.....	II
Contents.....	III
1 Abstract.....	1
1.1 English.....	1
1.2 Deutsch.....	4
2 General introduction.....	7
2.1 Background.....	7
2.2 Study sites.....	15
2.3 Framework of RESPONSE.....	16
2.4 Objectives of the thesis.....	17
2.5 Literature.....	19
3 Publications.....	24
3.1 Genetic structure of the protist <i>Physarum albescens</i> (Amoebozoa) revealed by multiple markers and genotyping by sequencing.....	25
3.2 Where do nivicolous myxomycetes occur? – Modeling the potential worldwide distribution of <i>Physarum albescens</i>	46
3.3 A workflow for low-cost automated image analysis of myxomycete spore numbers, size and shape.....	56
3.4 High environmental induced plasticity in spore size and numbers of nuclei per spore in <i>Physarum albescens</i> (Myxomycetes).....	82
4 Conclusion and perspective.....	115
4.1 Main findings.....	115
4.2 Outlook: Challenges and limitations.....	118
4.3 Literature.....	120
5 Affidavits.....	122
5.1 Eidesstattliche Erklärung / statutory declaration.....	122
5.2 Erklärung bei Gemeinschaftsarbeiten selbständig.....	123
6 Acknowledgement.....	126

1 Abstract

1.1 English

Myxomycetes or Myxogastria (supergroup Amoebozoa) are one of several Protistean groups dispersing via airborne spores. The model organism for the group, so far exclusively studied in a laboratory environment, is *Physarum polycephalum*. Here, molecular evolution, distribution and the ecology of spores dispersal was investigated for the non-model species *Physarum albescens*. This nivicolous myxomycete fruits with snow melt in most mountain ranges of the northern hemisphere and disperses via spherical, dark-colored and melanin-rich spores. Fruit body development and subsequent spore dispersal occurs within a short time window of a few days. At this time, the fruiting plasmodium is fully exposed to the harsh environment if the protecting snow melts away. The spores, with a diameter of 10–13 μm of the typical size for myxomycetes, can potentially reach all suitable habitats worldwide, which led to the assumption that not only *Ph. albescens* but most myxomycete species should be ubiquitously distributed over the world.

In the first part of this study (article 1), the question was, if spore dispersal can realize a gene flow sufficient to meet the above-mentioned assumption. A total of 324 accessions of *Ph. albescens*, collected all over the northern hemisphere, was sequenced for 1-3 genetic markers (SSU, EF1A, COI), and 98 specimens were further analyzed using the genotyping by sequencing technique. As a result, at least 18 reproductively isolated units, which can be seen as cryptic biological species, emerged as phylogroups in a three-gene phylogeny, but as well in a SNP-based phylogeny and were confirmed by a recombination analysis between the three markers. However, this evolutive radiation is not simply caused by geographic fragmentation due to low dispersal capability: within a certain region, multiple phylogroups coexisted next to each other, although some appeared to be regional endemics. Most likely, mutations in mating-type genes, as shown to exist for the cultivable *Ph. polycephalum*, are the main drivers of speciation. This challenges the hypothesis of ubiquitous distribution of *Ph. albescens* and corroborates the results of the few available studies for other myxomycete species. In addition, groups of clonal specimens, mostly but not always restricted to a certain slope or valley indicated that sexual and asexual reproduction coexists in the natural populations of *Ph. albescens*.

In the second part (articles 2), the fundamental niche for *Ph. albescens* was described using all available records for the species. The resulting set of 537 unique occurrence points was subjected to a correlative spatial approach using the software MaxEnt. In dependence on the predictor variables three species distribution models emerged which differed only in details. The first consisted of only 19 bioclimatic variables and an elevation map from the WorldClim dataset. The second was corrected for pseudo-absences resulting from missing survey activities, and the third was expanded with an

additional categorical environment variable on snow cover. High mean AUC (area under the curve) values above 0.97 could be reached with all three models. Variables for snow cover, precipitation of the coldest quarter (of the year), and elevation correlated highly to predict the distribution of *Ph. albescens*. Only in mid-northern latitudes, elevation alone was a good predictor, but it would cause false-positive predictions in arid mountain ranges and failed to explain occurrence in lowland sites at higher latitudes. Mountains in humid climates showed the highest incidences, confirming recent studies that long-lasting snow covers combined with mild summers are crucial for the ecological guild of nivicolous myxomycetes, with *Ph. albescens* as a typical species.

Spore size is crucial for dispersal ability and should thus be a character under strong selection. In addition, spores carrying two nuclei with opposite mating types should have a colonization advantage. This was the hypothesis for the last part of this study (articles 3 and 4), which investigated this trait in a quantitative manner. This required a method to analyze thousands of spores automatically (article 3) and with high precision for size and the number of nuclei enclosed. Human errors should be excluded, to reveal even subtle differences in the resulting spore size distributions. Two challenges had to be met for this approach. First, a preparation technique was developed to reduce false segmentations due to overlaying spores by aligning spores on one common plane with a high-frequency vibration device. Second, the segmentation process was automated to allow separating spores that are densely packed in the respective images. A machine learning algorithm was set up and trained to reliably identify and measure dark-colored spores. The technique produced consistent results with high accuracy, and the large number of spores allowed to compile spore size distributions, to check for the constancy of this character, which is impossible with manual measurements limited to low numbers.

The resulting spore size distributions, obtained from over 80 specimens (article 4), were mostly narrow, which is in accordance with our hypothesis. Spore size was as well fairly constant within fructifications from one colony. However, mean spore size within different accessions of *Ph. albescens* showed large variation (ca. 10%, a range often indicated to key out different morphospecies of myxomycetes), and this was explained only by a minor part with differences between biospecies. Not much smaller (8%) was the variation within a group of clonal specimens collected within 25 m distance. This points to a strong influence of environmental factors even at a micro spatial scale, perhaps caused by microclimatic differences and high phenotypic plasticity for spore size. The influence of large-scale covariates like altitude or latitude was negligible. However, spore size correlated with the variance in this trait, indicating that oversized spores may be caused by detrimental environmental conditions. Two aberrations in spore development were found: First, a few specimens showed a multimodal distribution for spore size with two or even three discernible spore populations. The estimated

volumes of those populations correspond to a multiple of the first and most abundant conspicuous spore size population. Second, not all spores were uninucleate as to be expected for meiotic products. This was revealed by fluorescence signals from staining the same spores with DAPI, with a second machine learning algorithm trained to identify the nuclei in a spore. A few specimens showed a significant proportion of binucleated spores in the size range of normal-sized ones, and these specimens were not the ones with multimodal spore size distributions. This indicates that the negative impacts (inbreeding) of multinucleate spores should outweigh a possible colonization advantage and is in accordance with the high genetic diversity found in the worldwide population of *Ph. albescens*, indicating predominantly sexual reproduction in wild populations of myxomycetes.

1.2 Deutsch

Myxomyceten oder Myxogastria (Supergruppe Amoebozoa) sind eine von mehreren Gruppen innerhalb der Protisten, die sich hauptsächlich über windverbreitende Sporen ausbreiten. Der bisher ausschließlich im Labor untersuchte Modellorganismus dieser Gruppe ist *Physarum polycephalum*. Hier wurde die molekulare Evolution, Verteilung und die Ökologie der Sporenausbreitung für den Nicht-Modellorganismus *Physarum albescens* untersucht. Diese nivicole Myxomyceten bildet Fruchtkörper mit dem Einsetzen der Schneeschmelze in den meisten Gebirgszügen der nördlichen Hemisphäre und verbreitet sich über kugelförmige, dunkel gefärbte und melaninreiche Sporen. Die Fruchtkörperentwicklung und anschließende Sporenausbreitung erfolgt innerhalb eines kurzen Zeitfensters von nur wenigen Tagen. Zu diesem Zeitpunkt ist das Plasmodium vollständig den rauen Umweltbedingungen ausgesetzt, sobald die schützende Schneeschicht nicht mehr besteht. Die Sporen mit einem Durchmesser von 10–13 µm, der für Myxomyceten typischen Größe, können potenziell alle geeigneten Lebensräume weltweit erreichen. Dies führte zur Annahme, dass nicht nur *Ph. albescens*, sondern die meisten Myxomycetenarten ubiquitär über die Welt vorkommen sollten.

Der erste Teil in dieser Arbeit (Artikel 1) war es daher zu klären, ob die Sporenausbreitung einen Genfluss realisieren kann, der ausreicht, um die eben genannte Annahme zu bestätigen. Insgesamt 324 Proben von *Ph. albescens*, die auf der gesamten nördlichen Hemisphäre gesammelt wurden, wurden für 1-3 genetische Marker (SSU, EF1A, COI) sequenziert und 98 Proben wurden mit der Genotypisierung durch Sequenzierungstechnik weiter analysiert. Infolgedessen konnten mindestens 18 reproduktiv isolierte Einheiten entdeckt werden, die als kryptische biologische Spezies angesehen werden können. Diese Phylogruppen waren das Ergebnis einer Drei-Gen-Phylogenie, aber auch einer SNP-basierten Phylogenie und wurden durch eine Rekombinationsanalyse zwischen diesen drei Markern weiter bestätigt. Diese evolutive Auffächerung wird jedoch nicht einfach durch geografische Fragmentierung aufgrund der geringen Ausbreitungsfähigkeit verursacht: Innerhalb einer bestimmten Region koexistierten mehrere Phylogruppen nebeneinander, obwohl einige regionale endemisch zu sein schienen. Höchstwahrscheinlich sind Mutationen in den "mating type" Genen, wie sie für den kultivierbaren *Ph. polycephalum* vorgewiesen wurden, die Haupttreiber der Artbildung. Dies stellt die Hypothese der ubiquitären Verteilung von *Ph. albescens* in Frage und bestätigt die Ergebnisse der wenigen verfügbaren Studien über andere Myxomycetenarten. Darüber hinaus deuteten Gruppen klonaler Exemplare, die meist, aber nicht immer auf einen bestimmten Hang oder ein bestimmtes Tal beschränkt sind, darauf hin, dass sexuelle und asexuelle Fortpflanzung in den natürlichen Populationen von *Ph. albescens* koexistieren.

Im zweiten Teil (Artikel 2) wurde die fundamentale Nische für *Ph. albescens* unter Verwendung aller verfügbaren Aufzeichnungen für die Art beschrieben. Der resultierende Datensatz von 537 eindeutigen Vorkommnissen wurde mit der Maximum-Entropie-Methode der Software MaxEnt genutzt, um eine Habitatmodellierung zu erstellen. In Abhängigkeit von den Einflussvariablen entstanden drei Verteilungsmodelle, die sich nur im Detail unterschieden. Das erste Modell bestand aus nur 19 bioklimatischen Variablen und einer Höhenkarte aus dem WorldClim-Datensatz. Das zweite wurde von Pseudo-Abwesenheiten korrigiert und die dritte wurde um eine zusätzliche kategoriale Einflussvariable, basierend auf Schneebedeckung, erweitert. Mit allen drei Modellen konnten hohe durchschnittliche AUC-Werte (Fläche unter der Kurve) über 0,97 erreicht werden. Die Variablen für Schneebedeckung, Niederschlag des kältesten Quartals (des Jahres) und Höhe korrelierten am stärksten, um die Verteilung von *Ph. albescens* vorherzusagen. Nur in mittleren nördlichen Breitengraden war die Variable "Höhe" allein ein guter Prädiktor, aber in den trockenen Gebirgszügen führte es zu falsch-positiven Vorhersagen und konnte zudem auch nicht das Vorkommen in Tieflandstandorten in höheren Breiten erklären. Berge in feuchten Klimazonen zeigten die höchsten Inzidenzen, was neuere Studien bestätigt, dass lang anhaltende Schneedecken in Kombination mit milden Sommern für die ökologische Gruppe der nivicolen Myxomyceten, mit *Ph. albescens* als typischer Art, von entscheidender Bedeutung sind.

Die Sporengröße ist ein entscheidender Faktor für die Ausbreitungsfähigkeit und sollte daher ein Charakter unter starker Selektion sein. Darüber hinaus sollten Sporen, die zwei Kerne mit komplementären Paarungstypen tragen ("mating type" System), einen Kolonisationsvorteil haben. Dies war die Hypothese für den letzten Teil dieser Studie (Artikel 3 und 4), der dieses Merkmal quantitativ untersuchte. Dies erforderte eine Methode, um Tausende von Sporen automatisch (Artikel 3) und mit hoher Präzision, bezüglich Größe und Anzahl, zu analysieren. Der menschliche Fehler sollte so gut wie möglich ausgeschlossen werden, um auch subtile Unterschiede in den resultierenden Sporengrößenverteilungen aufzudecken. Für diesen Ansatz mussten zwei Herausforderungen bewältigt werden. Zuerst wurde eine Präparierungstechnik entwickelt, um falsche Segmentierungen aufgrund von Überlagerungen zu reduzieren. Dazu wurden Sporen auf einer gemeinsamen Raumebene mit einer hochfrequenten Vibrationsvorrichtung ausgerichtet. Zweitens wurde der Segmentierungsprozess automatisiert und optimiert, um Sporen zu trennen, die in den jeweiligen Bildern zu dicht gepackt sind. Ein maschineller Lernalgorithmus wurde eingerichtet und trainiert, um dunkel gefärbte Sporen zuverlässig zu identifizieren und zu messen. Die Technik lieferte stabile Ergebnisse mit hoher Genauigkeit. Die große Anzahl von untersuchten Sporen erlaubte es, Sporengrößenverteilungen zu erstellen, um die Konstanz dieses Charakters zu überprüfen, was mit manuellen Messungen, die auf niedrige Zahlen beschränkt sind, unmöglich ist.

Die resultierenden Sporengrößenverteilungen, die für über 80 Exemplare (Artikel 4) erhalten wurden, waren meist schmal verteilt, was unserer Hypothese entsprach. Die Sporengröße war innerhalb von Fruktifikationen aus einer Kolonie konstant. Die durchschnittliche Sporengröße innerhalb verschiedener Sammlungen von *Ph. albescens* zeigte jedoch große Unterschiede (ca. 10%, ein Bereich, der oft angegeben wird, um verschiedene Morphospezies von Myxomyceten herauszufiltern), und dies wurde nur durch einen kleinen Teil mit Unterschieden zwischen Biospezies erklärt. Nicht viel kleiner (8%) war die Variation innerhalb einer Gruppe klonaler Exemplare, die innerhalb von 25 m Entfernung gesammelt wurden. Dies deutet auf einen starken Einfluss von Umweltfaktoren auch auf mikroräumlicher Skala hin, der möglicherweise durch mikroklimatische Unterschiede und einer hohen phänotypischen Plastizität für die Sporengröße verursacht wird. Der Einfluss großräumiger Kovariate wie Höhe oder Breitengrad war vernachlässigbar. Die Sporengröße korrelierte jedoch mit der Varianz dieses Merkmals, was darauf hindeutet, dass übergroße Sporen durch schädliche Umweltbedingungen verursacht werden können. Zwei Abweichung in der Sporenentwicklung wurden gefunden: Erstens zeigten einige Exemplare eine multimodale Verteilung für die Sporengröße mit zwei oder sogar drei erkennbaren Sporenpopulationen. Die geschätzten Volumina dieser Populationen entsprechen einem Vielfachen der ersten und am häufigsten vorkommenden Population in Sporengröße. Zweitens waren nicht alle Sporen einkernig, wie es bei meiotischen Produkten zu erwarten ist. Dies wurde durch Fluoreszenzsignale aus der Färbung der gleichen Sporen mit DAPI aufgedeckt, wobei ein zweiter maschineller Lernalgorithmus trainiert wurde, um die Kerne in einer Spore zu identifizieren. Einige Exemplare zeigten einen signifikanten Anteil an zweikernigen Sporen im Größenbereich normaler Sporengröße, und diese Exemplare waren nicht diejenigen mit multimodalen Sporengrößenverteilungen. Dies deutet darauf hin, dass die negativen Auswirkungen (Inzucht) von mehrkernigen Sporen einen möglichen Kolonisationsvorteil überwiegen sollten, und steht damit im Einklang mit der hohen genetischen Vielfalt, die in der weltweiten Population von *Ph. albescens* gefunden wurde. Das wiederum weist auf eine überwiegend sexuelle Fortpflanzung in wilden Populationen von Myxomyceten hin.

2 General introduction

2.1 Background

Spores are not unique to plants but have emerged independently in different groups of terrestrial organisms. Spore dispersal is especially successful in macroscopically visible and sessile organisms like plants or fungi – these cannot spread themselves. This study aims to show the mechanisms and limitations of this type of dispersal.

Life on earth is almost as old as our planet, about 4 billion years. In the beginning, all life forms were aquatic, small, and therefore self-spreading. In water as a medium, which is almost a thousand times denser than air, rather large particles can drift – we know these life forms as plankton. With the conquest of the land, the dispersal problem arose: on the one hand, actively living organisms must be resistant to desiccation, which means being larger, preferably multicellular. On the other hand, the much lower density of air compared to water allows only very small particles to propagate in air. Evolution's (almost universal) answer to this challenge is the spore: microscopic particles with minimal metabolism yet resistant to UV radiation and desiccation that "float" in air.

Spores evolved in many, often not closely related groups of terrestrial organisms: fungi (Asco- and Basidiomycetes as the most important groups) (Corner 1947), mosses (Miles and Longton 1992), clubmosses (Lycopodiophyta) as well as ferns and fern relatives (such as horsetails or moss ferns) (Kenrick and Crane 1997; Edwards and Kenrick 2015). Seed plants also have spores, but they are called pollen and they have lost the ability to germinate independently in the evolution of life cycles (Williams and Reese 2019). However, to mediate gene flow via pollination they must spread anyway: this also happens through the air in wind-pollinated plants (Ellstrand 1992; Kwak et al. 1998). But lesser-known groups of terrestrial organisms also form spores. A good model are the plasmodial slime molds (Myxomycetes), a group of protists belonging to the Amoebozoa (Stephenson S. L. and Schnittler M. 2017), which form small, mushroom-like fruiting bodies, usually with nearly spherical spores (Schnittler M et al. 2012) most all sessile terrestrial organisms form spores; the big exception is higher animals: they move themselves. The "zoospores" (cells that move actively utilizing flagella) occurring in aquatic organisms are excluded here since the purpose of this work is to focus on passive dispersal over the air.

How large can airborne spores become? Physics, more precisely Stokes' law (Stokes 1845), provides an answer. It describes the case of small, spherical particles falling through the air:

$$v = \frac{2}{9} \frac{(\rho_p - \rho_f)}{\mu} g R^2$$

Already the formula, with R as the radius of a particle (the spore) raised to the power of two, shows that spore size must be the crucial factor for the terminal velocity v . The density of the spore particle is given by ρ_p . Water has a density of 1.0 g cm^{-3} . However, spores dry out in the air, which is why we must assume a slightly lower density. The other variables are approximately constant (gravitational constant $g = 981 \text{ cm s}^{-2}$, the density of air $\rho_f = 1.29 \times 10^{-3} \text{ g cm}^{-3}$ at sea level and approx. 25°C , and the viscosity of air $\mu = 1.82 \times 10^{-4} \text{ g cm}^{-2} \text{ s}^{-1}$). The terminal velocity v is the velocity that occurs as a balance between gravitational acceleration and air friction; it describes the chances of a spore dispersing and can be measured experimentally (Tesmer and Schnittler 2007, Fig. 1).

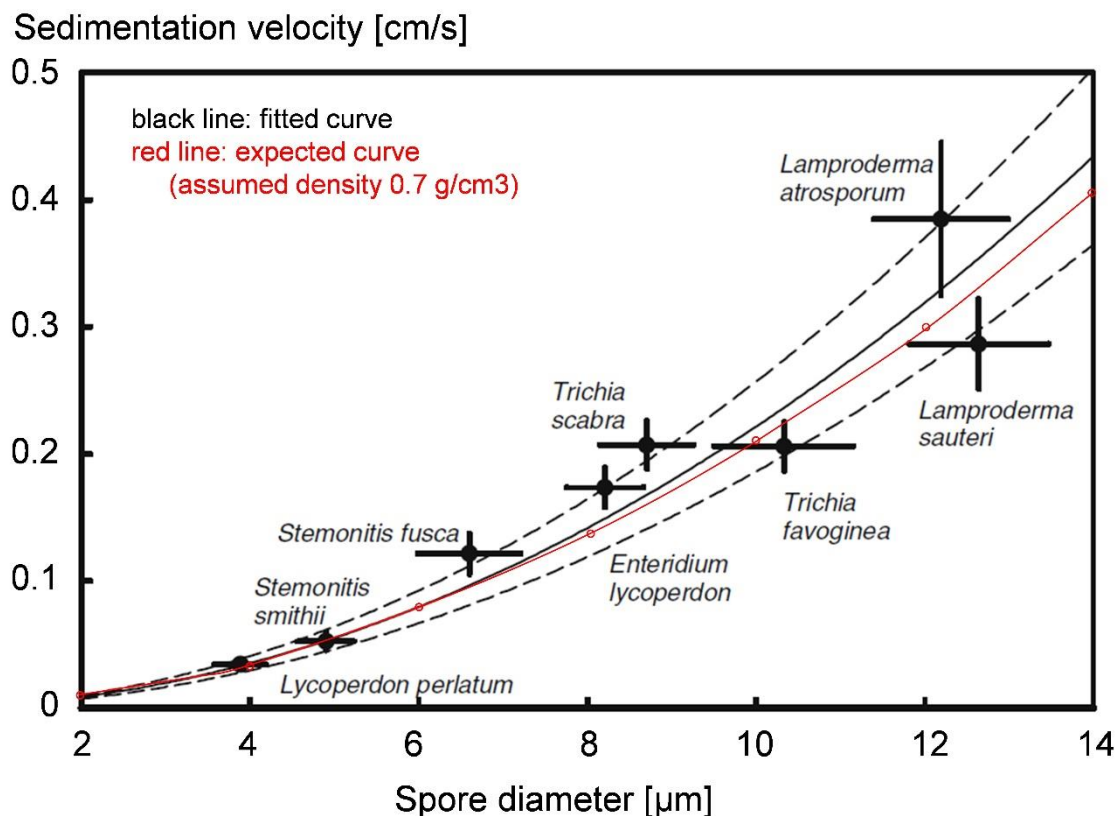


Fig. 1. Measurements of the terminal velocity of spores of myxomycetes and fungi (Bovist puffball, *Lycoperdon perlatum*). Horizontal bars show the standard deviations of spore size (25 spores measured); vertical bars are the standard deviations of the measured terminal velocity. Black line: a fitted curve according to Stokes' law with confidence intervals (dotted black lines), red line: theoretical terminal velocity of a spore with a density of 0.7 g cm^{-3} . According to Tesmer and Schnittler 2007, modified.

The slower a spore falls, the greater the chance of being drifted away by horizontal air streams or even updrafts. Therefore, spores should be as small as possible, but they must transport the entire genome of an organism. This is at least one haploid genome, which in prokaryotes usually entails a single

circular DNA molecule (Thanbichler et al. 2005), but in eukaryotes consists of several linear molecules that become visible as chromosomes (stainable bodies) during cell division. The DNA needs to be packed into the pollen grain of a wind-pollinating plant. In maize, a monocotyledonous plant with a rather large genome, pollen grains reach diameters of 76–80 μm , with a theoretically expected terminal velocity of 21 cm/s. For pollen grains with a diameter of 103–106 μm already 32 cm/s can be estimated (Aylor 2002), which is about the maximum of what is functional with airborne pollen or spores. Terminal velocity increases rapidly with diameter, at 1 mm it would already be 37–47 m/s. Thus, even if the genome can be transported, there is no space in spores for additional resources, comparable to the endosperm of a seed. Therefore, a spore can only successfully establish a new organism (fern, fungus, myxomycete, etc.) if optimum conditions are met from the beginning. This brings us to the first limitation, which favors quantity before quality: the lower the chances of establishment, the more spores are produced. This can be seen in the evolution of the study group mentioned above, the myxomycetes.

Myxomycetes or Myxogastria belong to the supergroup Amoebozoa within the domain of Eukaryota. This group of organisms, also often called plasmodial slime molds, are currently classified into 14 families and approximately 1000 species (Leontyev et al. 2019; Lado 2005-2022). They are free-living predators preying on other microorganisms like fungi, bacteria, and other protists. So far, they are recorded in every terrestrial habitat and build often distinct local communities (Stephenson et al. 2008). In history, they were falsely classified as plants, animals, or fungi based on their fungal-like dispersal ecology via airborne spores. Bary (1863) was the first to recognize their Amoebozoan nature. Today we know that fruit bodies dispersing spores evolved in several groups within Amoebozoa (Hillmann et al. 2018) but as well non-related Protistean groups (Schnittler et al. 2006). As predators, amoebae hatching from spores prey on other microorganisms. However, terrestrial habitats with a high density of microorganisms are confined to small spots (a dead trunk, litter that has been blown together in a depression, a dying fungal fruit body), so new habitats have to be colonized via spores (Schnittler and Tesmer 2008). In the simplest case, the amoeba forms a stalk and becomes a spore; this solution was found several times in this group (Kang et al. 2017, Hillman et al. 2018). In myxomycetes, however, the amoeba grows into a giant cell called a plasmodium. Through differentiation of the cell mass, entire fruiting bodies are formed, which contain many spores instead of one. A phylogeny of the corresponding Amoebozoan subgroups shows not only their multiple independent evolution, but reveals as well that the number of spores per fruiting body increases rapidly in terminal clades especially in the Myxomycetes (Fig. 2). There are similar evolutionary trends in ferns (Rose and Dassler 2017) and large mushrooms (Ingold. 1965), here species with larger fruiting bodies also seem to produce slightly larger spores (Meerts 1999).

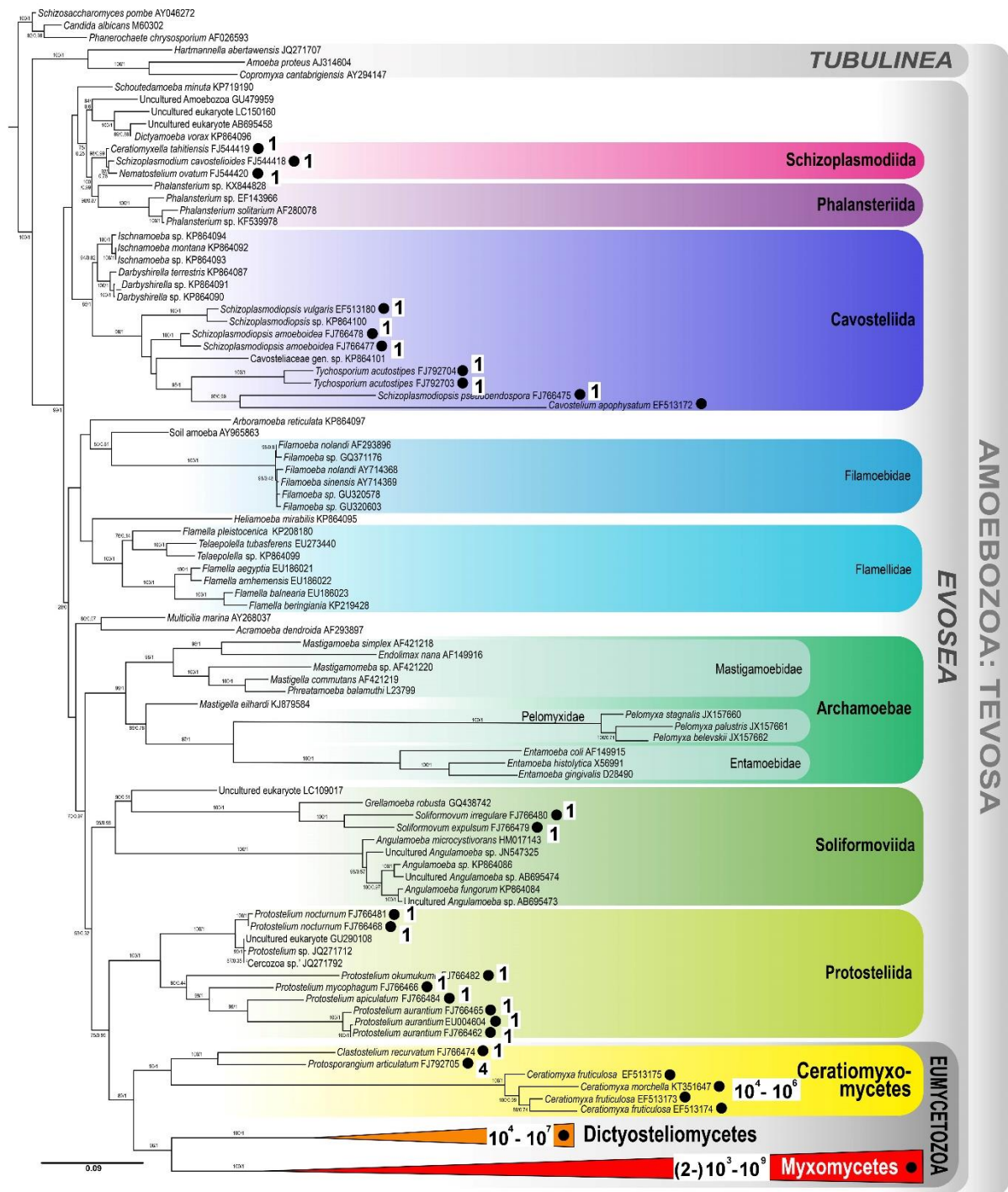


Fig. 2. Simplified phylogeny of the Amoebozoa, subgroup Tevosea (maximum likelihood method, 18S rRNA gene sequences, calculation with IQ-Tree 1.5.5, 1000 bootstrap replicates, GTR+R7 model). Clades forming spores are highlighted (•); the numbers are estimates of spore counts (as number of spores per fruit body). Modified after Leontyev et al. (2019).

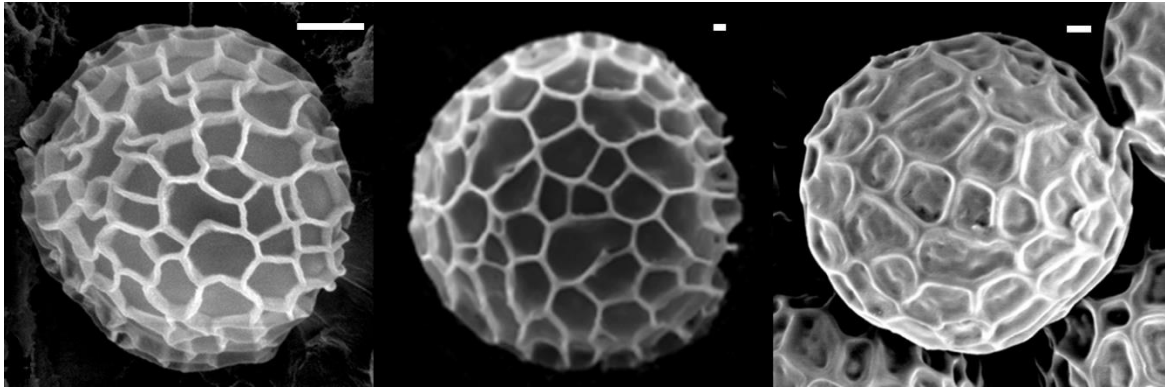


Fig. 3. Spores of different groups of organisms that are not closely related. The examples show the most water-repellent type of ornamentation: a network of elevated ridges. **A** Myxomycetes (plasmodial slime molds): *Tubifera* spp., 7–8 μm , a new taxon to be described (photo D. Leontyev), **B** Lycopodiophyta (clubmosses): *Diphasiastrum* spp., 32–36 μm (photo W. Bennert), **C** Tilletiales (smut fungi): *Tilletia caries*, 16–20 μm (Photo from (Shivas et al. 2014), smut fungi of Australia, collections.daff.qld.gov.au). Size scale: 1 μm .

There are similar developmental tendencies in several eukaryotic phyla, including the classic spore "plants" such as mosses, fungi, and ferns. The independently evolved solutions for spore shape and ornamentation are strikingly similar, as shown by scanning electron micrographs of spores (Fig. 3). A natural polymer, sporopollenin coats the spores (Mackenzie et al. 2015; Atkin et al. 2011). Ornaments with attached proteins ensure a hydrophobic surface, a prerequisite for spores not immediately sticking to moist surfaces, but instead being able to drift off repeatedly. The ornaments of these particles usually vary from small warts and spines to ridges. Similar ornaments occur repeatedly in life forms that are not closely related. These ornaments are very likely to be differently hydrophobic (Hoppe and Schwippert 2014). The more hydrophobic the spore surface is, the lower the chance that the spore will stick to moist surfaces, which are common in nature; or washed out of the air by rain drops. In this way, they can possibly be stirred up again several times and spread further. However, here is a trade-off, spores with hydrophobic surfaces are more difficult to become wet and therefore absorbing water becomes more difficult, but this is necessary for germination. Therefore, spore ornaments may vary from high to less hydrophobic depending on the environmental conditions in which a species lives.

How effective is spore dispersal? Can spores fly around the world? The principal answer is yes, and there are indications that they do so with the help of the jet stream, an extremely strong, equator-parallel high-altitude air current (Díez et al. 2020; Geiger et al. 2007; Wolf et al. 2001). However, all

experimental studies indicate that only a very few of the many spores or pollen that organism forms manage this. Most spores do not get thus far, so the number of spores falling on an area decreases exponentially with distance from the source (Fig. 5). In the case of ferns, it has been shown that the large number of spores formed enables effective colonization of distant habitats at least over longer (decades to centuries) periods of time (Groot et al. 2012); the same applies to fungi (Golan and Pringle 2017).

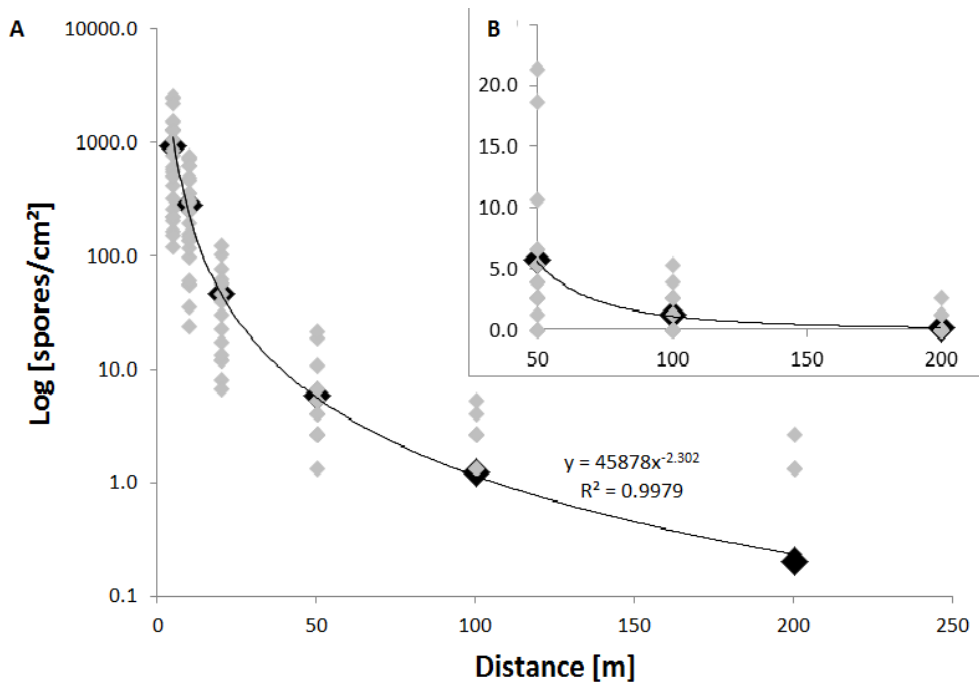


Fig. 5. Spore dispersal curve for the clubmoss species *Lycopodium clavatum*. Slides with double-sided adhesive film were placed vertically at an appropriate distance from an isolated stand to serve as spore traps. The spores captured on an area of 1 cm² were counted in eight different directions (each with three parallel slides). **A** Triple measurements (grey diamonds) for eight cardinal points and distances between 5 and 200 m; black diamonds denote the average value for these 24 measurements (fit: decaying exponential function). **B** Same data set with linear scaling. Data: R. Kaufmann (unpublished).

The question for speciation and population biology of spore-dispersing organisms is not whether all spores are spread over long distances, but how often this happens and how effective gene flow can be maintained between distant populations. Indeed, spore-dispersed plants seem to have larger areas than seed-dispersed ones: for example, some ferns and clubmosses occur in both Europe and North America, in contrast to native ranges of seed plants (Smith 1972). But: detailed studies often show that the corresponding populations differ slightly - whether they are described as a separate species

or subspecies is at the discretion of the taxonomists (Fayle et al. 2011; Kinoshian et al. 2020; Masuyama et al. 2002; Aguilar et al. 2014; Borg Dahl et al. 2018).

At least population genetics can provide a theoretical answer as to whether evolutionary trends always lead to better and better dispersal mechanisms. Here two phenomena can occur called inbreeding depression and outbreeding depression. For inbreeding, the fitness tends to decrease when a population has little genetic exchange with others (see work of Moraes (2018) on *Tigriopus californicus*). Alleles for genetic defects, for example, have a higher chance of being homozygous when relatives mate so that the corresponding defect manifests itself.

On the other hand, there is as well the opposite effect. As the selection conditions for a species change from place to place, for example with climate, the genotypes best adapted to local conditions will ultimately prevail in a population. A specimen of the same species from a more distant population then shows a lower fitness locally than the individuals of the local population (see work of Brown (1991) on *Tigriopus californicus*). If we now imagine the extremes of dispersal ability, a lack of dispersal possibilities tends to cause "inbreeding depression", but unlimited dispersal will favor "outbreeding depression": the emergence of locally adapted genotypes is prevented by the constant immigration of non-adapted genotypes. This leads to the assumption that evolution does not automatically progress in the direction of better and better possibilities of dispersal, especially since the resources brought by a spore or a seed are decisive for the establishment of the individual, especially in dry terrestrial habitats. Again, a trade-off will result between a) effective dispersal (colonization of new habitats, depending on the length of time a population remains in a habitat; avoidance of inbreeding depression through gene flow between populations) and b) local adaptation by limited dispersal (need to carry nutrients for establishment; avoidance of outcrossing depression). Obviously, the optimum setting differs for each species because it depends on many factors, such as:

- the reproductive system (in plants: probability of self-fertilization),
- the probability of establishment of the propagation units (are many or only a few resources needed), and
- the steepness of gradients in environmental conditions over a species' range.

At least theoretically, there must be a species-specific optimum for the efficiency of dispersal, which on the one hand avoids inbreeding depression and on the other hand enables local adaptation. This should also apply to species that produce so many spores that the probability of establishment is sufficiently high despite a large lack of resources. Regional differentiation of the populations is therefore the rule, at least for spore-dispersed eukaryotes, and could also be confirmed for myxomycetes, the model group for this study (Dagamac et al. 2017a; 2017b).

The species studied here, *Physarum albescens*, belongs to the nivicolous myxomycetes that fruit usually but not exclusively (Ronikier and Ronikier 2009) on mountain ranges with a seasonal snow cover. During its plasmodial stage, the organisms are foraging on bacteria, yeast, and other microorganisms (Gray and Alexopoulos 1968). Feeding on under snow microbial communities, the plasmodium is protected against harsh and sudden changes of environmental factors by the snow cover, for example, a sudden temperature shock (Schnittler et al. 2015; Dahl et al. 2018). As soon as the cover starts to melt, the sporulation process is initiated, and plasmodia fragment to colonies of multiple fruiting bodies, each filled with 10^5 - 10^6 spores (Schnittler and Tesmer 2008). During this process the plasmodium is exposed to the harshest environment during its lifetime, with rapid changes in temperature and radiation upon snow melt (Schnittler et al. 2015). This is enhanced by the positive phototropic behavior of fruiting plasmodia, ensuring an elevated starting point for spore dispersal. Only the spore itself will experience even more drastic environmental impacts but at the same time is protected by a spore wall mixed with melanin and amino sugars (Rakoczy and Panz 1994; Loganathan et al. 1989; McCormick et al. 1970). Following the ideas outlined above, spore size should be under strong genetic control. However, in the short time window for sporulation, with rapidly changing weather and different microenvironmental conditions, environmental conditions may overrule that. Genetic differentiation within *Ph. albescens* and the influence of genetic and environmental factors on spore size is the focus of this study. With samples collected over several mountain ranges all over the northern hemisphere we will look at the influence of large-scale factors like altitude (stronger winds on higher altitudes may allow for larger spores with a higher chance of establishment), genetic factors (isolated populations may differ from each other in spore size) or small-scale factors like microenvironment (spore size in different colonies found close by).

2.2 Study sites

The accessions used for this work are a mix between an existing collection (M. Schnittler, to be deposited at the Botanical State Museum Munich) and newly collected specimens during this Ph.D. project. The goal was to achieve a maximum in geographical variation, therefore various mountain ranges around the northern hemisphere were targeted. Besides the very well surveyed transect in the German Alps (in the Kreuzjoch region near the Alpspitz, close to the city Garmisch-Partenkirchen), collections from the Rocky Mountains (Colorado, United States of America), Sierra Nevada (Granada, Spain), Lapland region and Khibiny Mountains (Murmansk Oblast, Russia), the Caucasus Mountains (Karachay-Cherkess Republic, Russia), the Ili-Alatau mountain range (near Almaty, Kazakhstan), and the mountain range southwest to the volcanoes Koryaksky and Avachinsky (Kamchatka Krai, Russia) were added. Field surveys were scheduled around late spring / early summer; at this time snowmelt starts at regions around 2 000 m elevation (with the most suited elevational belt depending on northern latitude). *Ph. albescens* is a prominent representative of a whole ecological guild, the nivicolous myxomycetes, and a number of other myxomycete species could be collected simultaneously with surveys focusing on *Ph. albescens*. During the collecting process, geographical information with the highest precision possible was recorded. Additionally, more detailed information for each specimen was documented, like inclination, the height of a colony on the substrate, the plant species where it fruits on, and coverage of shadowing trees and shrubs. Since the species is relatively common in suitable places but cannot be cultivated (Shchepin et al. 2014), finding these sites was one of the challenges for this study.

2.3 Framework of RESPONSE

This thesis is part of the research projects in the graduate school “Biological Responses to Novel and Changing Environments“(in short RESPONSE). Two research clusters were planned, with cluster A focusing on local adaptation and cluster B on dispersal-related traits. In the latter cluster, factors related with the colonization of new habitats by a species are of major interest (RESPONSE¹, for further details). For this project, dealing with an organism producing airborne spores, the size of these particles is obviously a trait directly linked to dispersal abilities.

For a non-model species in a lesser-known group of organisms like *Physarum albescens* (the only species of the genetically extremely diverse group of protists, making up for the clear majority of deep lineages in eukaryotes), we first needed to study a number of subjects which are well studied for the most other organisms in RESPONSE: distribution range, reproductive mode, or gene flow between populations. Therefore, first goal was to analyze the species concept for the chosen study species (myxomycetes are of the few Protistean groups following a mainly morphological species concept) and to elucidate the importance of sexual and asexual reproduction in wild populations. The second goal is to understand environmental influences on morphological traits important for dispersal of this species, here especially spore size.

In the following section for this work investigated research goals are summarized.

¹ From the RESPONSE web site: <https://biologie.uni-greifswald.de/forschung/dfg-graduierntenkollegs/research-training-group-2010/research-projects/> accesses 30.01.2022.

2.4 Objectives of the thesis

The main focus of this thesis was (i) to investigate gene flow, genetic differentiation and the putative distribution range of *Ph. albescens*. This forms the foundation to (ii) investigate the balance between genetic and environmental factors on spore features, here spore size distribution and the number of nuclei transported, with the idea to detect signs of local adaptation. Therefore, the first part of the thesis focuses on population-genetic analyses, the second on a quantitative analysis of spore features in *Ph. albescens*.

Question 1: Is there intraspecific genetic differentiation in the morphologically described species *Ph. albescens*? Judged on the few available studies, the existence of reproductively isolated groups, furthermore, called phylogroups, could be expected. These constitute putative (and cryptic) biological species, with no or a certain extent of admixture between them.

To answer this, the first research project included:

- Sequencing of multiple collections of *Ph. albescens* from multiple mountain ranges around the northern hemisphere with three independent gene markers.
- A test for reproductive isolation between genetic variants (phylogroups), assuming random recombination of independent genetic markers.
- Genotyping by Sequencing methods to find out about the extent of asexual reproduction via detection of groups of clonal specimens in a wide range of collections.
- A species distribution model to define the fundamental niche of the study species, assuming snow cover to be an environmental factor of crucial importance.

The results are reported in articles 1 and 2.

Question 2: Is the genetic difference between biospecies or local populations of *Ph. albescens* large enough to be as well visible on phenotypic characters like spore size? If so, can the variation of spore size be explained rather by genetic factors (biospecies and clonal identity) or by recorded environmental factors (large scale: mountain range, elevation; small scale: microenvironmental differences between close by locations)?

To answer this, the second research project included:

- A novel method to align spore or pollen samples to a monolayer for imaging analysis.
- New segmentation models based on machine learning algorithms for automatically analyzing thousands of spores.

- Analysis of the resulting detailed spore size distributions of collections of *Ph. albescens* from multiple mountain ranges around the northern hemisphere
- Statistical analysis on to test for correlation between genetic / environmental factors with spore size in different phylogroups and clonal specimens of *Ph. albescens*.

The results are reported in articles 3 and 4.

In Addition to Q1, besides spore size measurements, fluorescence staining of the nucleus was added to the methods to acquire further information on spore formation for *Ph. albescens*.

2.5 Literature

Aguilar M; Fiore-Donno A-M; Lado C; Cavalier-Smith T (2014): Using environmental niche models to test the 'everything is everywhere' hypothesis for *Badhamia*. In *The ISME journal* 8 (4), pp. 737–745. DOI: 10.1038/ismej.2013.183.

Atkin SL; Barrier S; Cui Z; Fletcher PDI; Mackenzie G; Panel V et al. (2011): UV and visible light screening by individual sporopollenin exines derived from *Lycopodium clavatum* (club moss) and *Ambrosia trifida* (giant ragweed). In *Journal of photochemistry and photobiology. B, Biology* 102 (3), pp. 209–217. DOI: 10.1016/j.jphotobiol.2010.12.005.

Aylor DE (2002): Settling speed of corn (*Zea mays*) pollen. In *Journal of Aerosol Science* 33 (11), pp. 1601–1607. DOI: 10.1016/S0021-8502(02)00105-2.

Bary A de (1863): Über die Fruchtentwicklung der Ascomyceten. Leipzig: Englemann. Available online at <https://agris.fao.org/agris-search/search.do?recordid=us201300210475>.

Borg DM; Brejnrod AD; Unterseher M; Hoppe T; Feng Y; Novozhilov Y et al. (2018): Genetic barcoding of dark-spored myxomycetes (Amoebozoa)-Identification, evaluation and application of a sequence similarity threshold for species differentiation in NGS studies. In *Molecular ecology resources* 18 (2), pp. 306–318. DOI: 10.1111/1755-0998.12725.

Brown AF (1991): Outbreeding Depression as a Cost of Dispersal in the Harpacticoid Copepod, *Tigriopus californicus*. In *The Biological bulletin* 181 (1), pp. 123–126. DOI: 10.2307/1542494.

Corner EJJ (1947): Variation in the Size and Shape of Spores, Basidia and Cystidia in Basidiomycetes. 46 (2), pp. 195–228. Available online at <http://www.jstor.org/stable/2428787>.

Dagamac NHA; Novozhilov YK; Stephenson SL; Lado C; Rojas C; Cruz TEE et al. (2017a): Biogeographical assessment of myxomycete assemblages from Neotropical and Asian Palaeotropical forests. In *Journal of Biogeography* 44 (7), pp. 1524–1536. DOI: 10.1111/jbi.12985.

Dagamac NHA; Rojas C; Novozhilov YK; Moreno GH; Schlueter R; Schnittler M (2017b): Speciation in progress? A phylogeographic study among populations of *Hemitrichia serpula* (Myxomycetes). In *PloS one* 12 (4), e0174825. DOI: 10.1371/journal.pone.0174825.

Dahl MB; Shchepin O; Schunk C; Menzel A; Novozhilov YK; Schnittler M (2018): A four year survey reveals a coherent pattern between occurrence of fruit bodies and soil amoebae populations for nivicolous myxomycetes. In *Scientific reports* 8 (1), p. 11662. DOI: 10.1038/s41598-018-30131-3.

Díez J; Moreno G; Del Peral L; Adams JH; Rodríguez Fías MD; Manjón JL (2020): *Fuligo septica* Spores Onboard a Stratospheric NASA Balloon and Its Complete In Vitro Life Cycle. In *Astrobiology* 20 (3), pp. 394–404. DOI: 10.1089/ast.2019.2097.

Edwards D; Kenrick P (2015): The early evolution of land plants, from fossils to genomics: a commentary on Lang (1937) 'On the plant-remains from the Downtonian of England and Wales'. In *Philosophical transactions of the Royal Society of London. Series B, Biological sciences* 370 (1666). DOI: 10.1098/rstb.2014.0343.

Ellstrand NC (1992): Gene Flow by Pollen: Implications for Plant Conservation Genetics. In *Oikos* 63 (1), p. 77. DOI: 10.2307/3545517.

Fayle TM; Dumbrell AJ; Turner EC; Foster WA (2011): Distributional Patterns of Epiphytic Ferns are Explained by the Presence of Cryptic Species. In *Biotropica* 43 (1), pp. 6–7. DOI: 10.1111/j.1744-7429.2010.00731.x.

Geiger JMO; Ranker TA; Neale JMR; Klimas ST (2007): Molecular biogeography and origins of the Hawaiian fern flora. In *Brittonia* 59 (2), pp. 142–158. DOI: 10.1663/0007-196X(2007)59[142:MBAOOT]2.0.CO;2.

Golan JJ; Pringle A (2017): Long-Distance Dispersal of Fungi. In *Microbiology spectrum* 5 (4). DOI: 10.1128/microbiolspec.FUNK-0047-2016.

Gray WD; Alexopoulos CJ (1968): *Biology of the myxomycetes*. New York, NY: Ronald Press Co.

Groot GA de; During HJ; Ansell SW; Schneider H; Bremer P; Wubs ERJ et al. (2012): Diverse spore rains and limited local exchange shape fern genetic diversity in a recently created habitat colonized by long-distance dispersal. In *Annals of botany* 109 (5), pp. 965–978. DOI: 10.1093/aob/mcs013.

Hillmann Falk; Forbes G; Novohradská S; Ferling I; Riege K; Groth M et al. (2018): Multiple Roots of Fruiting Body Formation in Amoebozoa. In *Genome biology and evolution* 10 (2), pp. 591–606. DOI: 10.1093/gbe/evy011.

Hoppe T; Schwippert WW (2014): Hydrophobicity of myxomycete spores: An undescribed aspect of spore ornamentation. In *Mycosphere* 5 (4), pp. 601–606. DOI: 10.5943/mycosphere/5/4/12.

Ingold CT (1965): *Spore Liberation*. Oxford: Clarendon Press.

Kang S; Tice AK; Spiegel FW; Silberman JD; Pánek T; Cepicka I et al. (2017): Between a Pod and a Hard Test: The Deep Evolution of Amoebae. In *Molecular biology and evolution* 34 (9), pp. 2258–2270. DOI: 10.1093/molbev/msx162.

Kenrick P; Crane PR (1997): The origin and early evolution of plants on land. In *Nature* 389 (6646), pp. 33–39. DOI: 10.1038/37918.

Kinosian SP; Pearse WD; Wolf PG (2020): Cryptic diversity in the model fern genus *Ceratopteris* (Pteridaceae). In *Molecular phylogenetics and evolution* 152, p. 106938. DOI: 10.1016/j.ympev.2020.106938.

Kwak MM; Velterop O; van Andel J (1998): Pollen and gene flow in fragmented habitats. In *Applied Vegetation Science* 1 (1), pp. 37–54. DOI: 10.2307/1479084.

Lado C (2005-2022): An online nomenclatural information system of Eumycetozoa. Real Jardín Botánico, CSIC. Madrid, Spain. Available online at <https://eumycetozoa.com>, updated on 1/14/2022, checked on 1/22/2022.

Leontyev DV; Schnittler M; Stephenson SL; Novozhilov YK; Shchepin ON (2019): Towards a phylogenetic classification of the Myxomycetes. In *Phytotaxa* 399 (3), p. 209. DOI: 10.11646/phytotaxa.399.3.5.

Loganathan P; Paramasivan P; Kalyanasundaram I (1989): Melanin as the spore wall pigment of some myxomycetes. In *Mycological research* 92 (3), pp. 286–292. DOI: 10.1016/S0953-7562(89)80067-X.

Mackenzie G; Boa AN; Diego-Taboada A; Atkin SL; Sathyapalan T (2015): Sporopollenin, The Least Known Yet Toughest Natural Biopolymer. In *Front. Mater.* 2. DOI: 10.3389/fmats.2015.00066.

Masuyama S; Yatabe Y; Murakami N; Watano Y (2002): Cryptic species in the fern *Ceratopteris thalictroides* (L.) Brongn. (Parkeriaceae). I. Molecular analyses and crossing tests. In *Journal of plant research* 115 (1118), pp. 87–97. DOI: 10.1007/s102650200013.

McCormick JJ; Blomquist JC; Rusch HP (1970): Isolation and Characterization of a Galactosamine Wall from Spores and Spherules of *Physarum polycephalum*. In *Journal of bacteriology* 104 (3), pp. 1119–1125. DOI: 10.1128/jb.104.3.1119-1125.1970.

Meerts P (1999): The evolution of spore size in Agarics: do big mushrooms have big pores? 12, pp. 161–165. Available online at http://164.15.59.215/sciences/lagev/fichiers/meerts_1999_jeb.pdf.

Miles CJ; Longton RE (1992): Deposition of moss spores in relation to distance from parent gametophytes. In *Journal of Bryology* 17 (2), pp. 355–368. DOI: 10.1179/jbr.1992.17.2.355.

Moraes MA; Kubota TYK; Rossini BC; Marino CL; Freitas MLM; Moraes MLT et al. (2018): Long-distance pollen and seed dispersal and inbreeding depression in *Hymenaea stigonocarpa* (Fabaceae: Caesalpinioideae) in the Brazilian savannah. In *Ecology and evolution* 8 (16), pp. 7800–7816. DOI: 10.1002/ece3.4253.

Rakoczy L; Panz T (1994): Melanin revealed in spores of the true slime moulds using the electron spin resonance method. In *Acta Protozoologica* 33.

Ronikier A; Ronikier M (2009): How 'alpine' are nivicolous myxomycetes? A worldwide assessment of altitudinal distribution. In *Mycologia* 101 (1), pp. 1–16. DOI: 10.3852/08-090.

Rose JP; Dassler CL (2017): Spore Production and Dispersal in Two Temperate Fern Species, With an Overview of the Evolution of Spore Production in Ferns. In *American Fern Journal* 107 (3), pp. 136–155. DOI: 10.1640/0002-8444-107.3.136.

Schnittler M; Erastova DA; Shchepin ON; Heinrich E; Novozhilov YK (2015): Four years in the Caucasus – observations on the ecology of nivicolous myxomycetes. In *Fungal Ecology* 14, pp. 105–115. DOI: 10.1016/j.funeco.2015.01.003.

Schnittler M; Tesmer J (2008): A habitat colonisation model for spore-dispersed organisms: does it work with eumycetozoans? In *Mycological research* 112 (Pt 6), pp. 697–707. DOI: 10.1016/j.mycres.2008.01.012.

Schnittler M; Unterseher M; Tesmer J (2006): Species richness and ecological characterization of myxomycetes and myxomycete-like organisms in the canopy of a temperate deciduous forest. In *Mycologia* 98 (2), pp. 223–232. DOI: 10.3852/mycologia.98.2.223.

Schnittler M; Novozhilov YK; Romeralo M; Brown M; Spiegel FW (2012): Myxomycetes and Myxomycete-like organisms. In Frey W. (Ed.): Engler's Syllabus of Plant Families, vol. 1. 13th ed.: Borntraeger (Myxomycetes and Myxomycete-like organisms, 1), pp. 40–88.

Shchepin ON; Novozhilov YK; Schnittler M (2014): Nivicolous myxomycetes in agar culture: some results and open problems 8 (2), pp. 53–61.

Shivas RG; Beasley DR; McTaggart AR (2014): Online identification guides for Australian smut fungi (Ustilaginomycotina) and rust fungi (Pucciniales). In *IMA fungus* 5 (2), pp. 195–202. DOI: 10.5598/imafungus.2014.05.02.03.

Smith AR (1972): Comparison of Fern and Flowering Plant Distributions with Some Evolutionary Interpretations for Ferns. In *Biotropica* 4 (1), p. 4. DOI: 10.2307/2989639.

Stephenson SL; Schnittler M; Novozhilov YK (2008): Myxomycete diversity and distribution from the fossil record to the present. In *Biodivers Conserv* 17 (2), pp. 285–301. DOI: 10.1007/s10531-007-9252-9.

Stephenson SL; Schnittler M (2017): Myxomycetes. In Archibald J, Simpson A, Slamovits C (Eds.): Handbook of the protists. 2nd ed. Cham: Springer, pp. 1405–1432.

Stokes GG (1845): On the Theories of Internal Friction of Fluids in Motion and of the Equilibrium and Motion of Elastic Solids 8, pp. 287–305.

Tesmer J; Schnittler M (2007): Sedimentation velocity of myxomycete spores. In *Mycol Progress* 6 (4), pp. 229–234. DOI: 10.1007/s11557-007-0539-8.

Thanbichler M; Wang SC; Shapiro L (2005): The bacterial nucleoid: a highly organized and dynamic structure. In *Journal of cellular biochemistry* 96 (3), pp. 506–521. DOI: 10.1002/jcb.20519.

Williams JH; Reese JB (2019): Evolution of development of pollen performance. In *Current topics in developmental biology* 131, pp. 299–336. DOI: 10.1016/bs.ctdb.2018.11.012.

Wolf PG; Schneider H; Ranker TA (2001): Geographic distributions of homosporous ferns: does dispersal obscure evidence of vicariance? In *Journal of Biogeography* 28 (2), pp. 263–270. DOI: 10.1046/j.1365-2699.2001.00531.x.

3 Publications

Chapters

3.1 Genetic structure of the protist <i>Physarum albescens</i> (Amoebozoa) revealed by multiple markers and genotyping by sequencing	25 – 45
3.2 Where do nivicolous myxomycetes occur? – Modelling the potential worldwide distribution of <i>Physarum albescens</i>	46 – 55
3.3 A workflow for low-cost automated image analysis of myxomycete spore numbers, size and shape	56 – 81
3.4 High environmental induced plasticity in spore size and numbers of nuclei per spore in <i>Physarum albescens</i> (Myxomycetes)	82 – 114

3.1 Genetic structure of the protist *Physarum albescens* (Amoebozoa) revealed by multiple markers and genotyping by sequencing

Oleg Shchepin^{1,2}, Yuri Novozhilov¹, Jan Woyzichovski², Manuela Bog², Ilya Prikhodko¹, Nadezhda Fedorova^{1,3}, Vladimir Gmoshinskiy^{4,5}, Mathilde Borg Dahl^{2,6}, Nikki H. A. Dagamac^{2,7}, Yuka Yajima⁸, Martin Schnittler²

¹Laboratory of Systematics and Geography of Fungi, Komarov Botanical Institute of the Russian Academy of Sciences, St. Petersburg, Russia

²General Botany and Plant Systematics, Institute of Botany and Landscape Ecology, University of Greifswald, Greifswald, Germany

³Faculty of Biology, Saint Petersburg State University, Saint Petersburg, Russia

⁴Faculty of Biology, Lomonosov Moscow State University, Moscow, Russia

⁵Polistovsky National Nature Reserve, Pskov Region, Russia

⁶Institute of Microbiology, Center for Functional Genomics of Microbes, University of Greifswald, Greifswald, Germany

⁷Department of Biological Sciences and Research Center for the Natural and Applied Sciences, University of Santo Tomas, Manila, Philippines

⁸Muroran Institute of Technology, Muroran, Japan


Corresponding author:

Oleg Shchepin, Laboratory of Systematics and Geography of Fungi, Komarov Botanical Institute of the Russian Academy of Sciences, St. Petersburg, Russia.

Email address: oshchepin@gmail.com

Manuscript published 22 October 2021 in *Molecular Ecology*.

Genetic structure of the protist *Physarum albescens* (Amoebozoa) revealed by multiple markers and genotyping by sequencing

Oleg Shchepin^{1,2}  | Yuri Novozhilov¹ | Jan Woyzichowski² | Manuela Bog² | Ilya Prikhodko¹ | Nadezhda Fedorova^{1,3} | Vladimir Gmoshinskiy^{4,5} | Mathilde Borg Dahl^{2,6} | Nikki H. A. Dagamac^{2,7} | Yuka Yajima⁸ | Martin Schnittler²

¹Laboratory of Systematics and Geography of Fungi, Komarov Botanical Institute of the Russian Academy of Sciences, St. Petersburg, Russia

²General Botany and Plant Systematics, Institute of Botany and Landscape Ecology, University of Greifswald, Greifswald, Germany

³Faculty of Biology, Saint Petersburg State University, Saint Petersburg, Russia

⁴Faculty of Biology, Lomonosov Moscow State University, Moscow, Russia

⁵Polistovsky National Nature Reserve, Pskov Region, Russia

⁶Institute of Microbiology, Center for Functional Genomics of Microbes, University of Greifswald, Greifswald, Germany

⁷Department of Biological Sciences and Research Center for the Natural and Applied Sciences, University of Santo Tomas, Manila, Philippines

⁸Muroran Institute of Technology, Muroran, Japan

Correspondence

Oleg Shchepin, Laboratory of Systematics and Geography of Fungi, Komarov Botanical Institute of the Russian Academy of Sciences, St. Petersburg, Russia.

Email: oshchepin@gmail.com

Funding information

Ministry of Science and Higher Education of the Russian Federation, Grant/Award Number: 075-15-2021-1056; Deutsche Forschungsgemeinschaft, Grant/Award Number: DFG, RTG 2010 RESPONSE and SCHN1080/2-1; Komarov Botanical Institute, Russian Academy of Sciences, Grant/Award Number: AAAA-A19-119020890079-6

Abstract

Myxomycetes are terrestrial protists with many presumably cosmopolitan species dispersing via airborne spores. A truly cosmopolitan species would suffer from outbreeding depression hampering local adaptation, while locally adapted species with limited distribution would be at a higher risk of extinction in changing environments. Here, we investigate intraspecific genetic diversity and phylogeography of *Physarum albescens* over the entire Northern Hemisphere. We sequenced 324 field collections of fruit bodies for 1–3 genetic markers (SSU, EF1A, COI) and analysed 98 specimens with genotyping by sequencing. The structure of the three-gene phylogeny, SNP-based phylogeny, phylogenetic networks, and the observed recombination pattern of three independently inherited gene markers can be best explained by the presence of at least 18 reproductively isolated groups, which can be seen as cryptic species. In all intensively sampled regions and in many localities, members of several phylogroups coexisted. Some phylogroups were found to be abundant in only one region and completely absent in other well-studied regions, and thus may represent regional endemics. Our results demonstrate that the widely distributed myxomycete species *Ph. albescens* represents a complex of at least 18 cryptic species, and some of these seem to have a limited geographical distribution. In addition, the presence of groups

of presumably clonal specimens suggests that sexual and asexual reproduction coexist in natural populations of myxomycetes.

KEYWORDS

cryptic species, DNA barcoding, phylogeography, protists, simulation, slime molds

1 | INTRODUCTION

Terrestrial soil protists have received much less scientific attention than prokaryotes, fungi, and viruses, despite their functional significance (Geisen et al., 2020). Their diversity and biogeography are generally understudied, but a few studies have found presumed cosmopolitan soil protist taxa to consist of multiple cryptic species (Pinseel et al., 2020; Ryšánek et al., 2015; Singer et al., 2019). Some of these cryptic species showed endemic distributions, and others proved to be cosmopolitan (Foissner, 2008). The fact that these endemic protist species exist implies that at least in some taxa, gene flow between remote populations is not frequent enough to prevent populations from diverging (Mann & Vanormelingen, 2013).

Among terrestrial protists, myxomycetes are especially convenient models to study biogeography and phylogeography. Myxomycetes are amoeboid protists with a complex life cycle that includes microscopic amoeboid flagellates, resting microcysts, multinuclear plasmodia, and fruiting bodies (sporocarps) containing airborne spores. Myxomycete spores have been detected in the air (Kamono et al., 2009), but no direct evidences for a long-distance dispersal have been found. Nevertheless, their ability for a long-distance dispersal is indirectly confirmed by presumably cosmopolitan distribution of many species and a relatively diverse myxomycete assemblages found on remote islands (see a detailed discussion in Schnittler et al., 2021). Myxomycete sporocarps are often conspicuous, easy to find in nature and preserve as dried herbarium specimens. Herbarium specimens can be used for DNA isolation and 18S rDNA (SSU) barcoding (Borg Dahl, Brejnrod, et al., 2018; Schnittler et al., 2017). However, virtually all studies on myxomycete diversity and distribution have been conducted at the morphological species (morphospecies) level.

The few studies that investigated the genetic structure of particular myxomycete morphospecies produced similar results. Aguilar et al. (2014) studied the geographical distribution of SSU variants in *Badhamia melanospora* (here and throughout the manuscript, myxomycete nomenclature follows Lado, 2005–2021). They found two geographically structured groups of ribotypes, which were congruent with slight morphological differences in spores. The authors suggested that this taxon constituted a complex formed by at least two cryptic species. In *Physarum pseudonotabile*, a SSU and EF1A gene phylogeny revealed several well-separated genetic lineages (Novozhilov et al., 2013). Analysis of three independent genes (SSU, EF1A, and COI) and group I introns in SSU demonstrated the existence of three cryptic species in *Trichia varia* (Feng & Schnittler,

2015). Similarly, *Lepidoderma chailletii* turned out to be a polyphyletic complex, which consisted of three cryptic species, as was shown by the analysis of SSU, EF1A, and COI (Shchepin et al., 2016). Dagamac et al. (2017) analysed two-gene data (SSU and EF1A) and revealed four putative cryptic species in *Hemitrichia serpula* with subtle morphological differences. Finally, several large phylogroups were found within *Didymium nivicola* in SSU and EF1A phylogenies, with striking differences in genetic diversity between the Northern and the Southern Hemisphere (Janik et al., 2020).

However, many intriguing questions remain unanswered. How common is the presence of cryptic species in myxomycetes? How widely are such species distributed? Trying to answer these questions, we applied a three-gene approach and, for the first time in myxomycetes, genotyping by sequencing to investigate the genetic structure of populations of the myxomycete *Physarum albescens*.

Ph. albescens (Figure 1a,b) abundantly occurs in mountains of the Northern Hemisphere but is rarely reported from the Southern Hemisphere. It belongs to the ecological guild of snowbank (nivicolous) myxomycetes (Schnittler et al., 2015), which makes up for c. 10% of the morphospecies diversity in myxomycetes. Myxamoebae inhabit the uppermost soil layer; fructifications emerge in spring at the edge of melting snow patches in mountainous areas (Figure 1c; Ronikier & Ronikier, 2009). *Ph. albescens* is morphologically clearly distinctive from other members of the guild. Moreover, it is one of the most common nivicolous species in some regions. Its brightly coloured sporocarps are easily visible in nature, and no infraspecific taxa are described within it, which makes it an ideal candidate for a large-scale phylogeographic study.

2 | MATERIALS AND METHODS

2.1 | Material studied

We studied 324 herbarium specimens of *Ph. albescens*, which were collected in several mountain ranges of the Northern Hemisphere between 2010 and 2018 (Europe, Central Asia, East Asia, and North America). A specimen was defined as a colony of closely located sporocarps that share the same hypothallus and probably have originated from one plasmodium. Additionally, we studied 44 herbarium specimens that were received from other collectors. Based on the GPS coordinates (WGS84) of collection sites, all specimens were assigned to standardized localities of approximately 50 m diameter using the python package GEOPY and a custom python script

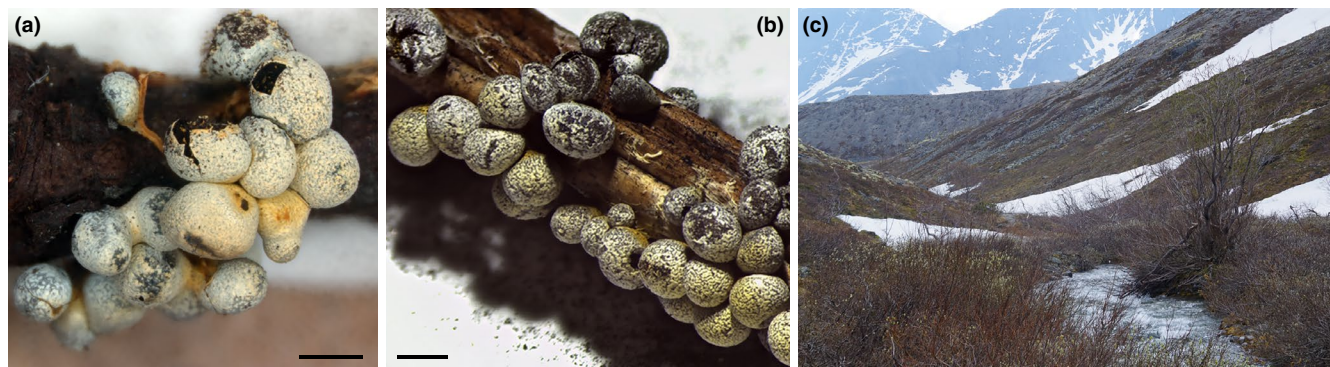


FIGURE 1 (a–b) Sporocarps of *Ph. albescens* from Khibiny Mts. (a, specimen LE305933) and Luvenga Tundra Mts. (b, MYX9295) at the Kola peninsula, Russia. (c) Typical habitat of *Ph. albescens* in Khibiny Mts. Scale bars = 1 mm

that performed greedy centroid-based clustering of collection sites. The resulting material included 368 specimens from 16 regions and 164 localities (Table S1).

2.2 | Genetic markers

Partial sequences of three independently inherited genetic markers were analysed. First, the beginning of the small ribosomal subunit gene (18S rDNA, SSU), including V2 region, located on nuclear minichromosomes. Second, the protein elongation factor subunit 1- α gene (EF1A) with nuclear chromosomal localization. Third, mitochondrial cytochrome c oxidase subunit one gene (COI). These markers proved to be highly variable in myxomycetes and valuable for species delimitation and phylogenetic inference (Schnittler et al., 2017).

For DNA extraction, approximately 2–5 sporocarps were sampled from a herbarium box and placed in 2 ml safe-lock tubes. Samples were homogenized either in a TissueLyser LT homogenizer (Qiagen) with 3 mm diameter steel balls or in a FastPrep-24 (MP Biomedicals) with sterilized sea sand and glass beads. DNA was extracted with PhytoSorb (Sintol) or with E.Z.N.A. Plant DNA Kit (Omega Bio-tek) according to the manufacturer's protocols.

The primers used were S1/SU19R or S3bF/S31R for SSU (Fiore-Donno et al., 2008, 2012; Hoppe & Schnittler, 2015; Schnittler et al., 2017), PB1F/PB1R for EF1A (Novozhilov et al., 2014), COIF1/COIR1 or COMF/COMRs for COI (Feng & Schnittler, 2015; Liu et al., 2015; Novozhilov et al., 2019). Amplification protocols were as follows: denaturation for 5 min at 95°C, 39 cycles (30 s at 95°C, 30 s at 56°C, 1 min at 72°C) and 5 min at 72°C with S1/SU19R; denaturation for 5 min at 95°C, 34 cycles (30 s at 95°C, 30 s at 57.6°C, 48 s at 72°C) and 5 min at 72°C with S3bF/S31R; denaturation for 5 min at 95°C, 35 cycles (30 s at 95°C, 30 s at 65.4°C, 1 min at 72°C) and 10 min at 72°C with PB1F/PB1R; denaturation for 5 min at 95°C, 34 cycles (30 s at 95°C, 50 s at 50.7°C or 52.0°C, 1 min at 72°C) and 10 min at 72°C with COIF1/COIR1 or COMF/COMRs.

Amplicons were sequenced on ABI 3500 automated DNA sequencer (Applied Biosystems) or by MacroGen Europe. Sequence

chromatograms were examined in BioEDIT 7.2.5 (Hall, 1999) and base-calling errors were corrected manually. New sequences were submitted to GenBank (accession numbers MW691477–MW691847, MW692988–MW693025, MW701443–MW701877, Table S1).

2.3 | Genotyping by sequencing (GBS)

For genotyping, 108 samples were prepared (Table S1). They represented 98 herbarium specimens of *Ph. albescens* from seven phylogenetic groups. Of them, two specimens were prepared in triplicates and six specimens in duplicates for evaluation of technical errors. From each specimen, 25–100 sporocarps (depending on their size and condition) were transferred into a 2 ml microtube with sterilized sea sand and glass beads and homogenized with a FastPrep-24 (MP Biomedicals). DNA was extracted with the E.Z.N.A. Plant DNA Kit (Omega Bio-tek) according to the manufacturer's protocol.

At least 100 ng of high molecular weight DNA per sample was required for GBS. DNA integrity was checked using gel electrophoresis with Lambda DNA/HindIII Marker. DNA concentration was measured using a Qubit 4 fluorometer (Invitrogen). GBS was performed by LGC Genomics with MsiI restriction endonuclease and paired-end sequencing (2 × 150 bp) on an Illumina NextSeq 500 platform (Illumina Inc.) with a sequencing depth of 0.5 million paired reads per sample. Preprocessing (demultiplexing, trimming sequencing adapters and restriction enzyme sites from raw sequence reads) was done by the sequencing facility. The raw data were submitted to the sequence read archive (PRJNA706537).

Preprocessed paired-end reads were de novo assembled and analysed using steps 3–7 of the IPYRAD 0.9.26 pipeline (Eaton & Overcast, 2020). In brief, reads were quality-filtered, dereplicated and clustered within samples with a specified sequence similarity threshold, maximum number of alleles per site, and minimum and maximum allowed sequencing depth. For each cluster, consensus sequence was produced. After that, consensus sequences from all samples were aligned together to obtain contigs. Only contigs that covered at least 10 samples were retained (value specified with the core parameter of step 7 “minimum number of samples per locus”).

We optimized the core assembly parameter “clustering threshold for de novo assembly” (*ct*) by running the analysis with three different values of *ct* (0.85, 0.90, 0.95) on the data of 10 technical replicates. The value 0.95 was chosen since the lower values produced apparent assembly errors leading to increased genetic distances between replicated samples. The resulting alignment of single-nucleotide polymorphisms (SNPs) was subjected to phylogenetic analysis and phylogenetic network construction.

ABBA-BABA statistics were calculated in Dsuite 0.4 (Malinsky et al., 2021) using DTRIOS command for 61 specimens from five phylogroups (Ha-He) and 25 specimens from phylogroup B as an outgroup. Relationships between phylogroups were specified by a simple tree based on the well-resolved maximum likelihood tree obtained for the SNP alignment: (Outgroup,((Hc, Hb),(Hd,(Ha, He)))). DTRIOS calculates Patterson's *D* and f_4 -ratio statistics and finds trios of phylogroups with significantly elevated *D* using Z-score, which is estimated with a block-Jackknife procedure that takes linkage among sites into account. The option Jknum (the number of jackknife blocks to divide the data set into) was left with its default value (20 blocks of 1278 SNPs), since different tested values (20, 30, 40, 50) did not alter the results. A Benjamini-Hochberg correction for multiple tests was applied to the resulting *p*-values to control the false-discovery rate. To aid the interpretation of correlated f_4 -ratio results, *f*-branch statistic ($f_b(C)$) was calculated using FBRANCH command, and its results were plotted using dtools.py. For the phylogroup trios with significantly elevated *D*, a sliding-window analysis was performed using DINVESTIGATE command to assess whether the admixture signal was confined to specific contigs (window size = 2, step = 1).

To test for the presence of clonal specimens, genetic distances between all pairs of specimens and between technical replicates were calculated using the Hamming Distances method (Hamming, 1950) with default options in SPLITREE5 5.0.0_alpha (Huson, 1998; Huson & Bryant, 2006). Groups of specimens that showed genetic distances not exceeding the maximum distances between technical replicates were classified as putative clones.

2.4 | Phylogeny construction

Four sequence data sets were built: (1) a two-gene data set (SSU and exons of EF1A) for *Ph. albescens* and diverse members of Physarales to infer phylogenetic relationships of *Ph. albescens* with other members of the order, (2) an SSU data set for all specimens of *Ph. albescens* for initial screening of species-wide genetic diversity, (3) a three-gene data set (SSU, exons of EF1A, and COI) for a subset of specimens from each clade of the SSU phylogeny to test for the presence of cryptic species within the morphologically defined species, and (4) a SNP data set resulting from the analysis of GBS data to get a phylogeny with a higher resolution for a subset of specimens.

In the first three data sets, sequences of different genes were aligned separately with MAFFT online service with default gap penalties (Katoh et al., 2019). Two alignment strategies were applied: E-INS-I for SSU, G-INS-I for EF1A and COI (Katoh et al., 2005). All

alignments were visually inspected, corrected if necessary, and trimmed. Poorly aligned regions with multiple indels in SSU alignment of the first data set were removed manually prior to the phylogenetic analyses (mask in Alignment S1 shows the remaining positions). Introns in all EF1A alignments were as well removed before the analyses.

Maximum likelihood (ML) phylogenies for all four data sets were built using W-IQ-TREE 1.6.11 (Trifinopoulos et al., 2016) with 1000 ultrafast bootstrap replicates (Minh et al., 2013). For the SNP data set, an ascertainment bias correction model was applied. Optimal substitution models for ML analysis were chosen independently for each partition with MODELFINDER on W-IQ-TREE web server (Kalyaanamoorthy et al., 2017) according to the Bayesian information criterion.

Bayesian inference was computed with MrBAYES 3.2.1 on CIPRES Science Gateway (Huelsenbeck & Ronquist, 2001; Miller et al., 2010). Five simultaneous runs with the evolutionary model set to GTR+G4+I included one cold and three heated Monte Carlo Markov chains. The number of generations, sample frequencies, and burnin ratio were set to 50 M, 1000, and 0.25, respectively. The convergence of MCMC chains in Bayesian inference analyses was assessed using TRACER 1.7.1 and R package RWTY 1.0.2 (Warren et al., 2017). Clade confidence scores based on the results of Bayesian inference analyses were placed on ML trees using IQ-TREE (it implements an algorithm that, similar to sumt command in MrBAYES, counts the proportion of the Bayesian trees where every taxon bipartition appears).

The two-gene data set included SSU and EF1A sequences for 298 myxomycete specimens belonging to 47 species of different Physarales, with three *Lamproderma* species as an outgroup (Alignment S1, Table S1). Of them, 194 specimens belonged to *Ph. albescens*. 66 SSU and 55 EF1A sequences were obtained from GenBank. The concatenated alignment contained 1434 sites, 505 of them parsimony informative. Four partitions were defined (Chernomor et al., 2016): one for SSU (model SYM+R4) and three for different codon positions in EF1A (models HKY+F+R4, TVM+F+I+G4, and TVM+F+G4 for the first, second, and third position, respectively).

The SSU data set included 372 nucleotide sequences (Alignment S2, Table S1). Of these, 368 sequences of *Ph. albescens* were obtained in this study and four sequences fetched from GenBank, with *Physarum polycephalum* as an outgroup. Among 565 nucleotide positions, 56 were parsimony informative. For phylogenetic inference, a single partition was defined with TNe+R2 model.

The three-gene data set included SSU, EF1A, and COI sequences for 182 specimens of *Ph. albescens*. SSU and EF1A sequences of three specimens of *Badhamia foliicola* were added as an outgroup, based on the two-gene analysis results (Alignment S3, Table S1). The concatenated alignment contained 1946 sites, 302 of them parsimony informative. Five partitions were defined (Chernomor et al., 2016): one for SSU (model K2P+R2), three for different codon positions in EF1A (models F81+F+I, F81+F+I, and TPM2u+F+G4 for the first, second, and third position, respectively), and one for COI (model K3Pu+F+I+G4).

The SNP data set included SNP data for 108 samples (98 specimens and technical replicates) of *Ph. albescens* (Alignment S4, Table S1). The alignment contained 25,589 positions, 10,364 of them parsimony informative. For phylogenetic inference, a single partition was defined with TVM+F+R3 model.

2.5 | Phylogenetic network construction

A phylogenetic network was built for the three-gene data set and the SNP data set. The analysis was performed using SPLITSTREE5 5.0.0_alpha (Huson, 1998; Huson & Bryant, 2006). A distance matrix was calculated using the Hamming Distances method (Hamming, 1950) with default options. The neighbor-net method (Bryant & Moulton, 2004) was used to obtain splits. The Splits Network Algorithm (Dress & Huson, 2004) produced a splits network with 5716 nodes and 10,883 edges for the three-gene data set, and with 1650 nodes and 3002 edges for the SNP data set.

2.6 | Phylogroup delimitation

Several approaches were applied to delimit phylogroups representing putative reproductively isolated cryptic species. First, we used species delimitation approach based on multilocus "fields for recombination" (ml-FFRs) concept proposed by Doyle (1995). Following the logic described in detail by Flot et al. (2010), we tried to determine groups of specimens that were not necessarily reciprocally monophyletic in each of the gene phylogenies, but their pools of alleles of three independently inherited genes were mutually exclusive (mutual allelic exclusivity criterion). For this, unique sequence variants of SSU, EF1A, and COI in *Ph. albescens* were determined by clustering sequences with a 100% similarity threshold using the --cluster_size command in VSEARCH 2.14.2 (Rognes et al., 2016). Each sequence variant received a numeric code. A custom GUI python program was written to visualize the combinations of the variants of three independently inherited genes (SSU, EF1A, and COI) within individuals (herbarium specimens) of *Ph. albescens* (Shchepin, 2021a). The resulting groups of individuals that do not have any allele in common (ml-FFRs) were compared with the topologies of the three-gene phylogeny and the SNP-based phylogeny, and ml-FFRs supported by the tree topologies were considered as putative cryptic species. If two distinct well-supported clades shared only one allele of one gene, they were still considered as two putative cryptic species. If a ml-FFR consisted of a single individual and it was closely related to another ml-FFR in a phylogeny, it was united with it into one phylogroup.

In addition, we employed two automatic species delimitation algorithms. First, multirate Poisson tree processes (mPTP) approach was employed. The analyses were run on mPTP 0.2.0 web server (Kapli et al., 2017) with default settings, using the three-gene ML phylogeny and SNP ML phylogeny as inputs. Second, assemble species by automatic partitioning (ASAP) analyses were run on a web

server with default settings using the three-gene and SNP alignments as inputs (Puillandre et al., 2021).

2.7 | Sequence clustering

To evaluate the taxonomical resolution of SSU-based DNA barcoding at the intramorphospecies level, SSU sequences of *Ph. albescens* were clustered with two similarity thresholds that were applied for species determination or clustering of the operational taxonomic units (OTUs) in previous studies: (1) 99.1% (Borg Dahl et al., 2019; Borg Dahl, Brejnrod, et al., 2018; Borg Dahl, Shchepin, et al., 2018; Shchepin et al., 2017, 2019) and (2) 98% (Clissmann et al., 2015; Gao et al., 2019; Kamono et al., 2013; Shchepin et al., 2019). SSU sequences were trimmed to match ca. 350 bp fragment covered by the primers S3bF/S31R used in DNA metabarcoding studies (columns 98–457 in Alignment S2). The --cluster_size command implemented in VSEARCH was used for clustering.

2.8 | Pairwise genetic distances

Genetic distances were calculated for all pairs of sequences from the three-gene data set and the SSU data set. Additionally, within-phylogroup and between-phylogroup pairwise genetic distances were computed for nonsingleton phylogroups. The analyses were conducted in MEGA X (Kumar et al., 2018). Genetic distance was defined as the number of base differences between two sequences. All ambiguous positions were removed for each sequence pair (pairwise deletion option). Standard error estimates were obtained by a bootstrap procedure (100 replicates).

2.9 | Diversity estimates

Phylogroup and SSU sequence variant diversity estimates (richness, sample completeness, Shannon and Simpson diversity) together with individual-based rarefaction and extrapolation sampling curves for phylogroup richness of *Ph. albescens* were obtained using the R package iNEXT2.0.20 (Hsieh et al., 2016). In addition, the same analyses were performed for six other myxomycete species based on data from published phylogeographic studies: *Badhamia melanospora*, *Didymium nivicola*, *Hemitrichia serpulula*, *Lepidoderma chailletii*, *Meriderma atrosporum*, *Trichia varia* (Aguilar et al., 2014; Dagamac et al., 2017; Feng et al., 2016; Feng & Schnittler, 2015; Janik et al., 2020; Shchepin et al., 2016).

2.10 | Computer simulation

To test for the presence of genetic isolation between members of different phylogroups of *Physarum albescens*, a python script was written (Shchepin, 2021b). It takes a table of observed combinations

of genetic variants of three independently inherited genes and creates 1000 times the first offspring generation, consisting of a specified number of individuals (equal to the number of studied specimens in the input table) with randomly combined multilocus genotypes.

To produce a new simulated individual, the algorithm randomly samples with replacement two "parent" individuals and randomly chooses one SSU variant (from parent 1 or parent 2, non-Mendelian inheritance), one COI variant (from parent 1 or parent 2, non-Mendelian inheritance), and two EF1A variants (one of the two alleles from parent 1 and one of the two alleles from parent 2, Mendelian inheritance). The simulation does not consider that in myxomycetes some variants of SSU and COI are preferentially preserved during the homogenization process (Ferris et al., 1983; Silliker & Collins, 1988; Silliker et al., 2002). To test if this factor would influence the results, an alternative simulation was created: here, a weight value (0, 1, or 2) was randomly assigned to each SSU and each COI variant. Whenever an individual was produced, the weights of the parental SSU and COI variants were compared, and the variant with a larger weight was inherited. If the weights were identical, the variant to be inherited was chosen randomly.

To minimize the possible influence of geographic isolation, the input data included only specimens collected in 2–3 adjacent valleys within a given mountain range. Five input data sets were compiled: (1) Forty-one specimens from Khibiny Mts. (phylogroups Ha, Hb, Hc), (2) Thirty-six specimens from Spanish Sierra Nevada (phylogroups B, D, Fa, G, M), (3) Sixteen specimens from Khibiny Mts. (phylogroup Hb only), (4) Twenty-two specimens from Khibiny Mts. (phylogroup Hc only), and (5) Eleven specimens from Spanish Sierra Nevada (phylogroup D only).

For each data set, the percentage of individuals with genetic variants coming from different phylogroups ("mixed" genotypes) in the observed and simulated data was calculated. Additionally, the average number of unique multilocus genotypes over 1000 simulated generations was calculated.

The Sierra Nevada data set was additionally tested with different values for generation size (from 100 to 5000, with an increment of 100) to determine the influence of generation size on the number of unique genotypes in the simulated offspring.

3 | RESULTS

3.1 | Genetic diversity of *Ph. albescens*

The 368 specimens of *Physarum albescens* collected throughout the Northern Hemisphere revealed 44 unique variants of partial SSU sequences. The monophyly of this morphospecies was confirmed by a two-gene phylogeny of Physaraceae (Figure S1). A phylogeny based on the SSU sequences (Figure S2) separated *Ph. albescens* into 13 clades of closely related specimens (phylogroups), with four additional phylogroups consisting of one specimen each (singletons). For a subset of specimens from each phylogroup, partial sequences of a mitochondrial gene COI and nuclear gene EF1A were obtained.

Among 204 COI sequences, 46 unique variants (haplotypes) were found. The highest number of genetic variants was found for the exons of the EF1A gene: 58 unique heterozygous variants (corresponding to 87 allelic variants) among 194 sequences. The three-gene genotypes' total diversity equalled 85, with 61% of them occurring in one specimen only (Figure 2a). In all studied specimens of *Ph. albescens*, the amplified fragment of EF1A contained a spliceosomal intron 59–110 bp in length near the end. This intron was absent in all other species of Physaraceae sequenced to date except for one accession of *Badhamia nitens* (MA-Fungi 57896) that was sister to *Ph. albescens* in the two-gene phylogeny (Alignment S1).

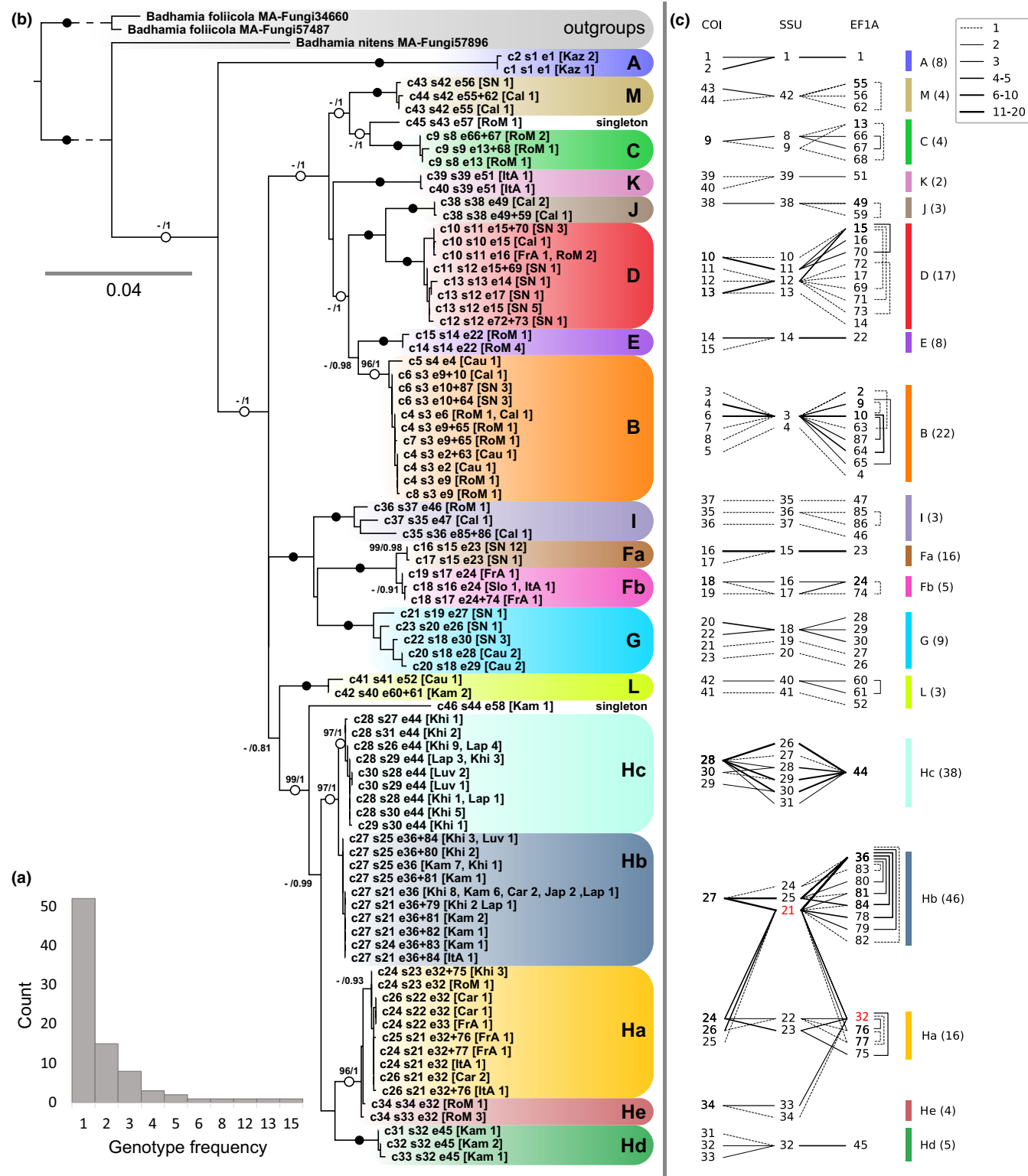
A robust phylogeny based on the three-gene data set separated *Ph. albescens* into multiple phylogroups with high statistical support. This pattern was reproduced in the phylogenetic network based on the same data (Figure 3a). The analysis of combinations between the sequence variants of three independently inherited gene markers (SSU, COI, and EF1A) revealed 22 ml FFRs, six of them consisting of a single specimen (Figure 2c). Based on these ml-FFRs and the topology of the three-gene tree, 18 phylogroups representing putative cryptic species and two singleton phylogroups were delimited according to the rules described in methods section (Figure 2b). The presence of ml-FFRs matching the clades in the three-gene phylogeny suggested the absence of recombination between the members of different phylogroups, that is, their reproductive isolation (Figure 2c). Only two exceptions were found: SSU variant 21 appeared in specimens from two closely related phylogroups (Ha and Hb), and the EF1A variant 32 was shared by sister phylogroups Ha and He.

Two species delimitation algorithms applied to the three-gene data set, MPTP and ASAP, suggested the presence of 17 and 19 species (including singletons), respectively (Table 1). Both algorithms united several phylogroups together (Fa+Gb, Ha+He, Hb+Hc). In addition, ASAP split the phylogroup I into three species.

For the three-gene data set, the pairwise genetic distance between specimens of *Ph. albescens* averaged 48.34 (SE 0.21, SD 27.47, min 0.00, max 102.00) base differences between two sequences. The average within-phylogroup distance was as low as 3.01 (SE 1.10, SD 4.69, min 0.00, max 19.67), while the average between-phylogroup distance was 62.48 (SE 1.32, SD 16.35, min 5.83, max 87.85). For SSU, the average between-phylogroup distance was 62.48 (SE 0.31, SD 4.05, min 0.896, max 22.56). Matrices of genetic distances and their descriptive statistics for SSU, COI, EF1A, and the three-gene data can be found in Table S2.

3.2 | GBS results

Raw Illumina sequencing data for 98 specimens representing seven phylogroups of *Ph. albescens* contained 87.6 million paired-end reads. After quality filtering, clustering withing samples, and filtering clusters by sequencing depth, 1,220,930 consensus reads were produced. Consensus reads were assembled into 76,192 contigs. Of them, 4521 contigs that covered at least 10 samples were retained (length: min 35, max 304, N50 200). Only 664 contigs were present



in at least half of the samples. Each sample was on average represented by 11,305 reads (min 1537, max 38,800) and 1180 contigs (min 111, max 1833).

SNP calling resulted in an alignment of 25,589 SNPs with 71.63% missing sites. A phylogenetic network (Figure 3b) that was produced using this alignment separated the specimens into the same seven phylogroups as the three-gene phylogeny (Figure 2b).

The SNP-based ML analysis produced a phylogeny with maximum bootstrap support for almost all major branches (Figure 4). Its topology again confirmed the separation of the investigated specimens into the same seven phylogroups as the SSU and the three-gene phylogenies.

Two species delimitation algorithms, mPTP and ASAP, produced different results when applied to the SNP data set (Table 1). mPTP

FIGURE 2 (a) Histogram showing the number of occurrences of three-gene genotypes with different frequencies among 182 specimens of *Ph. albescens*. (b) ML tree based on partial SSU, EF1A, and COI sequences of 182 specimens of *Ph. albescens*, with two species of the genus *Badhamia* as outgroups. Only unique three-gene genotypes are shown. Phylogroups of *Ph. albescens* are highlighted with different colours and named with letters. Labels list sequence variants of the three analysed genes in the following format: cN for COI, sN for SSU, and eN for EF1A (or eN+N for heterozygous sequences). The number of specimens bearing each three-gene genotype and their regions of origin is provided in square brackets (see abbreviations below). Bayesian posterior probability values above 0.7 and ultrafast bootstrap values above 95 are indicated. Fully supported branches (100/1) are marked with a solid circle. Branches fully supported by only one statistic are marked with a hollow circle. (c) Combinations of the variants of three independently inherited genes for 214 specimens of *Ph. albescens* that were sequenced for at least two genes. Numbers indicate unique sequence variants of each gene. Line type indicates the number of specimens where a particular combination of sequence variants was observed (see legend). For specimens with heterozygous EF1A, combinations of EF1A alleles are shown with vertical square brackets. Numbers in round brackets after the phylogroup names indicate the number of analysed specimens from each phylogroup. One SSU and one EF1A variant that each occur in more than one phylogroup are marked in red. Abbreviations: Cal, San Jacinto Mt. and Sequoia National Park, California, USA; Car, Western Carpathians, Poland; Cau, Northern Caucasus, Russia; FrA, French Alps; ItA, Italian Alps; Jap, Hokkaido, Japan; Kam, Kamchatka, Russia; Kaz, Ile Alatau Mts., Kazakhstan; Khi, Khibiny Mts., Russia; Lap, Chunutundra Mts., Lapland Reserve, Russia; Luv, Luvenga Tundra Mts., Russia; RoM, Rocky Mts., Colorado, USA; Slo, Slovenian Alps; SN, Sierra Nevada Mts., Spain

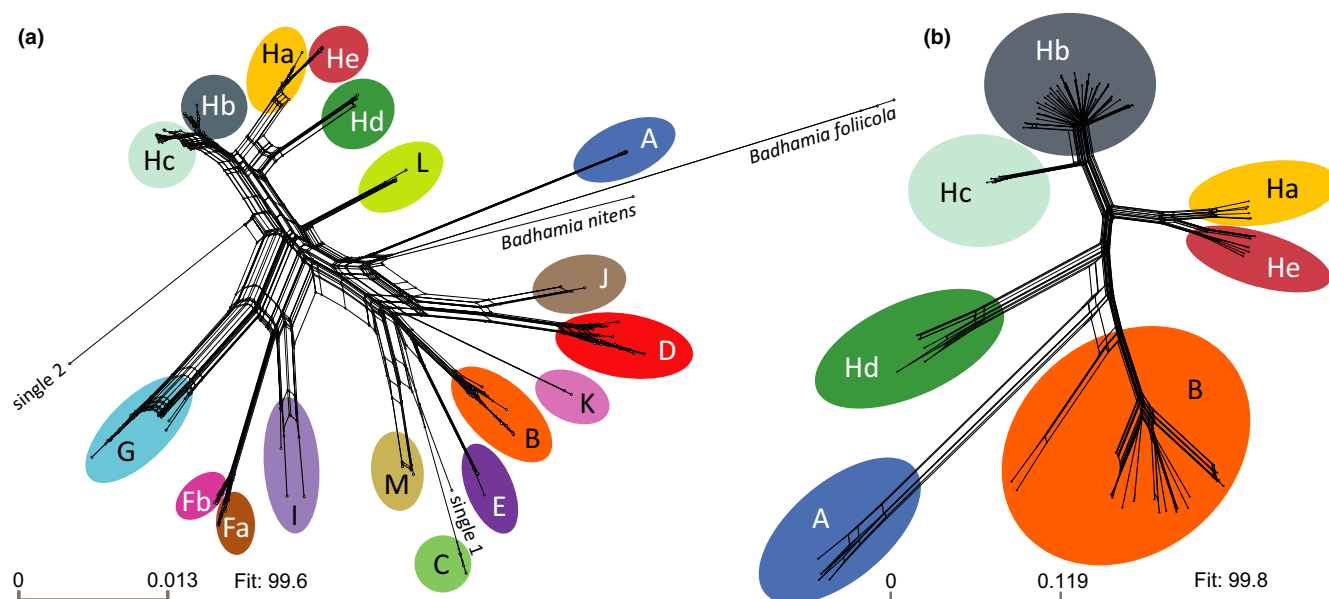


FIGURE 3 Phylogenetic networks produced for *Ph. albescens* in SPLITSTREE5 using the three-gene data set (a) and the SNP data set for seven phylogroups investigated with GBS (b). Phylogroups are highlighted with the same colours as in Figure 2. Scale bar indicates the number of substitutions per site

supported delimitation of the phylogroups Ha, Hb, Hc, Hd, and He, but suggested splitting of B into six species. ASAP supported delimitation of A and Hd, but suggested splitting B into two species and uniting Hb with Hc and Ha with He.

ABBA-BABA tests were conducted for ten trios of closely related phylogroups Ha–He to detect possible introgression events. Four trios showed D statistic significantly different from zero ($Z > 3$, p -adjusted $< .00135$) and large f_4 -ratio values (0.18–0.23) (Table S3). A sliding-window analysis demonstrated that SNPs showing ABBA-BABA patterns for each trio were distributed over 25–29 different contigs (Table S3). However, a single gene-flow event can lead to multiple elevated D and f_4 -ratio results. When a branch-specific $f_b(C)$ was calculated that partially disentangles correlated f_4 -ratio results, only two of the eight branches in the phylogeny showed significant excess sharing of derived alleles

with at least one other phylogroup (Figure 5). Specifically, an internal branch representing the common ancestor of phylogroups Ha and He showed an excess sharing of derived alleles with phylogroups Hb and Hc. One more $f_b(C)$ signal involves two of the same four phylogroups: Hc and Ha. These results are consistent with the observation of an SSU variant shared by Ha and Hb and an EF1A variant shared by Ha and He (Figure 2c), which, however, could be also explained by incomplete lineage sorting. It should also be taken into account that a single introgression event can still lead to significant $f_b(C)$ values across multiple related phylogroups (Malinsky et al., 2018).

Pairwise genetic Hamming distances between technical replicates ranged between 0.0011 and 0.0097, while distances between unique specimens averaged 0.2446 (min 0.0012, max 0.5292). Among the phylogroups A, B, Ha, Hb, Hd, and He, some pairs of

TABLE 1 Results of delimitation of cryptic species within *Physarum albescens* obtained using different methods

Phylogroup	SSU barcode		Three-gene data		GBS SNPs	
	98% similarity	99.1% similarity	mPTP	ASAP	mPTP	ASAP
A	5	6	17	10	1	4
B	3*	4	6	9	2^, 3^, 4^, 5^, 6^, 7^	1^, 5^
C	8^, 9^	15	10	18		
D	6*	7	4	2		
E	3*	13	7	14		
Fa	2*	3*	1*	1*		
Fb	2*	3*	1*	1*		
G	4*	5	3	3		
Ha	1*	1*	13*	6*	10	3*
Hb	1*	1*	12*	5*	9	2*
Hc	1*	1*	12*	5*	8	2*
Hd	1*	19	14	15	12	6
He	1*	14^, 17^	13*	6*	11	3*
I	4^, 7^, 8^	8^, 10^	2	8^, 13^, 17^		
J	6*	9	5	4		
K	8*	11	8	12		
L	1*	2	16	11		
M	3*	12	9	16		
Single1	8*	16	11	19		
Single2	10	18	15	7		

Note: "Phylogroup" – species delimited manually based on ml-FFRs and topologies of the three-gene and SNP phylogenies. "SSU barcode" – species delimited based on two different SSU barcoding similarity thresholds. mPTP and ASAP delimitations are presented separately for the three-gene data and for the GBS SNP data. GBS SNP data are available only for seven phylogroups. Predicted species that contain members of more than one phylogroup are marked with *. Predicted species that split one phylogroup into several species are marked with ^.

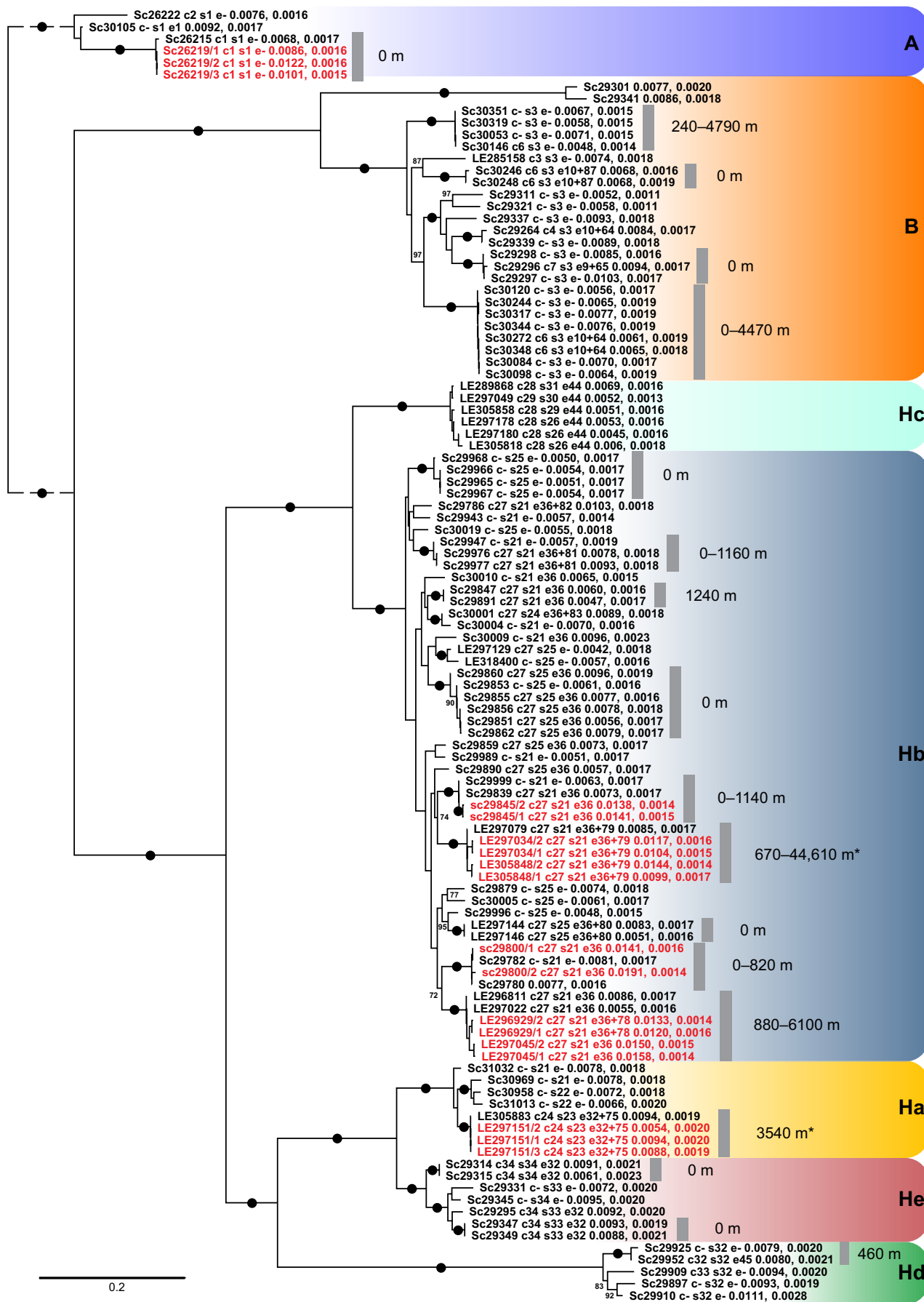
specimens showed a genetic distance comparable to the distance between technical replicates (0.0012–0.0094). Due to this, 18 groups of specimens that showed pairwise genetic distances not exceeding 0.01 were denoted as putative clones (Figure 4, Table S3). In total, 57 of 98 specimens were included into putatively clonal groups, with groups consisting of 2–8 specimens. Within phylogroup Hb, nine putatively clonal groups were found.

In most pairs of putatively clonal specimens, both specimens were collected from the same locality. However, in 10 of 18 putatively clonal groups, some specimens were collected from distant localities (240–44,610 m), including different valleys of the same mountain range and different mountain ranges in a region (Figure 4, Table S3). Two groups included putatively clonal specimens that were collected in two different years and at large distances from each other (44,610 and 3540 m).

3.3 | Observed and simulated number of unique multilocus genotypes

Five data sets containing information on genetic variants of three independently inherited genes (SSU, EF1A, COI) in specimens of *Ph. albescens* were used to test for the presence of reproductive isolation between different phylogroups. For populations of *Ph. albescens* from the Khibiny Mts. (data set 1, phylogroups Ha, Hb, and Hc) and Spanish Sierra Nevada (data set 2, phylogroups B, D, Fa, G, and M), the observed number of unique multilocus genotypes was outside the distance of three standard deviations (3σ) from the mean number of unique multilocus genotypes for 1000 simulated offspring generations consisting of the same number of individuals as the parent generation (Table S4, Figure S3). In other words, the observed number of combinations of three genetic variants is

FIGURE 4 ML tree based on 25,589 single-nucleotide polymorphisms from the GBS analysis for 108 samples (98 specimens plus technical replicates) of *Ph. albescens*. Phylogroups are highlighted with the same colours as in Figure 2. Labels show specimen numbers with sequence variants of the three analysed genes (same format as in Figure 2b; "-" stands for missing data), followed by figures for the estimated heterozygosity and error rate. Labels of technical replicates are shown in red font. Groups of putatively clonal specimens are marked with grey vertical lines, and geographic distances (minimal and maximal) between the localities where members of a group were collected are shown, with "0 m" denoting specimens collected from the same locality. Putatively clonal groups that include specimens collected in different years are marked with an asterisk. Bootstrap values above 70 are indicated. Fully supported branches (100) are marked with a solid circle



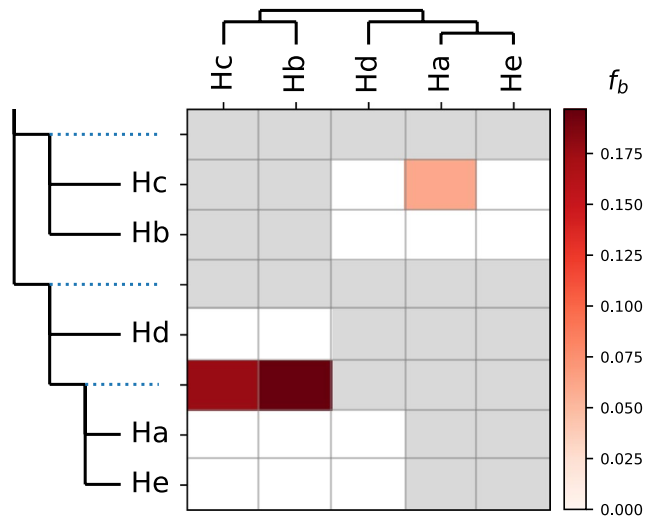


FIGURE 5 Results of f -branch inference for five phylogroups of *Ph. albescens* performed in Dsuite. The branch-specific statistic $f_b(C)$ identifies excess sharing of derived alleles between the tree branch on the y-axis and the phylogroup C on the x-axis. Grey data points in the matrix correspond to tests that are not applicable to the provided phylogeny

significantly lower than what would be expected in a randomly sampled panmictic population.

In the case of the data sets 3–5, the simulation was run separately for three phylogroups that were represented by more than 10 specimens and more than three unique multilocus genotypes within a region, assuming that they were reproductively isolated from other phylogroups (phylogroups Hb and Hc from Khibiny Mts., and D from Sierra Nevada). For these data sets, the observed number of combinations of three genetic variants did not differ significantly from the simulation results (Table S4).

When the influence of generation size on the mean genotype number over 1000 simulated generations was tested for the data set from the Sierra Nevada, a strong positive correlation was found ($R = 0.89$, $p < .01$) (Figure S4a). However, when generations of different sizes were sub-sampled to the size of the parent generation, this correlation disappeared ($R = 0.02$, $p < .88$), and the mean genotype number showed a negligible variation (mean 28.69, SD 0.07) (Figure S4b).

3.4 | Recombination patterns in simulated populations

Each of the 1000 offspring generations simulated under the assumption of panmictic populations for data sets 1 and 2 contained 34%–83% or 50%–94% (for Khibiny Mts. and Sierra Nevada, respectively) of individuals with “mixed” genotypes, consisting of genetic variants from different phylogroups (Table S4). Such “mixed” multi-locus genotypes were completely absent in the input data on *Ph. albescens*.

The observed patterns of combinations of genetic variants of three genes clearly differ from the combinations simulated under the

assumption that individuals from different phylogroups recombine freely. As seen from the examples shown in Figure 6, phylogroups cannot be separated in the simulated generations, since COI, SSU, and EF1A variants from different phylogroups combine freely with each other, while this never happens among the combinations observed in the input data.

3.5 | Species-level similarity thresholds for SSU

Clustering SSU sequences at 98% and 99.1% similarity threshold resulted in 10 and 19 clusters, respectively (Table 1). None of the two thresholds allowed to differentiate all phylogroups. Clustering at 98% similarity formed separate clusters only for the phylogroup A and one of the singletons. Six clusters contained sequences from more than one phylogroup. Clustering at 99.1% similarity produced separate clusters for 13 phylogroups and both singletons; only two clusters included more than one phylogroup. In both cases, they united phylogroups that appeared closely related in phylogenies (Fa and Fb; Ha, Hb, and Hc).

3.6 | Regional phylogroup diversity

Diversity estimates for the 20 phylogroups (two represented by singletons only) in the investigated regions revealed a sample coverage of 99.44% (the probability that the next sampled specimen would belong to one of the previously found phylogroups; Chao & Jost, 2012) (Figure 7a, Table S1). The asymptotic estimate of the total phylogroup richness was 21.99 ± 3.73 (for the formula, see Chao et al., 2014). Among the five regions that were sampled most intensively, the sample coverage varied from 94.41% in the Rocky Mts. to 100% in the mountains of the Kola Peninsula (Figure 7b, Table S1). The same two regions showed the highest and the lowest phylogroup richness estimates: for the Rocky Mts., the observed and estimated phylogroup richness was eight and 12.41 ± 7.06 , respectively; for the Kola Pen., these numbers were 3 and 3.00 ± 0.02 (Figure 8).

Some phylogroups showed a very restricted distribution in the Northern Hemisphere. For example, the phylogroups C, E, He, I, and J occurred only in the mountains of western North America, Fa – only in Spanish Sierra Nevada, Fb – in European Alps and the Pyrenees, Hc – mountains of the Kola Pen., and Hd – in the mountains of the Kamchatka Pen. (Figure 8).

3.7 | Diversity comparison with other species

Ph. albescens showed the highest observed phylogroup and SSU sequence diversity compared to the other six species that were extensively studied with molecular markers (Figure S6, Table S5). When extrapolated diversity values were compared, *Ph. albescens* still showed the highest expected phylogroup diversity, while

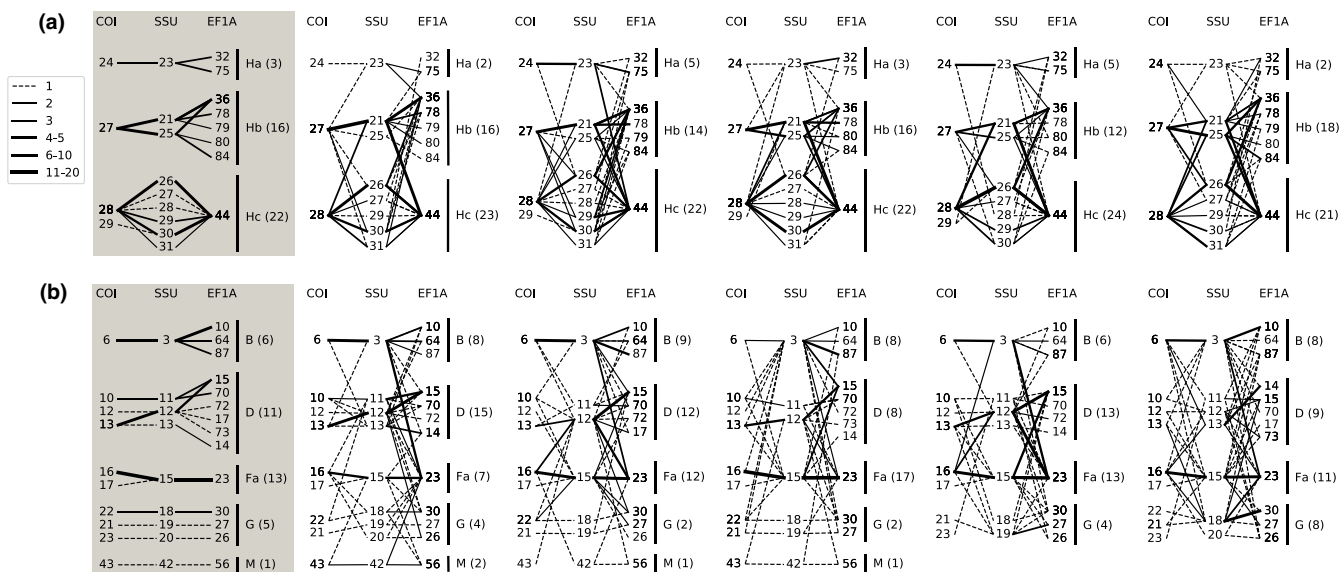


FIGURE 6 Observed and simulated combinations of the variants of three independently inherited genes for two data sets: a – Khibiny Mts., b – Sierra Nevada. The first graph on the left represents combinations observed in the input data (parent generation). The other graphs depict five generations randomly chosen from 1000 simulated offspring generations. In the graphs with simulated data, phylogroups are assigned according to the respective SSU variant. For more explanations, see caption for Figure 2c

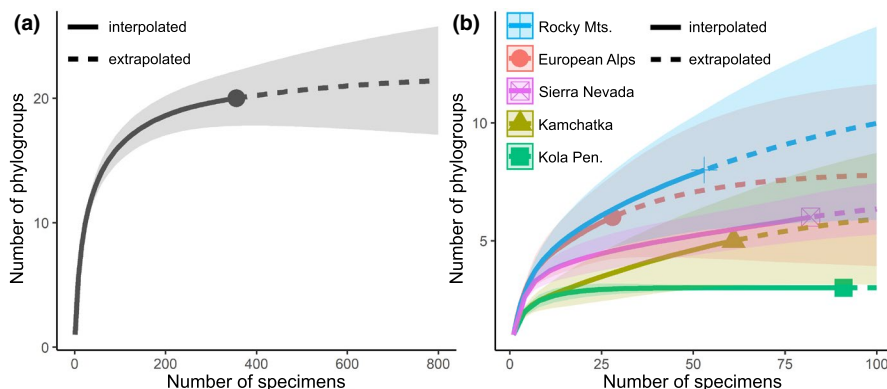


FIGURE 7 Individual-based interpolation (rarefaction) and extrapolation sampling curves for phylogroup richness of the *Ph. albescens*. This graph shows the number of detected (including singletons) and expected phylogroups within the investigated regions. The 95% confidence interval is shown as a transparent area. (a) Curve for the total phylogroup richness. (b) Curves for phylogroup richness in five regions that were sampled most intensively

SSU sequence diversity was expected to be higher in *Hemitrichia serpula*.

3.8 | Small-scale phylogroup distribution

Among the 164 localities of approx. 50 m diam., in 60 localities more than one specimen of *Ph. albescens* was collected. In many cases, specimens from different phylogroups occurred in the same locality: of the 60 localities, 24 (40%) harboured members of two or more different phylogroups (mean 1.53, SD 0.79) (Figure S5). The highest number of phylogroups per locality was found in the Rocky Mts.: up to five in one locality.

4 | DISCUSSION

4.1 | Phylogroups in *Ph. albescens*

We investigated the genetic structure of populations of the nivicolous myxomycete *Physarum albescens* in different mountain ranges of the Northern Hemisphere using three independent genetic markers (SSU, EF1A, COI). With 324 studied specimens, *Ph. albescens* becomes the most extensively sequenced species of myxomycetes to date. The results of our study show an extraordinarily high intraspecific phylogroup diversity that largely exceeds the observed and expected phylogroup diversity in other studied myxomycete species (Figure S6, Table S5). Our main finding is that *Ph. albescens*

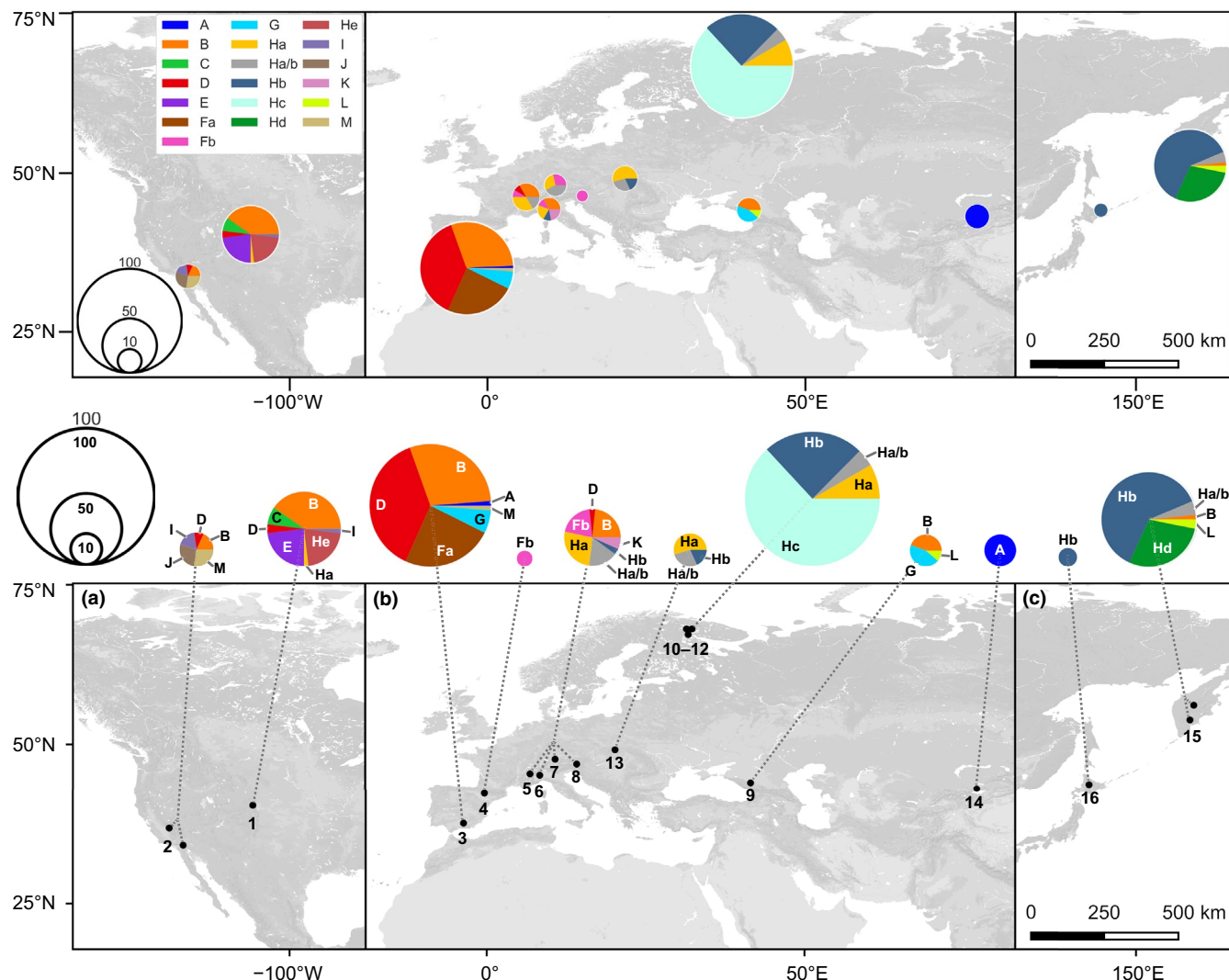


FIGURE 8 Regions sampled for *Ph. albescens*. The circle diameter reflects the number of studied specimens collected from a region. The area of the coloured sectors shows proportions of phylogenetic groups among the specimens collected from a region (see details in the Results section). Specimens sequenced only for SSU and showing sequence variant s21 shared by Ha and Hb are shown in grey. (a) North America (1, Rocky Mts., 2, Angeles National Forest, San Bernardino National Forest, San Jacinto Mt., and Sequoia National Park). (b) Europe (3, Sierra Nevada Mts.; 4, French Pyrenees; 5, French Alps; 6, Italian Alps; 7, German Alps; 8, Slovenian Alps; 9, Northern Caucasus; 10–12, Kola Peninsula: Khibiny Mts., Chunutundra Mts., Luvenka Tundra Mts., 13, Western Carpathians) and Central Asia (14, Ile Alatau Mts.). (c) East Asia (15, Kamchatka; 16, Hokkaido). Maps were produced with QGIS 3.12.1 and Mapbox online service

represents not a single species, but a species complex, since this morphologically defined species splits into at least 18 phylogroups that can be considered as cryptic species. According to the extrapolated diversity estimates, even more phylogroups could be found with an extended sampling. Previous studies reported two to seven large phylogroups (putative cryptic species) per morphospecies in other complexes of myxomycete species (Aguilar et al., 2014; Dagamac et al., 2017; Feng et al., 2016; Feng & Schnittler, 2015; Janik et al., 2020; Novozhilov et al., 2013; Shchepin et al., 2016).

The three-gene data set used here included 302 parsimony-informative variable sites, which allowed to construct a robust phylogeny and a phylogenetic network that, in combination with the analysis of ml-FFRs, showed the separation into 18 phylogroups

(Figures 2b and 3a). Two automatic species delimitation algorithms applied to the three-gene data set (mPTP and ASAP) agreed in delimitation of 13 phylogroups and suggested uniting some of the closely related phylogroups together (Table 1), partly supporting our manual phylogroup delimitation. High-resolution GBS data that were obtained for a subset of samples from seven phylogroups further supported the separation revealed from the three-gene data. Judging by the topology of the phylogenetic tree and network (Figures 3b and 4) and mPTP results for the GBS data (Table 1), it is possible that some of these phylogroups split into even more cryptic species (for example, phylogroup B). We applied here a conservative approach and tried to keep the number of recognized phylogroups to a minimum.

4.2 | Reproductive isolation

In all intensively sampled mountain ranges, members of several different phylogroups of *Ph. albescens* occur together, and even within one locality, two or more phylogroups were often found. However, even though members of different phylogroups may share habitats (Figure S5), they do not exchange genetic information, as seen from the observed combinations of genetic variants in 214 sampled colonies of sporocarps (Figure 2c). This observation supports the hypothesis of reproductive isolation between phylogroups. We consider incomplete lineage sorting or hybridization to be the most probable explanation for the two exceptions (one SSU variant shared by Ha and Hb and one EF1A variant shared by Ha and He). There are three reasons for this: (1) in both cases, these variants are shared by two closely related phylogroups separated by short branches, which is indicative of a recent speciation event, (2) the separation of the phylogroups Ha, Hb, and He is strongly supported by the SNP phylogenies (Figures 3b and 4), and (3) ABBA-BABA tests and *f*-branch statistics indicate a possible gene flow event(s) between the discussed phylogroups. The fact that only two of the eight branches in the input tree for Fbranch showed an excess of shared derived alleles with other branches supports the idea that gene flow is generally restricted even between the most closely related phylogroups.

The computer simulation results showed that the observed numbers of combinations of three genetic variants in populations of *Ph. albescens* from neighbouring valleys in the Khibiny Mts. and the Sierra Nevada were significantly lower than what would be expected for a single randomly sampled panmictic population. Moreover, among the individuals sampled from each of the 1000 replicates of the simulated panmictic populations, 34%–94% of individuals showed “mixed” genotypes consisting of genetic variants from different phylogroups, while such genotypes did not occur in the individuals sampled from the real populations, although the sample size was the same.

Based on the observations listed above and the simulation results, we conclude that the revealed phylogroups of *Ph. albescens* are reproductively isolated from each other, although rare hybridization events between recently diverged phylogroups cannot be excluded. As such, they can be seen as biological species in Mayr's strict sense (1942). In this case, another biological feature, the monophyly of the respective phylogroups, supports this (compare de Queiroz, 2005), but we do not expect to find consistent morphological differences between all phylogroups. The frequent coexistence of different phylogroups (cryptic species) in one region can be explained by sympatric speciation caused by mutations in the mating-type systems or polyploidisation (see review in Clark & Haskins, 2010). Alternatively, the observed phylogroup distribution could have resulted from an allopatric or parapatric speciation followed by range expansion.

4.3 | Mode of reproduction

The reproduction mode of myxomycetes in natural populations has long been in question. Amoebzoa are principally capable of sexual

reproduction (Lahr et al., 2011), but amoebae reproduce as well asexually by cell fission. Although myxomycetes are considered to be predominantly heterothallic sexual organisms, in vitro experiments with several easily cultivable species have shown that at least in culture exceptions do often occur (see discussion in Feng et al., 2016; Walker & Stephenson, 2016).

From the observed pattern of combinations of genetic variants within phylogroups in the current study and the high number of three-marker genotypes found, we can assume that in most lineages from time to time sexual recombination does occur. However, the GBS data show a considerable percentage of specimens of putatively clonal origin, forming 18 putatively clonal groups within six of the seven genotyped phylogroups (Figure 4). The most obvious explanation for this could be the fragmentation of a single plasmodium, with different parts of it moving in different directions and forming genetically identical colonies of sporocarps. However, in 10 of 18 groups, some specimens showing nearly identical genotypes (genetic distance within the range of technical errors) were found on a large distance from the others (240–44,610 m) (Figure 4, Table S3). Moreover, in two cases, members of a putatively clonal group were collected in two different years (2013 and 2015). In such cases, the genotypic identity of different specimens cannot be explained by fragmentation of a single plasmodium, as it can be done for the specimens found in one season in a few metres from each other. In the Sierra Nevada and Khibiny Mts., members of some putatively clonal groups were found in different valleys, so their distribution cannot be explained by a passive drift of pieces of plasmodia with streams of water running down from melting snow patches. This could be a sign of asexual lineages dispersing via airborne spores, as suggested for *Didymium nivicola* (Janik et al., 2020). A second possible explanation (as well speculative) could be that these genetically nearly identical specimens result from repeated mating of a few dominating myxamoebal strains that are widely distributed within a large area and persist from year to year.

Our results demonstrate that sexual and asexual reproduction coexist in natural populations of *Ph. albescens*. Despite these intriguing results, the proportions of sexual and asexual reproduction remain unclear. Crossing experiments or studies of ploidy levels at different life cycle stages could shed light on this question. However, these methods require in vitro cultivation of *Ph. albescens* at least from spore to plasmodium, which we failed to achieve (Shchepin et al., 2014).

4.4 | Geographical distribution

The cryptic species in the *Ph. albescens* complex show well-pronounced phylogeographical patterns (Figure 8). Most of the 18 cryptic species have a limited geographical distribution, and none was found in all of the studied regions. Moreover, some phylogroups were found to be abundant in only one region and totally absent in all other studied regions and thus may represent local endemics. Nevertheless, in most studied regions, several phylogroups coexist

and are often found in one habitat. The observed geographical distribution may be at least partially due to the niche differentiation among the members of the *Ph. albescens* complex (hypothesis not tested herein). The presence of niche differentiation between closely related cryptic species was demonstrated previously for *Badhamia melanospora* and *Hemitrichia serpula* using environmental niche modeling (Aguilar et al., 2014; Dagamac et al., 2017).

While reports of *Ph. albescens* from the Southern Hemisphere are rare, the largest observed and predicted phylogroup diversity in the Northern Hemisphere is recorded from the Rocky Mts., which may represent the centre of diversity for this species complex. However, since other mountains in North America are sampled poorly or not sampled at all, the real centre of diversity can be somewhere else on this continent.

4.5 | Resolution of SSU barcoding

Species determination based on the similarity of short nucleotide sequences to references (DNA barcoding) is becoming a widely used method in myxomycete research. Here, with only one exception (SSU variant 21 shared by Ha and Hb), a partial SSU sequence is sufficient to unambiguously classify a herbarium specimen of *Ph. albescens* as belonging to a particular phylogroup. However, in environmental DNA studies, sequences are usually clustered prior to taxonomic assignment to reduce sequencing noise. Several different similarity thresholds were applied previously for the determination of myxomycete species in SSU-based DNA barcoding studies and clustering OTUs in metabarcoding studies: (1) 99.1% (Borg Dahl et al., 2019; Borg Dahl, Brejnrod, et al., 2018; Borg Dahl, Shchepin, et al., 2018; Shchepin et al., 2017, 2019), (2) 98% (Clissmann et al., 2015; Gao et al., 2019; Kamono et al., 2013; Shchepin et al., 2019), (3) 97% (Fiore-Donno et al., 2016), and (4) 96% (Kamono et al., 2013). We have evaluated the ability of the two more popular similarity thresholds (98% and 99.1%) to differentiate between the cryptic species within *Ph. albescens*.

With a 98% similarity threshold, the species complex split into ten clusters, six of them containing sequences of more than one phylogroup. The 99.1% similarity threshold showed better results: 13 cryptic species and both singleton phylogroups could be separated, and only two clusters included more than one phylogroup (in both cases, they united closely related phylogroups within clades F and H).

However, none of the two thresholds can differentiate all 18 cryptic species. This can present a serious limitation for the barcoding-based identification of environmental sequences due to two reasons: (1) in DNA metabarcoding studies, usually only one genetic marker is sequenced. Thus, the taxonomic resolution cannot be increased by the analysis of additional genes; even if two or more different gene markers are sequenced from the same environmental sample, it can often be impossible to show that two sequences of different genes originate from the same species; (2) environmental sequencing data are inherently noisy due to PCR artifacts and high

error rates of the high-throughput sequencing platforms, thus clustering at thresholds higher than 98% may lead to a high number of erroneous OTUs. In comparison, lower thresholds would lump even more species together into one OTU. In a DNA metabarcoding study based on OTUs, the phylogroup Hc from the Kola Peninsula would not differ from Hb distributed over Eurasia and from Ha, which occurs in Europe and North America; Fa from Sierra Nevada would form one OTU with Fb from European Alps and Pyrenees. A possible solution could be the use of amplicon sequence variants (ASVs) instead of OTUs. ASVs represent every unique biological sequence in the analysed sample (Callahan et al., 2017). This approach could increase the taxonomic resolution of the amplicon-based eDNA studies, but very stringent data filtering is required to reduce sequencing noise. However, even the use of ASVs in some cases would not help to differentiate between SSU sequences of the phylogroups Ha and Hb due to the presence of at least one shared SSU sequence variant. In contrast, COI sequences are unique for each of the 18 phylogroups and more genetically diverse, and could potentially serve as DNA barcodes with better resolution than SSU sequences. COI has been promoted as a barcode for metazoans since the very appearance of the concept of DNA barcoding (Hebert et al., 2003). Later this gene was shown to be a more suitable barcode than SSU for different groups of protists, including some members of Amoebozoa (Nassonova et al., 2010; Zlatogursky et al., 2016) and SAR (Heger et al., 2011; Zhao et al., 2016). Taxonomic resolution and convenience of COI as a DNA barcode for myxomycetes needs to be tested on a broader taxon sample.

5 | CONCLUSIONS

Although the nivicolous myxomycete *Ph. albescens* seems to have a cosmopolitan distribution over the mountains of the Northern Hemisphere, our results demonstrate that it represents a complex of at least 18 cryptic species, each of them showing a much narrower distribution than the morphospecies as a whole. This again challenges the ubiquity hypothesis for myxomycetes and supports the moderate endemism hypothesis. Despite the fact that members of different phylogroups co-occur in most of the studied regions and many microhabitats, our data suggest that introgression events between phylogroups, if they happen, should be rare and occur mostly between recently diverged phylogroups.

On the one hand, such patterns of multiple cryptic species within morphospecies seem to be common in myxomycetes and may represent a general mode of evolution in this group: all hitherto investigated morphospecies turned out to be complexes of several cryptic species (Aguilar et al., 2014; Dagamac et al., 2017; Feng & Schnittler, 2015; Janik et al., 2020; Leontyev et al., 2015; Shchepin et al., 2016). This means that we should expect the real number of myxomycete species to be several times bigger than c. 1050 currently recognized species (Lado, 2005–2021). Further efforts should be made to identify cryptic species within other myxomycete species and their geographical distribution, to find new morphological

traits that could help to differentiate between them, and to test for the presence of niche differentiation between members of cryptic species complexes. This data would allow us to better estimate the total expected myxomycete species diversity and to re-evaluate our knowledge on ecology and distribution of some presumably ubiquitous morphospecies.

On the other hand, the presence of groups of presumably clonal specimens together with a high genotypic diversity within phylogroups suggests that sexual and asexual reproduction coexist in natural populations of *Ph. albescens*. This conclusion is consistent with the results of crossing experiments conducted for other species of myxomycetes, which revealed a frequent occurrence of apomictic strains, including facultatively apomictic ones (Clark & Haskins, 2013). If the presence of apomictic strains among sexual strains is usual in myxomycetes, this makes species delimitation and interpretation of species-level ecological data even more complicated.

In addition, it should be pointed out that SSU barcode proved to lack resolution in some cases to differentiate some closely related phylogroups in *Ph. albescens*. Since COI showed a better resolution in current study, it should be evaluated on a broader sample of taxa as a possibly better DNA barcode for myxomycetes.

The large cryptic diversity and biogeographical patterns revealed for *Ph. albescens* are consistent with the presence of multiple cryptic species with restricted distribution found for other soil-inhabiting protists as different as diatoms, streptophyte algae, and testate amoebae (Pinseel et al., 2020; Ryšánek et al., 2015; Singer et al., 2019). It seems possible that these patterns of diversity and distribution can be universal for soil-inhabiting protists. Further research on soil protist diversity and biogeography is essential to estimate the number of endemic protist species and their ability to persist in changing environments.

ACKNOWLEDGEMENTS

This research was funded by the the German Research Council (DFG: SCHN1080/2-1, RTG 2010 RESPONSE) and the state task of the Komarov Botanical Institute RAS "Biodiversity, ecology, structural and functional features of fungi and fungus-like protists" (AAAA-A19-119020890079-6). The work was partially performed under the Agreement with the Ministry of Science and Higher Education of the Russian Federation on the provision of a grant from the federal budget in the form of a subsidy No. 075-15-2021-1056. The authors are grateful to Ángela López-Villalba, Anna Ronikier, Daria Erastova, Gabriel Moreno, Marianne Meyer, Paulina Janik, Renato Cainelli, and other researchers for sharing specimens, sequences, photos, and expertise. We thank Anja Klahr for help with sequencing. MBD thanks Prof. Steven K. Schmidt, Prof. William Bowman and MSc Adam Solon for hosting, providing access to field sites and help during the field collection in the Rocky Mountains. We acknowledge the use of equipment of the Core Facility Center 'Cell and Molecular Technologies in Plant Science' at the Komarov Botanical Institute RAS (St. Petersburg). Open access funding enabled and organized by ProjektDEAL.

AUTHOR CONTRIBUTIONS

OS, YN and MS designed the study. OS, YN, JW, IP, NF, VG, MBD, NHAD, YY and MS collected samples. OS, MBD, NHAD, MS, IP and NF acquired sequencing data. OS, MB and NHAD prepared samples for GBS. OS performed all bioinformatic analyses. OS, YN and MS wrote the manuscript. All authors edited and approved the final manuscript.

CONFLICT OF INTEREST

The authors declare that they have no conflict of interest.

DATA AVAILABILITY STATEMENT

The GBS data: NCBI Sequence Read Archive BioProject PRJNA706537 (Shchepin et al., 2021). DNA sequences: GenBank accessions MW691477–MW691847, MW692988–MW693025, MW701443–MW701877. Sequence alignments are included in the supplementary materials (Additional files 1–4). Information on studied samples and collection sites is included in the supplementary materials (Additional file 6). Source code for the program visualizing recombination patterns: https://github.com/Gurdhhu/recombination_graph. Source code for the computer simulation: https://github.com/Gurdhhu/recombination_simulation.

ORCID

Oleg Shchepin  <https://orcid.org/0000-0001-9327-7655>

REFERENCES

- Aguilar, M., Fiore-Donno, A. M., Lado, C., & Cavalier-Smith, T. (2014). Using environmental niche models to test the 'everything is everywhere' hypothesis for *Badhamia*. *The ISME Journal*, 8, 737–745. <https://doi.org/10.1038/ismej.2013.183>
- Borg Dahl, M., Brejnrod, A. D., Russel, J., Sørensen, S. J., & Schnittler, M. (2019). Different degrees of niche differentiation for bacteria, fungi, and myxomycetes within an elevational transect in the German Alps. *Microbial Ecology*, 78(3), 764–780. <https://doi.org/10.1007/s00248-019-01347-1>
- Borg Dahl, M., Brejnrod, A. D., Unterseher, M., Hoppe, T., Feng, Y., Novozhilov, Y., Sørensen, S. J., & Schnittler, M. (2018). Genetic barcoding of dark-spored myxomycetes (Amoebozoa) – Identification, evaluation and application of a sequence similarity threshold for species differentiation in NGS studies. *Molecular Ecology Resources*, 18(2), 306–318. <https://doi.org/10.1111/1755-0998.12725>
- Borg Dahl, M., Shchepin, O. N., Schunk, C., Menzel, A., Novozhilov, Y. K., & Schnittler, M. (2018). A four year survey reveals a coherent pattern between occurrence of fruit bodies and soil amoebae populations for nivicolous myxomycetes. *Scientific Reports*, 8, 11662. <https://doi.org/10.1038/s41598-018-30131-3>
- Bryant, D., & Moulton, V. (2004). Neighbor-net: An agglomerative method for the construction of phylogenetic networks. *Molecular Biology and Evolution*, 21(2), 255–265. <https://doi.org/10.1093/molbev/msh018>
- Callahan, B., McMurdie, P., & Holmes, S. (2017). Exact sequence variants should replace operational taxonomic units in marker-gene data analysis. *The ISME Journal*, 11, 2639–2643. <https://doi.org/10.1038/ismej.2017.119>
- Chao, A., Gotelli, N. J., Hsieh, T. C., Sander, E. L., Ma, K. H., Colwell, R. K., & Ellison, A. M. (2014). Rarefaction and extrapolation with Hill numbers: A framework for sampling and estimation in species

- diversity studies. *Ecological Monographs*, 84(1), 45–67. <https://doi.org/10.1890/13-0133.1>
- Chao, A., & Jost, L. (2012). Coverage-based rarefaction and extrapolation: Standardizing samples by completeness rather than size. *Ecology*, 93(12), 2533–2547. <https://doi.org/10.1890/11-1952.1>
- Chernomor, O., von Haeseler, A., & Minh, B. Q. (2016). Terrace aware data structure for phylogenomic inference from supermatrices. *Systematic Biology*, 65(6), 997–1008. <https://doi.org/10.1093/sysbio/syw037>
- Clark, J., & Haskins, E. F. (2010). Reproductive systems in the myxomycetes: A review. *Mycosphere*, 1, 337–353.
- Clark, J., & Haskins, E. F. (2013). The nuclear reproductive cycle in the myxomycetes: A review. *Mycosphere*, 4, 233–248. <https://doi.org/10.5943/mycosphere/4/2/6>
- Clissmann, F., Fiore-Donno, A. M., Hoppe, B., Krüger, D., Kahl, T., Unterseher, M., & Schnittler, M. (2015). First insight into dead wood protistean diversity: A molecular sampling of bright-spored Myxomycetes (Amoebozoa, slime moulds) in decaying beech logs. *FEMS Microbiology Ecology*, 91(6), fiv050.
- Dagamac, N. H. A., Rojas, C., Novozhilov, Y. K., Moreno, G. H., Schlueter, R., & Schnittler, M. (2017). Speciation in progress? A phylogeographic study among populations of *Hemitrichia serpula* (Myxomycetes). *PLoS One*, 12(4), e0174825. <https://doi.org/10.1371/journal.pone.0174825>
- De Queiroz, K. (2005). Ernst Mayr and the modern concept of species. *Proceedings of the National Academy of Sciences*, 102, 6600–6607. <https://doi.org/10.1073/pnas.0502030102>
- Doyle, J. J. (1995). The irrelevance of allele tree topologies for species delimitation, and a non-topological alternative. *Systematic Botany*, 20, 574–588. <https://doi.org/10.2307/2419811>
- Dress, A. W. M., & Huson, D. H. (2004). Constructing splits graphs. *IEEE/ACM Transactions on Computational Biology and Bioinformatics*, 1(3), 109–115. <https://doi.org/10.1109/TCBB.2004.27>
- Eaton, D., & Overcast, I. (2020). ipyrad: Interactive assembly and analysis of RADseq datasets. *Bioinformatics (Oxford, England)*, 36(8), 2592–2594. <https://doi.org/10.1093/bioinformatics/btz966>
- Feng, Y., Klahr, A., Janik, P., Ronikier, A., Hoppe, T., Novozhilov, Y. K., & Schnittler, M. (2016). What an intron may tell: Several sexual bio-species coexist in *Meriderma* spp. (Myxomycetes). *Protist*, 167(3), 234–253. <https://doi.org/10.1016/j.protis.2016.03.003>
- Feng, Y., & Schnittler, M. (2015). Sex or no sex? Independent marker genes and group I introns reveal the existence of three sexual but reproductively isolated biospecies in *Trichia varia* (Myxomycetes). *Organisms Diversity & Evolution*, 15, 631–650.
- Ferris, P. J., Vogt, V. M., & Truitt, C. L. (1983). Inheritance of extrachromosomal rDNA in *Physarum polycephalum*. *Molecular and Cellular Biology*, 3(4), 635–642. <https://doi.org/10.1128/mcb.3.4.635>
- Fiore-Donno, A. M., Kamono, A., Meyer, M., Schnittler, M., Fukui, M., & Cavalier-Smith, T. (2012). 18S rDNA phylogeny of *Lamproderma* and allied genera (Stemonitidales, Myxomycetes, Amoebozoa). *PLoS One*, 7(4), e35359.
- Fiore-Donno, A. M., Meyer, M., Baldauf, S. L., & Pawlowski, J. (2008). Evolution of dark-spored Myxomycetes (slime molds): Molecules versus morphology. *Molecular Phylogenetics and Evolution*, 46, 878–889. <https://doi.org/10.1016/j.ympev.2007.12.011>
- Fiore-Donno, A. M., Weinert, J., Wubet, T., & Bonkowski, M. (2016). Metacommunity analysis of amoeboid protists in grassland soils. *Scientific Reports*, 11(6), 19068. <https://doi.org/10.1038/srep19068>
- Flot, J. F., Couloux, A., & Tillier, S. (2010). Haplowebs as a graphical tool for delimiting species: A revival of Doyle's "field for recombination" approach and its application to the coral genus *Pocillopora* in Clipperton. *BMC Evolutionary Biology*, 10, 372. <https://doi.org/10.1186/1471-2148-10-372>
- Foissner, W. (2008). Protist diversity and distribution: Some basic considerations. *Biodiversity and Conservation*, 17, 235–242. <https://doi.org/10.1007/s10531-007-9248-5>
- Gao, Y., Zhang, X., He, G., Shchepin, O. N., Yan, S., & Chen, S. (2019). Influence of forest type on dark-spored myxomycete community in subtropical forest soil, China. *Soil Biology and Biochemistry*, 139, 107606. <https://doi.org/10.1016/j.soilbio.2019.107606>
- Geisen, S., Lara, E., Mitchell, E. A., Völcker, E., & Krashevska, V. (2020). Soil protist life matters! *Soil Organisms*, 92(3), 189–196. <https://doi.org/10.25674/so92iss3pp189>
- Hall, T. A. (1999). BioEdit: A user-friendly biological sequence alignment editor and analysis program for Windows 95/98/NT. *Nucleic Acids Symposium Series*, 41, 95–98.
- Hamming, R. W. (1950). Error detecting and error correcting codes. *Bell System Technical Journal*, 29(2), 147–160. <https://doi.org/10.1002/j.1538-7305.1950.tb00463.x>
- Hebert, P. D. N., Cywinska, A., Ball, S. L., & DeWaard, J. R. (2003). Biological identifications through DNA barcodes. *Philosophical Transactions of the Royal Society B: Biological Sciences*, 270(1512), 313–321.
- Heger, T. J., Pawlowski, J., Lara, E., Leander, B. S., Todorov, M., Golemansky, V., & Mitchell, E. A. (2011). Comparing potential COI and SSU rDNA barcodes for assessing the diversity and phylogenetic relationships of cyphoderiid testate amoebae (Rhizaria: Euglyphida). *Protist*, 162(1), 131–141. <https://doi.org/10.1016/j.protis.2010.05.002>
- Hoppe, T., & Schnittler, M. (2015). Characterization of myxomycetes in two different soils by TRFLP analysis of partial 18S rRNA gene sequences. *Mycosphere*, 6(2), 216–227. <https://doi.org/10.5943/mycosphere/6/2/11>
- Hsieh, T. C., Ma, K. H., & Chao, A. (2016). iNEXT: An R package for rarefaction and extrapolation of species diversity (Hill numbers). *Methods in Ecology and Evolution*, 7, 1451–1456.
- Huelsenbeck, J. P., & Ronquist, F. (2001). MrBayes: Bayesian inference of phylogenetic trees. *Bioinformatics*, 17(8), 754–755. <https://doi.org/10.1093/bioinformatics/17.8.754>
- Huson, D. H. (1998). SplitsTree: Analyzing and visualizing evolutionary data. *Bioinformatics (Oxford, England)*, 14(1), 68–73. <https://doi.org/10.1093/bioinformatics/14.1.68>
- Huson, D. H., & Bryant, D. (2006). Application of phylogenetic networks in evolutionary studies. *Molecular Biology and Evolution*, 23, 254–267. <https://doi.org/10.1093/molbev/msj030>
- Janik, P., Lado, C., & Ronikier, A. (2020). Range-wide phylogeography of a nivicolous protist *Didymium nivicola* Meyl. (Myxomycetes, Amoebozoa): Striking contrasts between the Northern and the Southern Hemisphere. *Protist*, 171, 125771.
- Kalyanamoorthy, S., Minh, B. Q., Wong, T. K. F., von Haeseler, A., & Jermini, L. S. (2017). ModelFinder: Fast model selection for accurate phylogenetic estimates. *Nature Methods*, 14(6), 587–589. <https://doi.org/10.1038/nmeth.4285>
- Kamono, A., Kojima, H., Matsumoto, J., Kawamura, K., & Fukui, M. (2009). Airborne myxomycete spores: Detection using molecular techniques. *Naturwissenschaften*, 96, 147–151. <https://doi.org/10.1007/s00114-008-0454-0>
- Kamono, A., Meyer, M., Cavalier-Smith, T., Fukui, M., & Fiore-Donno, A. M. (2013). Exploring slime mould diversity in high-altitude forests and grasslands by environmental RNA analysis. *FEMS Microbiology Ecology*, 94, 98–109. <https://doi.org/10.1111/1574-6941.12042>
- Kapli, T., Lutteropp, S., Zhang, J., Kobert, K., Pavlidis, P., Stamatakis, A., & Flouri, T. (2017). Multi-rate Poisson tree processes for single-locus species delimitation under maximum likelihood and Markov chain Monte Carlo. *Bioinformatics*, 33(11), 1630–1638. <https://doi.org/10.1093/bioinformatics/btx025>
- Katoh, K., Kuma, K., Toh, H., & Miyata, T. (2005). MAFFT version 5: Improvement in accuracy of multiple sequence alignment. *Nucleic Acids Research*, 33, 511–518. <https://doi.org/10.1093/nar/gki198>
- Katoh, K., Rozewicki, J., & Yamada, K. D. (2019). MAFFT online service: Multiple sequence alignment, interactive sequence choice and

- visualization. *Briefings in Bioinformatics*, 20(4), 1160–1166. <https://doi.org/10.1093/bib/bbx108>
- Kumar, S., Stecher, G., Li, M., Knyaz, C., & Tamura, K. (2018). MEGA X: Molecular Evolutionary Genetics Analysis across computing platforms. *Molecular Biology and Evolution*, 35, 1547–1549. <https://doi.org/10.1093/molbev/msy096>
- Lado, C. (2005–2021). *NomenMyx: An on line nomenclatural information system of Eumycetozoa* [Electronic database]. Retrieved from <http://www.nomen.eumycetozoa.com>
- Lahr, D. J. G., Parfrey, L. W., Mitchell, E. A., Katz, L. A., & Lara, E. (2011). The chastity of amoebae: Re-evaluating evidence for sex in amoeboid organisms. *Proceedings of the Royal Society B*, 278, 2081–2090. <https://doi.org/10.1098/rspb.2011.0289>
- Leontyev, D., Schnittler, M., & Stephenson, S. L. (2015). A critical revision of the *Tubifera ferruginosa*-complex. *Mycologia*, 107, 959–985.
- Liu, Q. S., Yan, S. Z., & Chen, S. L. (2015). Further resolving the phylogeny of Myxogastria (slime molds) based on COI and SSU rRNA genes. *Russian Journal of Genetics*, 51, 46–53. <https://doi.org/10.1134/S1022795414110076>
- Malinsky, M., Matschiner, M., & Svardal, H. (2021). Dsuite - Fast D-statistics and related admixture evidence from VCF files. *Molecular Ecology Resources*, 21(2), 584–595. <https://doi.org/10.1111/1755-0998.13265>
- Malinsky, M., Svardal, H., Tyers, A. M., Miska, E. A., Genner, M. J., Turner, G. F., & Durbin, R. (2018). Whole-genome sequences of Malawi cichlids reveal multiple radiations interconnected by gene flow. *Nature Ecology & Evolution*, 2(12), 1940–1955. <https://doi.org/10.1038/s41559-018-0717-x>
- Mann, D. G., & Vanormelingen, P. (2013). An inordinate fondness? The number, distributions, and origins of diatom species. *The Journal of Eukaryotic Microbiology*, 60(4), 414–420. <https://doi.org/10.1111/jeu.12047>
- Mayr, E. (1942). *Systematics and the origin of species*. Colombia University Press.
- Miller, M. A., Pfeiffer, W., & Schwartz, T. (2010). Creating the CIPRES Science Gateway for inference of large phylogenetic trees. In *Proceedings of the Gateway Computing Environments Workshop (GCE)* (pp. 1–8).
- Minh, B. Q., Nguyen, M. A., & von Haeseler, A. (2013). Ultrafast approximation for phylogenetic bootstrap. *Molecular Biology and Evolution*, 30(5), 1188–1195. <https://doi.org/10.1093/molbev/mst024>
- Nassonova, E., Smirnov, A., Fahrni, J., & Pawlowski, J. (2010). Barcoding amoebae: Comparison of SSU, ITS and COI genes as tools for molecular identification of naked lobose amoebae. *Protist*, 161(1), 102–115. <https://doi.org/10.1016/j.protis.2009.07.003>
- Novozhilov, Y. K., Mitchell, D. W., Okun, M. V., & Shchepin, O. N. (2014). New species of *Diderma* from Vietnam. *Mycosphere*, 5, 554–564. <https://doi.org/10.5943/mycosphere/5/4/8>
- Novozhilov, Y. K., Okun, M. V., Erastova, D. A., Shchepin, O. N., Zemlyanskaya, I. V., García-Carvajal, E., & Schnittler, M. (2013). Description, culture and phylogenetic position of a new xerotolerant species of *Physarum*. *Mycologia*, 105(6), 1535–1546. <https://doi.org/10.3852/12-284>
- Novozhilov, Y. K., Prikhodko, I. S., & Shchepin, O. N. (2019). A new species of *Diderma* from Bidoup Nui Ba national park (southern Vietnam). *Protistology*, 13, 126–132. <https://doi.org/10.21685/1680-0826-2019-13-3-2>
- Pinseel, E., Janssens, S. B., Verleyen, E., Vanormelingen, P., Kohler, T. J., Biersma, E. M., Sabbe, K., Van de Vijver, B., & Vyverman, W. (2020). Global radiation in a rare biosphere soil diatom. *Nature Communications*, 11(1), 2382. <https://doi.org/10.1038/s41467-020-16181-0>
- Puillandre, N., Brouillet, S., & Achaz, G. (2021). ASAP: Assemble species by automatic partitioning. *Molecular Ecology Resources*, 21(2), 609–620. <https://doi.org/10.1111/1755-0998.13281>
- Rognes, T., Flouri, T., Nichols, B., Quince, C., & Mahé, F. (2016). VSEARCH: A versatile open source tool for metagenomics. *PeerJ*, 4, e2584. <https://doi.org/10.7717/peerj.2584>
- Ronikier, A., & Ronikier, M. (2009). How 'alpine' are nivicolous myxomycetes? A worldwide assessment of altitudinal distribution. *Mycologia*, 101(1), 1–16. <https://doi.org/10.3852/08-090>
- Ryšánek, D., Hřčková, K., & Škaloud, P. (2015). Global ubiquity and local endemism of free-living terrestrial protists: Phylogeographic assessment of the streptophyte alga *Klebsormidium*. *Environmental Microbiology*, 17(3), 689–698.
- Schnittler, M., Dagamac, N. H. A., Woyzichowski, J., & Novozhilov, Y. K. (2021). Biogeographical patterns in myxomycetes. In S. L. Stephenson, & C. Rojas (Eds.), *Myxomycetes. Biology, systematics, biogeography and ecology* (2nd ed., pp. 377–416). Elsevier, Academic Press.
- Schnittler, M., Erastova, D. A., Shchepin, O. N., Heinrich, E., & Novozhilov, Y. K. (2015). Four years in the Caucasus – Observations on the ecology of nivicolous myxomycetes. *Fungal Ecology*, 14, 105–115. <https://doi.org/10.1016/j.funeco.2015.01.003>
- Schnittler, M., Shchepin, O. N., Dagamac, N. H. A., Borg Dahl, M., & Novozhilov, Y. K. (2017). Barcoding myxomycetes with molecular markers: Challenges and opportunities. *Nova Hedwigia*, 104, 323–341. https://doi.org/10.1127/nova_hedwigia/2017/0397
- Shchepin, O. N. (2021a, March 21). Visualization of recombination patterns [Source code]. https://github.com/Gurdhhu/recombination_graph
- Shchepin, O. N. (2021b, March 21). Recombination simulation [Source code]. https://github.com/Gurdhhu/recombination_simulation
- Shchepin, O. N., Dagamac, N. H., Sanchez, O. M., Novozhilov, Y. K., Schnittler, M., & Zemlyanskaya, I. V. (2017). DNA barcoding as a tool for identification of plasmodia and sclerotia of myxomycetes (*Myxogastria*) appearing in moist chamber cultures. *Mycosphere*, 8(10), 1904–1913. <https://doi.org/10.5943/mycosphere/8/10/13>
- Shchepin, O. N., Novozhilov, Y. K., & Schnittler, M. (2014). Nivicolous myxomycetes in agar culture: Some results and open problems. *Protistology*, 8(2), 53–61.
- Shchepin, O. N., Novozhilov, Y. K., & Schnittler, M. (2016). Disentangling the taxonomic structure of the *Lepidoderma chailletii-carestianum* species complex (*Myxogastria*, Amoebozoa): Genetic and morphological aspects. *Protistology*, 10(4), 117–129. <https://doi.org/10.21685/1680-0826-2016-10-4-1>
- Shchepin, O. N., Novozhilov, Y. K., Woyzichowski, J., Bog, M., Prikhodko, I. S., Fedorova, N. A., & Schnittler, M. (2021). GBS data for herbarium specimens of a myxomycete *Physarum albescens*. *NCBI Sequence Read Archive. BioProject PRJNA706537*.
- Shchepin, O. N., Schnittler, M., Erastova, D. A., Prikhodko, I. S., Borg Dahl, M., Azarov, D. V., Chernyaeva, E. N., & Novozhilov, Y. K. (2019). Community of dark-spored myxomycetes in ground litter and soil of taiga forest (Nizhne-Svirskiy Reserve, Russia) revealed by DNA metabarcoding. *Fungal Ecology*, 39, 80–93. <https://doi.org/10.1016/j.funeco.2018.11.006>
- Silliker, M. E., & Collins, O. R. (1988). Non-mendelian inheritance of mitochondrial DNA and ribosomal DNA in the myxomycete, *Didymium iridis*. *Molecular & General Genetics*, 213(2–3), 370–378. <https://doi.org/10.1007/BF00339605>
- Silliker, M. A., Liles, J. L., & Monroe, J. A. (2002). Patterns of mitochondrial inheritance in the myxogastriid, *Didymium iridis*. *Mycologia*, 94, 939–946. <https://doi.org/10.2307/3761862>
- Singer, D., Mitchell, E. A. D., Payne, R. J., Blandenier, Q., Duckert, C., Fernández, L. D., Fournier, B., Hernández, C. E., Granath, G., Rydin, H., Bragazza, L., Koronatova, N. G., Goia, I., Harris, L. I., Kajukalo, K., Kosakyan, A., Lamentowicz, M., Kosykh, N. P., Vellak, K., & Lara, E. (2019). Dispersal limitations and historical factors determine the biogeography of specialized terrestrial

- protists. *Molecular Ecology*, 28(12), 3089–3100. <https://doi.org/10.1111/mec.15117>
- Trifinopoulos, J., Nguyen, L. T., von Haeseler, A., & Minh, B. Q. (2016). W-IQ-TREE: A fast online phylogenetic tool for maximum likelihood analysis. *Nucleic Acids Research*, 44(W1), W232–W235. <https://doi.org/10.1093/nar/gkw256>
- Walker, L. M., & Stephenson, S. L. (2016). The species problem in myxomycetes revisited. *Protist*, 167(4), 319–338. <https://doi.org/10.1016/j.protis.2016.05.003>
- Warren, D. L., Geneva, A. J., & Lanfear, R. (2017). RWTY (R We There Yet): An R package for examining convergence of Bayesian phylogenetic analyses. *Molecular Biology and Evolution*, 34(4), 1016–1020. <https://doi.org/10.1093/molbev/msw279>
- Zhao, Y., Yi, Z., Gentekaki, E., Zhan, A., Al-Farraj, S. A., & Song, W. B. (2016). Utility of combining morphological characters, nuclear and mitochondrial genes: An attempt to resolve the conflicts of species identification for ciliated protists. *Molecular Phylogenetics and Evolution*, 94(Pt B), 718–729. <https://doi.org/10.1016/j.ympev.2015.10.017>
- Zlatogursky, V. V., Kudryavtsev, A., Udalov, I. A., Bondarenko, N., Pawlowski, J., & Smirnov, A. (2016). Genetic structure of a morphological species within the amoeba genus *Korotnevella* (Amoebozoa:

Discosea), revealed by the analysis of two genes. *European Journal of Protistology*, 56, 102–111. <https://doi.org/10.1016/j.ejop.2016.08.001>

SUPPORTING INFORMATION

Additional supporting information may be found in the online version of the article at the publisher's website.

How to cite this article: Shchepin, O., Novozhilov, Y., Woyzichowski, J., Bog, M., Prihodko, I., Fedorova, N., Gmshinskiy, V., Borg Dahl, M., Dagamac, N. H. A., Yajima, Y., & Schnittler, M. (2022). Genetic structure of the protist *Physarum albescens* (Amoebozoa) revealed by multiple markers and genotyping by sequencing. *Molecular Ecology*, 31, 372–390. <https://doi.org/10.1111/mec.16239>

3.2 Where do nivicolous myxomycetes occur? – Modeling the potential worldwide distribution of *Physarum albescens*

Nikki Heherson A.Dagamac^{ab}, BarbaraBauer^a, JanWoyzichowski^a, Oleg N.Shchepin^{ac}, Yuri K.Novozhilov^c, MartinSchnittler^a

^aInstitute of Botany and Landscape Ecology, University of Greifswald, Soldmannstr. 15, D-17489, Greifswald, Germany

^bDepartment of Biological Sciences and Research Center for the Natural and Applied Sciences, University of Santo Tomas, España, 1008, Manila, Philippines

^cKomarov Botanical Institute of the Russian Academy of Sciences, Prof. Popov Str. 2, 197376, St. Petersburg, Russia

Corresponding author:

Nikki Heherson A.Dagamac Institute of Botany and Landscape Ecology, University of Greifswald, Soldmannstr. 15, D-17489, Greifswald, Germany.

Email address: nhadagamac@gmail.com

Manuscript published 11 June 2021 in *Fungal Ecology*.



Where do nivicolous myxomycetes occur? – Modeling the potential worldwide distribution of *Physarum albescens*

Nikki Heherson A. Dagamac^{a,b,*}, Barbara Bauer^a, Jan Woyzichowski^a, Oleg N. Shchepin^{a,c}, Yuri K. Novozhilov^c, Martin Schnittler^a

^a Institute of Botany and Landscape Ecology, University of Greifswald, Soldmannstr. 15, D-17489, Greifswald, Germany

^b Department of Biological Sciences and Research Center for the Natural and Applied Sciences, University of Santo Tomas, España, 1008, Manila, Philippines

^c Komarov Botanical Institute of the Russian Academy of Sciences, Prof. Popov Str. 2, 197376, St. Petersburg, Russia

ARTICLE INFO

Corresponding Editor: Yu Fukasawa

Keywords:

Biogeography

Dispersal

Protists

Species distribution modeling

Slime molds

ABSTRACT

To identify potentially suitable areas for the mostly alpine ecological guild of nivicolous (snowbank) myxomycetes, the worldwide distribution of a distinct morphospecies, *Physarum albescens*, was modelled with a correlative spatial approach using the software MaxEnt from 537 unique occurrence points. Three models were developed, first with only the 19 bioclimatic variables plus elevation from the WorldClim database, second with regularization to correct for pseudo-absence, and third with additional categorical environmental layer on snow cover. All three models showed high mean AUC (area under the curve) values (>0.970). Output maps were comparable, with the third model perhaps the most realistic. For this model, *snow cover*, *precipitation of the coldest quarter* (of the year), and *elevation* predicted best the distribution of *Ph. albescens*. Elevation alone is a good predictor only in some regions, since (i) elevation of the occurrence points decreases with increasing latitude, and (ii) elevation wrongly predicts the species' occurrence in arid mountain ranges. The model showed mountains in humid climates with highest incidence, which confirmed field studies: a long-lasting snow cover fluctuating with comparatively mild summers is the decisive factor. As such, the model can serve as a predictive map where fructifications of nivicolous myxomycetes can be expected. Limitations of the model are discussed: cryptic speciation within a morphospecies, including the evolution of reproductively isolated units which may lead to local adaptation and niche differentiation, and wider ranges for myxamoebal populations.

1. Introduction

Among protists, myxomycetes (Amoebozoa) are one of the few exceptions from an entirely microbial life style: they form macroscopically visible fruit bodies which are comparatively easy to detect that release airborne spores (Stephenson and Schnittler 2017). The group includes slightly over 1000 formally named species (see Lado, 2005–2021 for species names mentioned herein) delimited upon morphological characters of the fructifications. These can be stored as herbarium specimens, which led to a solid body of data on the distribution of species (Stephenson et al., 2008) within distinct communities across terrestrial habitats (Novozhilov et al., 2017a; Schnittler et al., 2017). As such, they are directly observable but will be detected usually only by a few specialists working with this group. This calls for the application of species distribution models (SDMs) to estimate their potential geographic distribution, although species persistence times (which can critically

influence the correctness of this approach, Suweis et al., 2012) are not yet known, since only the fructifications are observable. However, studies of other ephemeral organisms like fungi (*Phellinus* sp., Yuan et al., 2015), protosteloid amoebae (Aguilar and Lado 2012) or marine ciliates (Williams et al., 2018) have shown that SDM give meaningful results.

Myxomycetes are assumed to be capable of long-distance dispersal (Kamono et al., 2009), a feature that suits SDMs, since they do not account for dispersal barriers by default. Even small habitat sections, so-called microhabitats, are sufficient to sustain an amoebal population. Prominent examples are floricolous myxomycetes (inhabiting inflorescences; Schnittler and Stephenson 2002; Rojas et al., 2017), or epiphyllous myxomycetes (inhabiting liverworts and lichens covering living leaves of understory woody plants in tropical regions; Schnittler 2001; Schnittler et al., 2002; Stephenson et al., 2004). These microhabitats, constituting a small piece of substrate exposed to a

* Corresponding author. Institute of Botany and Landscape Ecology, University of Greifswald, Soldmannstr. 15, D-17489, Greifswald, Germany.

E-mail address: nhadagamac@gmail.com (N.H.A. Dagamac).

microclimate suitable for the respective species, may exist in very different regions of the world and can be reached by spores, at least over long periods of time. This was shown first for *Barbeyella minutissima*, a rare species with minute fructifications appearing on decorticated logs of (mostly) conifers covered by algae and liverworts that stay continuously moist but are somewhat sheltered from wind and rain (Schnittler et al., 2000). The fragmentary data on the very patchy worldwide distribution of this species were well reflected by the distribution of montane spruce-fir forests that provide suitable habitats for *B. minutissima* (Schnittler et al., 2000). A follow-up study showed that the potential distribution of this myxomycete is not limited by the distribution of conifers, but still remains patchy (Stephenson et al., 2019). Therefore, the question arises if a myxomycete species can fill out its entire potential range, i.e., conquer all suitable habitats world-wide.

In recent years, there is a growing evidence that the “*everything is everywhere*” hypothesis does not apply for many protists (e.g. Foissner et al., 2007, ciliates; Bass et al., 2007, protozoa; Azovsky et al., 2016, marine benthic flagellates). For myxomycetes, only a few species seem to be really cosmopolitan in distribution, as a comparison between assemblages of the Neo- and Paleotropics has shown (Dagamac et al., 2017a). Even within smaller regions, species are not uniformly distributed, as it has been shown by regional distribution models for abundantly occurring tropical myxomycetes species in Costa Rica (*Arcyria cinerea*, *Didymium iridis*, *D. squamulosum*, *Hemitrichia calyculata*, *Physarum compressum*; Rojas et al., 2015) and in the Philippines (*Diderma hemisphaericum*, Almadrones-Reyes and Dagamac 2018).

In this study, we employed the MaxEnt algorithm (Phillips et al., 2008) to explore the potential world-wide distribution of nivicolous myxomycetes, a distinct ecological guild of species fruiting on the edge of melting snow banks preferentially in mountains (Novozhilov et al., 2013). These organisms are most likely predators of under-snow microbial communities, where amoebae benefit from the rather constant soil temperatures under insulating snow beds (Schnittler et al., 2015). They grow at low but positive temperatures, and may survive frost events by encystment, if those are not too severe and do not come too fast (Shchepin et al., 2014). These conditions are usually, but not always, fulfilled best in mountains (Ronikier and Ronkier 2009). Nivicolous myxomycetes constitute an ecological guild with ca. 100 described species, discovered first by Meylan (1908) in the Swiss Jura mountains, where he described numerous species in subsequent publications (Kowalski 1975). Most members belong to the dark-spored clade of myxomycetes (Fiore-Donno et al., 2012). Our target species, *Physarum albescens*, was described already in the 19th century by T. Macbride from Denver (Colorado) as *Leocarpus fulvus* (Macbride 1899). After confusion with *Diderma albescens*, which is today known as *D. niveum*, another species of nivicolous myxomycetes (Singer et al., 2004), it was recognized as a *Physarum*, and Macbride reported occurrences at Lake Tahoe, Nevada, and from Montana (Macbride 1922). All these localities are situated in mountainous regions of the American west, and Macbride suggested the species to be “*No doubt common at high altitudes near the snow-line in mountainous regions, probably around the world.*” *Physarum albescens* is one of the most easily recognizable nivicolous myxomycetes, since its fruit bodies are brightly colored and appear often in large groups. The species is easily distinguishable from *Diderma niveum* by the type of capillitium (reticulate, tubular and with lime nodes in *Ph. albescens*, but mostly solid and simply branched threads without lime nodes in *D. niveum*) and the presence of a stalk. According to the experience of the authors, its occurrence usually indicates locations rich in other nivicolous species. As such, the modelled distribution map of this species should give us an idea, in which regions of the world fruiting of nivicolous myxomycetes can be expected.

2. Materials and methods

2.1. Data sources

GBIF lists 1225 entries named as *Physarum albescens* (<http://GBIF.org/GBIF.org>, 2020). All accession numbers were traced back to the respective survey, and numerous records had to be excluded due to confusion with *Ph. Album*, a non-nivicolous species. This left 1117 entries. Additional five records came from published papers (Yamamoto 1993; Ing, 2009; Tamayama 2000; Ronikier and Lado 2013; Antonopoulos et al., 2018) mentioning localities of *Ph. albescens* not provided by GBIF. The last source of data (594 records) constituted the private collections of the authors and the collections of M. Meyer, R. Cainelli and Y. Yajima. However, many records overlapped with entries in GBIF or referred to multiple collections from one place, thus only 537 observations turned out to be really unique and were used for modeling. Geographical coordinates were reconstructed for all records where the locality could be determined with a precision of at least ± 50 km; and elevation data were taken from Google Earth for all localities determined with a precision of less than 250 m (Supplement 1). Since most of our records are rather recent and have relatively precise geographical coordinates we did not investigate the influence of spatial uncertainty (Naimi et al., 2014).

Data for the respective environmental conditions were first obtained from the 19 BioClimatic variables with 30 arc seconds (~ 1 km²) spatial resolution (Hijmans et al., 2005; Fick and Hijmans 2017) of the WorldClim database (version 2, www.worldclim.org). These variables represent trends in temperature and precipitation, seasonality, and extreme or limiting environmental factors. Mean elevation (variable 20, see list of all environmental variables in Table S1) of each grid is as well available. In addition, snow cover (21) was obtained from the ERA5-Land data set (Muñoz-Sabater, 2019).

2.2. Correlative modeling approach employed in MaxEnt

We first created an occurrence matrix showing rasterized presences of all records. Together with various matrices of the environmental variables, it was subjected to MaxEnt v. 3.3.3. (<http://www.cs.princeton.edu/~schapire/maxent/>). This software is one of the most robust (Thapa et al., 2018) bioclimatic modeling approaches that relies on presence-only data and performs well even if the species occurrence data are scarce (Pearson 2007; Townsend-Peterson et al., 2007; Elith et al., 2011), which certainly is the case for a myxomycete with ephemeral fruiting which will be found mostly by specialists.

We did three model runs: first with default values of the BioClim data set, second adding a correction for pseudo-absence (not all mountain ranges of the world are surveyed) and third adding snow cover as the decisive parameter for the suitable ecological niche. The first run (model 1) considered all BioClim variables (1–19) and elevation (20), using only the default regularization settings in Maxent.

In the second run (model 2) the ENMeval package in R (Muscarella et al., 2014) was utilized to correct for possible pseudo-absences. It balances the goodness of fit with model complexity and (for spatially independent data) it establishes the equivalent of a penalty for pseudo-absences. In our case, the fine-tuned setting generated from the ENMeval analysis (method = randomkfold, kfold = 10) suggested the adjustment of a regularization multiplier of 3 with Linear settings to be selected.

For the last approach (model3) snow cover (21) was considered. Monthly values from the ERA5-Land data set were converted into a categorical map of regions with suitable snow cover: grid cells receiving (i) three successive months with snow cover (average 2000–2010, >1 cm considered as presence) and (ii) three successive months free of snow (allowing vegetation to develop). In addition, we conducted a variance inflation factor analysis to identify correlated environmental variables within the WorldClim data set. To reduce computational load, we only

analyzed this for grids with suitable snow cover and elevation >350 m. Within these areas, we randomly selected 5000 points and extracted climate information (19 BioClimatic variables and elevation) at those points and used the extracted data as input for the *vifcor* function from the *usdm* R package (v. 1.1.18), which uses a stepwise procedure to exclude variables that are highly correlated to each other (Pearson's $R > 0.7$). We repeated the random sampling procedure 10 times to ensure that the results were not sensitive to the random selection of points. The Bioclimatic variables 2, 3, 5, 8, 15, and 18–20 were always retained as non-correlated (Table S1); variable 9 was retained in six cases. These nine variables were finally used for the model, together with snow cover (21) as a categorical environmental layer (see Table S1). In this case ENMeval suggested that a regularization multiplier of 3 and Linear, Quadratic, Hinge, Product and Threshold settings should also be selected.

In accordance with Yang et al. (2013), the random test percentage was adjusted to 30% and the file format turned into logistic for all models. A total of 100 runs were set for the model building (Flory et al., 2012). The algorithm runs either 1000 iterations of these processes or continues until it reaches a convergence threshold of 0.00001 (Yuan et al., 2015). The resulting models were then evaluated using the receiver operating characteristic (ROC) analysis, which eventually generated the area under the curve (AUC) scores (Phillips et al., 2006) to determine the model's goodness-of-fit. A *Jackknife* procedure was used to calculate the contribution of the variables used for the model prediction. The final output of all models produced a distribution map that with potential incidence values for each grid cell, ranging from 0 to 1. For easier visualization these values were subsequently grouped into five classes from very low (0.0–0.2), low (0.21–0.40), medium (0.41–0.60), high (0.61–0.80), to very high (0.81–1.00) probability. The final output file generated by MaxEnt was then exported as an ASCII file format so that it could be imported in ArcMap v. 10.4. for a better map visualization.

To visualize the elevation preferred by *Ph. albescens* in dependence from the latitude of the localities, we plotted altitude over latitude for all records from the Northern Hemisphere, where elevation was given or could be reconstructed with a precision of at least 100 m. To test for a correlation between altitude and incidence of occurrence, all land-locked grid cells of the Northern Hemisphere provided by the WorldClim database were assigned to latitudinal belts of 5° extension. The Pearson correlation coefficient was calculated for each belt.

3. Results

Not surprisingly for a small and ephemeral organism, the known records of *Physarum albescens* are very unevenly distributed and span a wide range of elevation (from low-mountain areas of northwestern Russia, ca 400–650 m a.s.l., up to the U.S. Rocky Mountains, nearly 3500 m a.s.l., Supplement 1). Fig. 1 shows the known distribution, together with localities that were surveyed for nivicolous myxomycetes (Supplement 2). Best represented are European countries, including Andorra (2), Austria (16), France (490), Germany (17), Greece (1), Italy (20), Norway (39), Poland (11), Slovenia (4), Spain (199), northwestern Russia (231; Erastova et al., 2015) and Switzerland (4). For the whole of Africa, a single older record is known from the Atlas Mts. (Morocco). The species is fairly common in the northwestern Caucasus (168 records; Novozhilov et al., 2013), was found in only one region of Central Asia (Trans-Ili Alatau, Kazakhstan, near Almaty, 9 records); but nothing is known for the Himalaya and the South Siberian Mountains. *Ph. albescens* is fairly common in the Russian Far East (Kamchatka; Novozhilov et al., 2017b) and northern Japan (Tamayama 2000). In the New World it is, despite lacking recent studies, known from numerous older records across the Rocky Mountains and the western US (California, 24; Colorado, 285; Montana, 8; South Dakota, 1; Utah, 9; Washington, 5; Wyoming, 4). The last author added one record for the Coastal Mountains from British Columbia. Despite several years of searching (S.L. Stephenson, pers. comm.), no records are known from the eastern US, although the Appalachians reach ca. 2600 m a.s.l. At the highest peak. For the Southern Hemisphere we have 35 records from southwestern Australia (Stephenson and Shadwick 2009) and New Zealand (Stephenson et al., 2007). A single occurrence is known from Argentina (Ronikier and Lado 2013).

Three, subsequently refined SDMs with the same distribution but different environmental data and degrees of regularization produced similar results (see Supplements 3–5 for maps of all three models in high resolution), yet with differences especially for lowland regions.

Although model 1 was most simple (all 19 WorldClim variables plus elevation), it produced high AUC values for both training (0.982) and test (0.981) data sets (see Supplement 3).

Model 2 (same variables, but with a regularization multiplier of 3) resulted in a lower AUC (0.970, mean of ten runs). Its incidence map (Supplement 4) is less restricted to mountain regions, e.g. highlighting with a low incidence as well the lowlands of northern Central Europe.

Model 3 (8 of 19 WorldClim variables selected by a collinearity test, elevation and categorical map of suitable snow cover plus

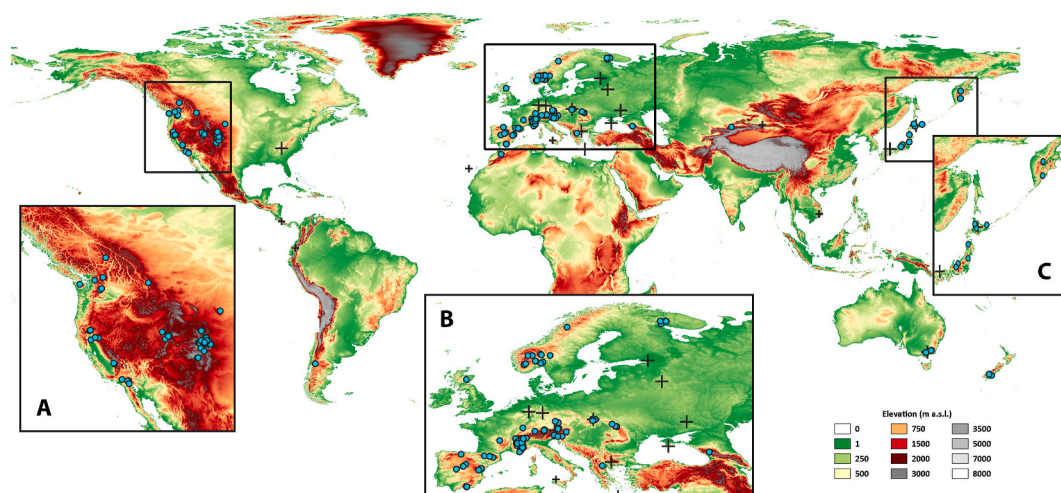


Fig. 1. Elevation map of the world built upon the elevational layers included in the WorldClim data set, showing the distribution of known records of *Physarum albescens* (circles) and selected studies for nivicolous myxomycetes (large hair crosses: other nivicolous species but not *Ph. albescens* found; small hair crosses: no nivicolous species found but alpine environment). Insets show the exact localities of (A) all occurrences from North America, (B) Europe and (C) Northeast Asia.

regularization) is again more centered around mountains, and indicates more correctly regions with no or a few known records but apparently suitable climate (Fig. 2, Supplement 5). The AUC value increased again (0.974, mean of ten runs).

The analysis of the percent contributions (Table S1) for the environmental predictors fed into the models listed *elevation* as very influential (26.2/19.1/20.5%) in all runs. In addition, environmental variables that yielded high percent contributions for the first and second model run were *precipitation of the driest quarter* (Bio17, 27.1%) and *precipitation seasonality* (Bio15, 37.2%), respectively. For the third model run, Bio19 (precipitation of the coldest quarter) and the additional categorical environmental layer of the suitable snow condition gave 31.9 and 27.5 percent contribution, respectively.

Our maps do not indicate all mountain ranges as equally suitable. Even the incidence map for model 3 (Fig. 2) that includes snow cover and corrects for possible pseudo-absence of records does not highlight most of the Central Asian mountains, the northeastern part of the Himalaya with the Tibetan plateau and most of the Andes. This indicates that elevation alone does not always predict species occurrence.

A plot for the known records for the Northern Hemisphere, making up for 68% of the land mass and 98% of all unique records, reveals a pattern of decreasing elevation with increasing latitude (Fig. 3A). If we compare the elevation belts preferentially inhabited by *Ph. albescens* (>25 to <75° latitude, Fig. 3A) with the map in Fig. 2, two remarkable exceptions become visible. The first regards arid mountain ranges (like Central Asia and the central and eastern Andes) with high altitudes where the species is predicted to be absent. The second exception is constituted by low-mountain regions in the northern boreal zone, where *Ph. albescens* is predicted in spite of low altitude (and was found).

As suggested by the plot in Fig. 3A, at latitudes below 25° no areas with sufficiently high altitudes seem to exist. This is confirmed by the incidence values (Fig. 3B). The mean altitudes in latitudinal belts of 5° show a bimodal distribution (peaks at 25–40 and above 70°N), but the mean incidence values are more unimodal and peak between 35 and 60°N (Fig. 3B). However, for the respective grids, mean altitude and incidence correlate best for this latitudinal range (Fig. 3B, red dots).

4. Discussion

The classical applications of SDMs are for large organisms, like vascular plants (*Chromolaena odorata*, Truong et al., 2017, *Thuja sutchuenensis*, Qin et al., 2017), although small organisms noticeable only by specialists have been studied as well (*Drosophila suzukii*, Wang et al., 2010; Dos Santos et al., 2017). Since nivicolous myxomycetes fruit in habitats hard to access (mountains) only for a short time in spring, we have chosen a species that is (relatively for the group) easy to spot in nature and has clear morphological characters (less likely to be confused with other nivicolous myxomycetes). As a common element of snow-bank assemblages, *Ph. albescens* has a high extent of surrogacy for other nivicolous species.

The predictive distribution map for this species (Fig. 2) shows a distribution pattern centered around mountainous regions, as expected from the known records, but revealed a much lower incidence for regions with a continental climate, i.e. with low winter precipitation. The suitable elevation belt generally decreases with increasing latitude, and incidence values reach a maximum between 35 and 65° northern latitude (Fig. 3B). At this belt, humid temperate to southern boreal climates prevail, and sufficient winter snow alternates with fairly humid and warm summers supporting herbaceous vegetation. Here, elevation alone has the highest predictive value, as indicated by the correlation between altitude and incidence (Fig. 3B, red dots).

Although a number of surveys enlarged our knowledge about the distribution and ecology of nivicolous myxomycetes since the time of Meylan, the mountains of Europe are still covered best (Supplement 2). Further surveys of the authors contributed records from British Columbia (Canada), Kamchatka (Russia), and the Trans-Ili Alatau range (Kazakhstan). The major “white spots” in need of surveys predicted by this study include the Himalayan mountain range (but some nivicolous myxomycetes are reported, Venkataramani and Kalyanasundaram 1986), the South Siberian Mountains, the Canadian province of Nova Scotia (nivicolous myxomycetes were seen to occur, S. Beland, pers. comm.), southern Greenland, and the Alaskan Mountains. Mountains in northern Africa (Atlas, only one occasional record) and the Middle East (e.g., the Golan Heights between Israel and Syria) deserve as well a place in the list of regions in need of studies.

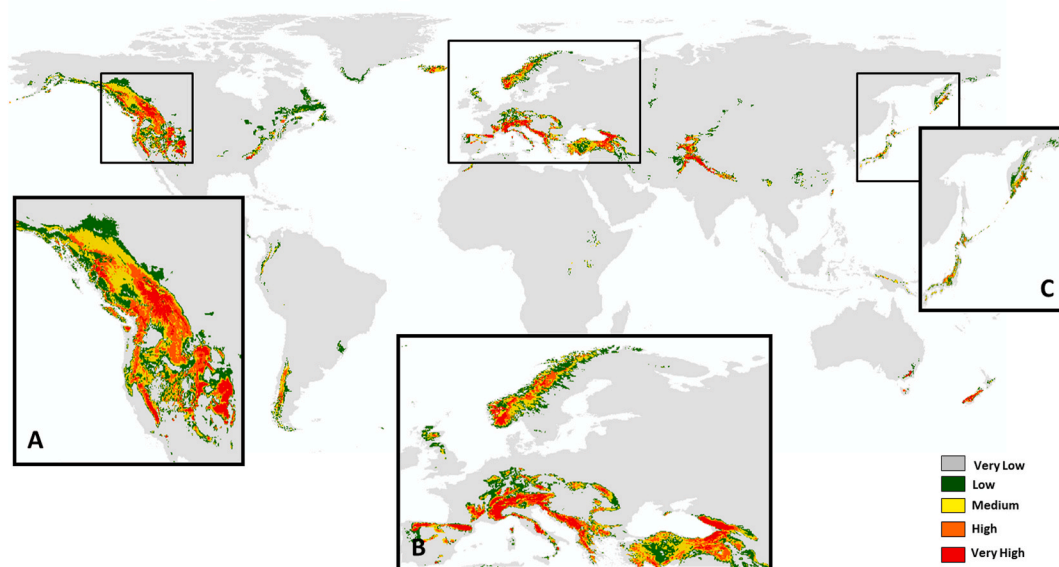


Fig. 2. Predicted worldwide distribution of *Ph. albescens* according to model 3 shown as a heat map with incidence (probability of occurrence) classified from very low (grey, 0–0.20), low (green, 0.21–0.40), medium (yellow, 0.41–0.60), high (orange, 0.61–0.80) to very high (red, 0.81–1.00). Insets show (A) Western North America, (B) Europe and (C) Northeast Asia. See Supplement 3 for a high-resolution map. (For interpretation of the references to color in this figure legend, the reader is referred to the Web version of this article.)

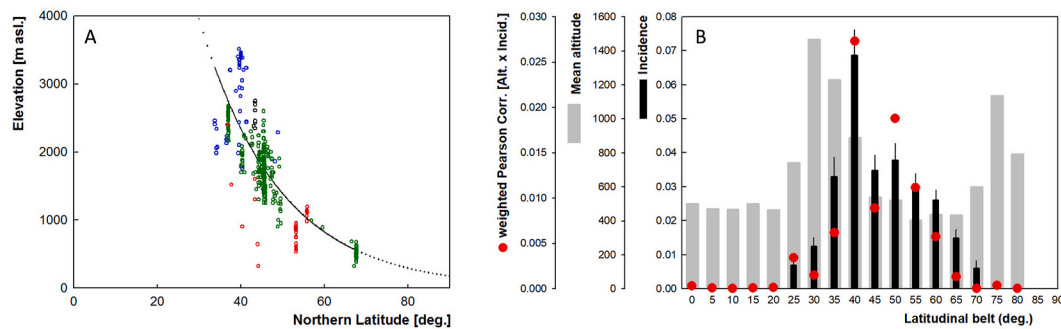


Fig. 3. (A) Plot of elevation vs. northern latitude for 991 records of *Physarum albescens* from the Northern Hemisphere, where elevation was given or could be reconstructed with a precision of ± 100 m. Data are fitted according to a modified decay function with $\text{elev} = a \exp^{-b(\text{Lat} - c)}$; obtained where figures of $a = 3351$, $b = 0.052$, $c = 33.16$, $R^2 = 0.665$ for the best fit. Dots are colored according to major world regions, showing western North America (blue), Europe (green), Northeast Asia (red), and Central Asian mountains (black). (B) Average incidence \pm SEM (black bars) in latitudinal belts of five degrees of the Northern Hemisphere, showing as well mean elevation (grey bars) and incidence-weighted Pearson correlation between elevation and incidence (red dots) for all land-locked grid cells of the WorldClim model. (For interpretation of the references to color in this figure legend, the reader is referred to the Web version of this article.)

4.1. Does the model reflect the ecological niche of nivicolous myxomycetes?

The correlative approach employed in the MaxEnt algorithm requires an easily scalable set of abiotic data; complex, especially biological, interactions are not included. The first question is to what extent the model appropriately describes the fundamental niche of *Ph. albescens*. Nivicolous myxomycetes are not necessarily alpine (Ronikier and Ronikier 2009, compare Fig. 3A). We therefore analyzed all grid cells above 350 m elevation for snow cover (the lowest record comes from 380 m a.s.l.).

What is known about the microhabitat of nivicolous myxomycetes, the uppermost soil layer? Studies employing data loggers measuring relative humidity and temperature revealed that the probability of soil frost is the decisive factor for the fruiting of nivicolous myxomycetes (Schnittler et al., 2015; Borg-Dahl et al., 2018). Amoebae can multiply under low but positive temperatures, but are susceptible to frost, especially to sudden frost events, where they fail to encyst and die (Shchepin et al., 2014). This probability is closely linked to the insulating power of snow beds, which can keep the soil at low but positive temperatures during the whole winter (Schnittler et al., 2015). In each of two long-term studies where local weather has been recorded by data loggers at ground level (Northwestern Caucasus, Schnittler et al., 2015, 4 y; German Alps, Borg Dahl et al., 2018, now 6 y), one year with few or no fructification has been observed, and this coincided with a single severe autumn frost occurring before the first snowfall. Snow falling on frozen soil conserved the below-zero temperatures in the uppermost soil layer for a long time.

At a world-wide scale, no data for soil surface temperature are available, and in addition this parameter is extremely variable over small distances, depending on local exposition, vegetation, and soil water content. Nivicolous myxomycetes fruit only after snow melt in spring around melting snow fields, thus snow cover must have a crucial influence – mitigating fluctuations in surface soil temperatures over the winter and sheltering the A-horizon (topsoil) from hard frosts, where amoebal density seems to be highest (Stephenson and Feest 2012). For this reason we included snow cover, where data are available at a world-wide scale. Guided by local investigations with data loggers (Schnittler et al., 2015) we considered a region with a minimum of three months of continuous snow cover as harboring suitable habitats for nivicolous myxomycetes.

These considerations coincide best with the map produced by model 3 that includes snow cover. In addition, this model corrects for pseudo-absence (which occurs in the data, as mentioned above), and takes into account the high correlation between some of the WorldClim (1–19) variables, which was indicated by shifts in the per cent contributions of

single variables shift between the model runs (Table S1). Here *precipitation of the coldest quarter* (Bio19), *snow cover* (20), and *elevation* (21) appear as the strongest predictors. This model corrects for some regions which were marked by the first two models as apparently suitable, but have never snow (for example, an area in the Brazilian Atlantic forests south of Sao Paulo, showed with much lower incidence in model 3 compared with model 2, see Supplements 4 and 5).

A few surveys negative for nivicolous myxomycetes can serve as “ground checks” to prove the “correctness” of the model. The species so far was not found in tropical mountains, where even at high elevations a continuous snow cover does not develop. This was confirmed in surveys for the Simien Mts. in Ethiopia (Dagamac et al., 2017c, max. elev. 4200 m, 13.2°N), Sierra de la Muerte in Costa Rica (Lado and Rojas 2018, ca. 3800 m, 9.5°N) and in southern Vietnam (Novozhilov et al., 2020, ca. 2400 m, 12.1°N): these regions were all negative for nivicolous myxomycetes (Supplement 2) and correctly not highlighted in the predictive map (Fig. 2).

Ronikier and Ronikier (2009) already suggested that elevation and incidence of occurrence do not always coincide for nivicolous myxomycetes. The two exceptions identified by the model are arid mountains (low to missing incidence but high altitude), and boreal lowlands (moderate incidence but low altitude). In arid mountains receiving only sporadic snowfall, the upper soil layer usually freezes in winter: amoebae cannot actively prey and multiply (Shchepin et al., 2014). This explains why in most of Central Asia, *Ph. albescens* (and nivicolous myxomycetes in general) seem to be rare. For example, in Kazakhstan they were found only in one spot within a week of surveying; in the Chinese Bogd-Shan (Xinjiang province) surveys in three different years (2004–2006) did not reveal a single record of a nivicolous myxomycete species (see brief habitat descriptions in Peterson et al., 2011). The mountains of western North America are also more arid than the European mountains: here, records of *Ph. albescens* are found on average at higher altitude (Fig. 1, average elevation of known records from western North America 2898 ± 632 m, 136 records; from Europe, 1852 ± 363 m, 763 records). Northeast Asia, influenced by the Pacific climate with high precipitation, shows the lowest mean altitude (869 ± 292 m, 74 records, see color codes in Fig. 3A).

Indeed, a number of nivicolous myxomycete species, especially of the genera *Diderma* and *Lamproderma*, are known to fruit in boreal lowlands (Erastova and Novozhilov 2015, 47 km NE from St. Petersburg, Russia, elev. 70 m a.s.l.; Gmshinskiy, 2018, near Tver, Russia, elev. 200–300 m a.s.l.; near Outokumpu, eastern Finland, elev. 120 m a.s.l., Marja Pennanen, pers. comm.). Even in eastern Ukraine, characterized by temperate deciduous forests, nivicolous *Lamproderma* spp. were found (Yatsiuk and Leontyev 2020). These species, apparently less strictly adapted to alpine conditions, can be expected as well in areas

with lower incidence values (Fig. 2). For *Physarum albescens* no true lowland occurrences are yet known, the lowest records come from ca. 380 m a.s.l. (Kola peninsula, Khibiny mountains, 67°N, Erastova et al., 2017).

In a given mountain range, nivicolous myxomycetes of the genera *Lamproderma* and *Meriderma* seem to be able to inhabit lower elevations (with a less durable continuous snow cover preventing soil frost), species of *Diderma* spp. are intermediate, and *Lepidoderma* and *Physarum albescens* are restricted to higher elevations (compare Fig. 1 in Schnittler et al., 2015). We hypothesize that this has to do with the water content of the soil: fructifications of especially *Lamproderma* spp. were often observed over waterlogged soils (Schnittler, pers. obs.). These will freeze more slowly than dry soils, giving the amoebae more time to encyst. In this genus transitions to the nivicolous life style can be seen: species like *L. arcyrroides* can be called cryophilous and are closely related to nivicolous members of the genus. Fructifications sometimes appear in deciduous forests in late autumn and winter in absence of snow (personal observ. of the authors). As such, the chosen species, *Physarum albescens*, is certainly not representative of all nivicolous myxomycetes but likely describes the “core” niche of this ecological guild: at all places where the authors found it, numerous other nivicolous species were recorded as well.

4.2. Dispersal barriers and local adaptation

Correlative SDMs as used in the present study are static (Convertino et al., 2014) and do not consider (i) possible dispersal limitations (Rodríguez-Rey et al., 2013) and (ii) local adaptation or any other within-species differentiation (Merow et al., 2013). They predict the suitable range for a species assuming unlimited dispersal capabilities. In other words, they neglect the history of speciation and the existence of possible dispersal barriers. We thus must ask if such barriers exist for myxomycetes. Even surveys on remote islands (Hawaii, Eliasson et al., 1983; Galapagos, Eliasson, 1991) did not discover endemic myxomycetes, at least not at the level of morphospecies. Nivicolous myxomycetes produce rather large spores for the group (12–16 µm vs. 7–12 µm as the usual range (Schnittler and Tesmer 2008)). This seems not to be the limiting factor: in ferns long-distance dispersal is common (Schneller et al., 1998; Dassler and Farrar 2001) despite a much higher average spore size (Tryon 1970; Gomez-Noguez et al., 2017). Like in ferns, myxomycete spores are primarily adapted to become airborne (Kamono et al., 2009). A study in the nivicolous myxomycete genus *Meriderma* (Feng et al., 2016) indicated that long distance dispersal exists but loses power over large distances: the more distant two mountain ranges are, the lower the proportion of shared genotypes.

Second, we should ask for local adaptation in myxomycete populations. Most myxomycete species are not simply ubiquitous (Schnittler et al., 2017). Several recent studies mounted evidence for biological, often cryptic, speciation in myxomycetes: molecular markers demonstrated the existence of reproductively isolated units within morphospecies. If occurring regionally, such units are expected to suffer less from outbreeding depression, which may facilitate local genetic adaptation. The respective biospecies may be cryptic (*Trichia varia*, 3 putative biospecies; Feng and Schnittler 2015), partially discernible by subtle morphological characters (*Hemitrichia serpulula*, 4; Dagamac et al., 2017b), or well discernible if novel traits can be found (*Tubifera ferruginosa* s.l., >5; Leontyev et al., 2015). Although the number of records included was very limited, two studies modeling the distribution of biospecies showed different geographical ranges for those (*Badhamia melanospora*, Aguilar et al., 2014; *Hemitrichia serpulula*, Dagamac et al., 2017b).

Within *Ph. albescens* as a morphospecies we can expect a similar differentiation, and studies with multiple molecular markers indeed point to the existence of more than ten reproductively isolated units (putative biospecies, Shchepin et al., unpubl. results). Currently, we do not have enough records to resolve the distribution of these putative

biospecies (which seem to occupy smaller ranges than the species as a whole). Therefore the model is valid only at the morphospecies level. At this level, it seems to predict well the distribution of *Ph. albescens*: mountain ranges with high incidence but no known records were indeed not well surveyed. This pattern may change if taxonomic resolution is increased, i.e. at the biospecies level: here only parts of the potential range may be filled. A recent study on the nivicolous species *Didymium nivicola* (Janik et al., 2020) mounted evidence for this: the genetically most distinct group (which likely constitutes a separate biospecies) is confined to the Southern Hemisphere and was not found in the Northern Hemisphere. We thus hypothesize that gene flow via spores is sufficient to conquer all suitable habitats over long periods of time. The emergence of regionally distributed reproductively isolated units, putative biospecies, may be a way to allow for local genetic adaptation.

4.3. Fruit bodies vs. amoebae

This model is solely based on the occurrence of fruit bodies for *Physarum albescens*. Data on the occurrence of the active trophic stage, the myxamoebae, are very limited, since myxamoebae cannot be determined to species and are hard to distinguish from free-living amoebae. Hence, such data must be generated via environmental PCR. The very few metabarcoding studies for myxomycetes indicated that amoebae of nivicolous myxomycetes seem to be wider distributed than their fructifications: Fiore-Donno et al. (2016) found sequences corresponding to nivicolous myxomycetes in three lowland areas of Germany; Shchepin et al. (2019) in boreal lowlands of Russia; Gao et al. (2019) in subtropical China. This pattern is confirmed by further, yet unpublished surveys of the authors which all indicated the presence of nivicolous myxomycetes in regions where fructifications have never been found. The abundance of the respective sequence reads seems to exclude the possibility that these results reflect simply spore fallout (Shchepin et al., 2019). An extensive study from the German Alps (Borg Dahl et al., 2019) found sequences corresponding to *Ph. albescens* as well at lower elevations, whereas fruit bodies occur only at higher elevations. In less suitable habitats, amoebae germinating from migrating spores might survive and vegetatively reproduce by cell division, but do not fruit. A similar case is known for the fern *Trichomanes speciosum*: sporophytes show much more limited distribution than gametophytes, which, like myxamoebae, in this species are capable of vegetative reproduction (Rumsey et al., 1998; Schuler et al., 2016). As such, our model only predicts the most suitable habitats for *Ph. albescens* (and likely for nivicolous myxomycetes in general), where these species can complete their life cycle and fruit.

Acknowledgements

Funding for this study was provided in the frame of Research Training Group RESPONSE (RTG 2010), supported by the Deutsche Forschungsgemeinschaft (DFG). YN and OS received support from the Russian program ‘Biodiversity, ecology, structural and functional features of fungi and fungus-like protists’ (AAAA-A19-119020890079-6). Thanks are extended to all people contributing data via GBIF or directly, by making the databases of their collections available, especially M. Meyer (France), but as well R. Cainelli (Italy), V.I. Gmoshinskiy (Russia), G. Moreno (Spain), M. Pennanen (Finland), A. Ronikier and P. Janik (Poland), and Y. Yajima (Japan). For suggestions with model improvement, we owe thanks to the reviewers of this paper.

Appendix A. Supplementary data

Supplementary data to this article can be found online at <https://doi.org/10.1016/j.funeco.2021.101079>.

References

- Aguilar, M., Lado, C., 2012. Ecological niche models reveal the importance of climate variability for the biogeography of protosteloid amoebae. *ISME J.* 6 (8), 1506–1514.
- Aguilar, M., Fiore-Donno, A.M., Lado, C., Cavalier-Smith, T., 2014. Using environmental niche models to test the ‘everything is everywhere’ hypothesis for *Badhamia*. *ISME J.* 8 (4), 737–745.
- Almadrones-Reyes, K.J., Dagamac, N.H.A., 2018. Predicting local habitat suitability in changing climate scenarios: applying species distribution modelling for *Diderma hemisphaericum*. *Curr. Res. Environ. Appl. Mycol.* 8 (5), 492–500.
- Antonopoulos, Z., Giannakis, T., Karagkizos, G., Athanasiadis, A., 2018. A contribution to the study of nivicolous myxomycetes in Greece. Part I: the genus *Physarum*. *Nova Hedwigia* 107 (3–4), 473–485.
- Azovsky, A.I., Tikhonov, D.V., Mazei, Y.A., 2016. An estimation of the global diversity and distribution of the smallest eukaryotes: biogeography of marine benthic heterotrophic flagellates. *Protist* 167 (5), 411–424.
- Bass, D., Richards, T.A., Matthai, L., Marsh, V., Cavalier-Smith, T., 2007. DNA evidence for global dispersal and probable endemicity of protozoa. *BMC Evol. Biol.* 7 (1), 162.
- Borg Dahl, M., Brejnrod, A.D., Russel, J., Sørensen, S.J., Schnittler, M., 2019. Different Degrees of niche differentiation for bacteria, fungi, and myxomycetes within an elevational transect in the German alps. *Microb. Ecol.* 78 (3), 764–780.
- Borg Dahl, M., Shchepin, O., Schunk, C., Menzel, A., Novozhilov, Y.K., Schnittler, M., 2018. A four year survey reveals a coherent pattern between occurrence of fruit bodies and soil amoebae populations for nivicolous myxomycetes. *Sci. Rep.* 8 (1), 1–12.
- Convertino, M., Muñoz-Carpena, R., Chu-Agor, M.L., Kiker, G.A., Linkov, I., 2014. Untangling drivers of species distributions: global sensitivity and uncertainty analyses of MaxEnt. *Environ. Model. Software* 51, 296–309.
- Dagamac, N.H.A., Hoffmann, M., Novozhilov, Y.K., Schnittler, M., 2017c. Myxomycetes from the highlands of Ethiopia. *Nova Hedwigia* 104, 111–127.
- Dagamac, N.H.A., Novozhilov, Y.K., Stephenson, L.S., Rojas, C., dela Cruz, T.E.E., Unterseher, M., Schnittler, M., 2017a. Biogeographical assessment of myxomycete assemblages across the Tropics. *J. Biogeogr.* 44 (7), 1524–1536.
- Dagamac, N.H.A., Rojas, C., Novozhilov, Y.K., Moreno, G.H., Schlueter, R., Schnittler, M., 2017b. Speciation in progress? A phylogeographic study among populations of *Hemitrichia serpulata* (Myxomycetes). *PLoS One* 12 (4), e0174825.
- Dassler, C.L., Farrar, D.R., 2001. Significance of gametophyte form in long-distance colonization by tropical, epiphytic ferns. *Brittonia* 53 (2), 352–369.
- dos Santos, L.A., Mendes, M.F., Krüger, A.P., Blauth, M.L., Gottschalk, M.S., Garcia, F.R., 2017. Global potential distribution of *Drosophila suzukii* (Diptera, Drosophilidae). *PLoS One* 12 (3), e0174318.
- Eliasson, U., 1991. The myxomycete biota of the Hawaiian Islands. *Mycol. Res.* 95, 257–267.
- Eliasson, U., Nannenga-Bremekamp, N.E., 1983. Myxomycetes from the scalesia forest, Galapagos islands. *Proc. Koninklijke Nederl. Akademie Wetenschappen C* 86, 148–153.
- Elith, J., Phillips, S.J., Hastie, T., Dudík, M., Chee, Y.E., Yates, C.J., 2011. A statistical explanation of MaxEnt for ecologists. *Divers. Distrib.* 17 (1), 43–57.
- Erastova, D.A., Novozhilov, Y.K., 2015. Nivicolous myxomycetes of the lowland landscapes of the North-West of Russia. *Mikol. Fitopatol.* 49 (1), 9–18.
- Erastova, D.A., Novozhilov, Y.K., Schnittler, M., 2017. Nivicolous myxomycetes of the Khibiny mountains, kola peninsula, Russia. *Nova Hedwigia* 104 (1–3), 85–110.
- Feng, Y., Schnittler, M., 2015. Sex or no sex? Group I introns and independent marker genes reveal the existence of three sexual but reproductively isolated biospecies in *Trichia varia* (Myxomycetes). *Org. Divers. Evol.* 15 (4), 631–650.
- Feng, Y., Klahr, A., Janik, P., Ronikier, A., Hoppe, T., Novozhilov, Y.K., Schnittler, M., 2016. What an intron may tell: several sexual biospecies coexist in *Meriderma* spp. (Myxomycetes). *Protist* 167, 234–253.
- Fick, S.E., Hijmans, R.J., 2017. WorldClim 2: new 1km spatial resolution climate surfaces for global land areas. *Int. J. Climatol.* 37 (12), 4302–4315.
- Fiore-Donno, A.M., Kamono, A., Meyer, M., Schnittler, M., Fukui, M., Cavalier-Smith, T., 2012. 18S rDNA phylogeny of *Lamproderma* and allied genera (Stemonitales, Myxomycetes, Amoebozoa). *PLoS One* 7 (4), e35359.
- Fiore-Donno, A.M., Weinert, J., Wubet, T., Bonkowski, M., 2016. Metacommunity analysis of amoeboid protists in grassland soils. *Sci. Rep.* 6 (1), 1–13.
- Flory, A.R., Kumar, S., Stohlgren, T.J., Cryan, P.M., 2012. Environmental conditions associated with bat white nose syndrome mortality in the north-eastern United States. *J. Appl. Ecol.* 49, 680–689.
- Foissner, W., Chao, A., Katz, L.A., 2007. Diversity and geographic distribution of ciliates (Protista: Ciliophora). In: *Protist Diversity and Geographical Distribution*. Springer, Dordrecht, pp. 111–129.
- Gao, Y., Zhang, X., He, G., Shchepin, O.N., Yan, S., Chen, S., 2019. Influence of forest type on dark-spored myxomycete community in subtropical forest soil, China. *Soil Biol. Biochem.* 138, e107606.
- GBIF.org, 2020. GBIF occurrence download. <https://doi.org/10.15468/dl.m04g7e>. (Accessed 29 May 2019).
- Gmshinskiy, V.I., 2018. First data on nivicolous myxomycetes (class myxomycetes) of central forest state biosphere reserve. In: Zheltukhin, A.S. (Ed.), *Nature Chronicle of the Central Forest Reserve*, pp. 146–152, 2018.
- Gómez-Noguez, F., León-Rossano, L.M., Mehltreter, K., Orozco-Segovia, A., Rosas-Pérez, I., Pérez-García, B., 2017. Experimental measurements of terminal velocity of fern spores. *Am. Fern J.* 107 (2), 59–71.
- Hijmans, R.J., Cameron, S.E., Parra, J.L., Jones, P.G., Jarvis, A., 2005. Very high resolution interpolated climate surfaces for global land areas. *Int. J. Climatol.* 25 (15), 1965–1978.
- Ing, B., 2009. Alpine myxomycetes in scotland. *Bot. J. Scotl.* 50, 47–53.
- Janik, P., Lado, C., Ronikier, A., 2020. Range-wide phylogeography of the nivicolous protist *Didymium nivicola* meyl. (Myxomycetes, Amoebozoa): striking contrasts between the northern and the southern Hemisphere. *Protist* 171, 125771.
- Kamono, A., Kojima, H., Matsumoto, J., Kawamura, K., Fukui, M., 2009. Airborne myxomycete spores: detection using molecular techniques. *Naturwissenschaften* 96, 147–151.
- Kowalski, D.T., 1975. The myxomycete taxa described by Charles Meylan. *Mycologia* 67, 448–494.
- Lado, C., 2005–2021. NomenMyx: an online nomenclatural information system of Eumycetozoa. Available at: (Accessed 5 May 2021) <http://www.nomen.eumycetozoa.com>.
- Lado, C., Rojas, C., 2018. Diversity patterns, ecological associations and future of research on Costa Rican myxomycetes. *Mycology* 9 (4), 250–263.
- Leontyev, D.V., Schnittler, M., Stephenson, S.L., 2015. A critical revision of the *Tubifera ferruginosa* complex. *Mycologia* 107 (5), 959–985.
- Macbride, T.H., 1899. The North American Slime-Moulds; Being a List of All Species of Myxomycetes Hitherto Described from North America, Including Central America. Macmillan and Co., New York, London, p. 269.
- Macbride, T.H., 1922. The North American Slime-Moulds, a Descriptive List of All Species of Myxomycetes Hitherto Reported from the Continent of North America with Notes on Some Extra-limital Species, second ed. Macmillan and Co., New York, London, p. 347.
- Merow, C., Smith, M.J., Silander Jr., J.A., 2013. A practical guide to MaxEnt for modeling species' distributions: what it does, and why inputs and settings matter. *Ecography* 36 (10), 1058–1069.
- Meylan, Ch., 1908. Contributions à la connaissance des Myxomycètes du Jura. *Bull. Soc. Vaudoise Sci. Nat.* 44, 285–302.
- Muñoz Sabater, J., 2019. ERA5-Land monthly averaged data from 1981 to present. In: Copernicus Climate Change Service (C3S) Climate Data Store (CDS). <https://doi.org/10.24381/cds.68d2bb30> accessed 06/11/2020.
- Muscarella, R., Galante, P.J., Soley-Guardia, M., Boria, R.A., Kass, J.M., Uriarte, M., Anderson, R.P., 2014. ENMeval: an R package for conducting spatially independent evaluations and estimating optimal model complexity for Maxent ecological niche models. *Methods in Ecology and Evolution* 5 (11), 1198–1205.
- Naimi, B., Hamm, N., Groen, T.A., Skidmore, A.K., Toxopeus, A.G., 2014. Where is positional uncertainty a problem for species distribution modelling? *Ecography* 37, 191–203.
- Novozhilov, Y.K., Shchepin, O.N., Schnittler, M., 2017b. A preliminary report of the diversity of nivicolous myxomycetes from the natural park «Vulkany Kamchatki». *Proceedings of the XVIII international scientific conference, dedicated to the 70th anniversary of P. Kamchatpress A. Khomentovskiy's birthday*. 371–378, 978–5–9610–0294–2.
- Novozhilov, Y.K., Rollins, A.W., Schnittler, M., 2017a. Ecology and distribution of myxomycetes. In: *Myxomycetes*. Academic Press, pp. 253–297.
- Novozhilov, Y.K., Schnittler, M., Erastova, D.A., Okun, M.V., Schepin, O.N., Heinrich, E., 2013. Diversity of nivicolous myxomycetes of the tiberda state biosphere reserve (northwestern Caucasus, Russia). *Fungal Divers.* 59 (1), 109–130.
- Novozhilov, Y.K., Shchepin, O.N., Schnittler, M., Dagamac, N.H., Alexandrova, A.V., Popov, E.S., Kuznetsov, A.N., 2020. Myxomycetes associated with mountain tropical forests of bidoup nui Ba and chu Yang sin national parks (dalat plateau, southern Vietnam). *Nova Hedwigia* 110 (1–2), 185–224.
- Pearson, R.G., 2007. Species' distribution modeling for conservation educators and practitioners. *Synthesis*. American Museum of Natural History. Available at: <http://ncep.amnh.org>.
- Peterson, A., Levichev, I., Peterson, J., Harpke, D., Schnittler, M., 2011. New insights into the phylogeny and taxonomy of Chinese species of *Gagea* (Liliaceae) – speciation through hybridization. *Org. Divers. Evol.* 11, 387–407.
- Phillips, S.J., Dudík, M., 2008. Modeling of species distributions with Maxent: new extensions and a comprehensive evaluation. *Ecography* 31 (2), 161–175.
- Phillips, S.J., Anderson, R.P., Schapire, R.E., 2006. Maximum entropy modeling of species geographic distributions. *Ecol. Model.* 190 (3–4), 231–259.
- Qin, A., Liu, B., Guo, Q., Bussmann, R.W., Ma, F., Jian, Z., Pei, S., 2017. Maxent modeling for predicting impacts of climate change on the potential distribution of *Thuja sutchuenensis* Franch., an extremely endangered conifer from southwestern China. *Global Ecology and Conservation* 10, 139–146.
- Rodríguez-Rey, M., Jiménez-Valverde, A., Acevedo, P., 2013. Species distribution models predict range expansion better than chance but not better than a simple dispersal model. *Ecol. Model.* 256, 1–5.
- Rojas, C., Valverde, R., Rollins, A.W., Murillo Roos, M., 2017. What can myxomycetes tell us about floricolous microbial systems? *Nova Hedwigia* 104 (1–2), 211–220.
- Rojas, C., Zuñiga, J.M., Stephenson, S.L., 2015. Ecological niche modeling of some Costa Rican myxomycetes. *Curr. Res. Environ. Appl. Mycol.* 5, 153–159.
- Ronikier, A., Lado, C., 2013. *Physarum andinum*, a new nivicolous species of myxomycete from the Patagonian Andes. *Mycologia* 105 (1), 162–171.
- Ronikier, A., Ronikier, M., 2009. How ‘alpine’ are nivicolous myxomycetes? A worldwide assessment of altitudinal distribution. *Mycologia* 101 (1), 1–16.
- Rumsey, F.J., Jermy, A.C., Sheffield, E., 1998. The independent gametophytic stage of *Trichomanes speciosum* Willd. (Hymenophyllaceae), the killarney fern and its distribution in the British isles. *Watsonia* 22, 1–19.
- Schneller, J., Holderegger, R., Gugerli, F., Eichenberger, K., Lutz, E., 1998. Patterns of genetic variation detected by RAPDs suggest a single origin with subsequent mutations and long-distance dispersal in the apomictic fern *Dryopteris remota* (Dryopteridaceae). *Am. J. Bot.* 85 (7), 1038–1042.
- Schnittler, M., 2001. Follicolous liverworts as a microhabitat for neotropical myxomycetes. *Nova Hedwigia* 72 (1–2), 259–270.

- Schnittler, M., Stephenson, S.L., 2002. Inflorescences of Neotropical herbs as a newly discovered microhabitat for myxomycetes. *Mycologia* 94 (1), 6–20.
- Schnittler, M., Tesmer, J., 2008. A habitat colonisation model for spore-dispersed organisms – does it work with eumycetozoans? *Mycol. Res.* 112, 697–707.
- Schnittler, M., Dagamac, N.H.A., Novozhilov, Y.K., 2017. Biogeographical patterns in myxomycetes. In: *Myxomycetes*. Academic Press, pp. 299–331.
- Schnittler, M., Erastova, D.A., Shchepin, O.N., Heinrich, E., Novozhilov, Y.K., 2015. Four years in the Caucasus – observations on the ecology of nivicolous myxomycetes. *Fungal Ecology* 14, 105–115.
- Schnittler, M., Lado, C., Stephenson, S.L., 2002. Rapid biodiversity assessment of a tropical myxomycete assemblage – maquipucuna Cloud Forest Reserve, Ecuador. *Fungal Divers.* 9, 135–167.
- Schnittler, M., Stephenson, S.L., Novozhilov, Y.K., 2000. Ecology and world distribution of *Barbeyella minutissima* (Myxomycetes). *Mycol. Res.* 104 (12), 1518–1523.
- Schuler, S.B., García-López, M., López-Flores, I., Nieto-Lugilde, M., Suárez-Santiago, V. N., 2016. Genetic diversity and population history of the Killarney fern, *Vandenboschia speciosa* (Hymenophyllaceae), at its southern distribution limit in continental Europe. *Bot. J. Linn. Soc.* 183, 94–105.
- Shchepin, O.N., Novozhilov, Y.K., Schnittler, M., 2014. Nivicolous myxomycetes in agar culture: some results and open problems. *Protistology* 8 (2), 53–61.
- Shchepin, O.N., Schnittler, M., Erastova, D.A., Prihodko, I.S., Borg Dahl, M., Azarov, D. V., Chernyaeva, E.N., Novozhilov, Y.K., 2019. Community of litter-inhabiting dark-spored myxomycetes in taiga forest (Nizhne-Svirskiy Reserve, Russia) revealed by DNA metabarcoding. *Fungal Ecology* 39, 80–93.
- Singer, H., Moreno, G., Illana, C., 2004. A SEM-study of some types of nivicolous Physarales. *Österreichische Zeitschrift für Pilzkunde* 13, 75–89.
- Stephenson, S.L., Shadwick, J.D., 2009. Nivicolous myxomycetes from alpine areas of south-eastern Australia. *Aust. J. Bot.* 57 (2), 116–122.
- Stephenson, S.L., Moreno, G., Singer, H., 2007. Notes on some nivicolous myxomycetes from Australia and New Zealand including the description of a new species of *Lamproderma*. *Österreichische Zeitschrift für Pilzkunde* 16, 11–23.
- Stephenson, S.L., Novozhilov, Y.K., Almadrones-Reyes, K.J., Dagamac, N.H.A., Schnittler, M., 2019. New records of *Barbeyella minutissima* (Myxomycetes, Echinosteliales) with an updated distribution map. *Nova Hedwigia* 109 (1–2), 177–186.
- Stephenson, S.L., Schnittler, M., Lado, C., 2004. Ecological characterization of a tropical myxomycete assemblage – maquipucuna cloud forest reserve, Ecuador. *Mycologia* 96 (3), 488–497.
- Stephenson, S.L., Schnittler, M., Novozhilov, Y.K., 2008. Myxomycete diversity and distribution from the fossil record to the present. *Biodivers. Conserv.* 17 (2), 285–301.
- Stephenson, S.L., Schnittler, M., 2017. Myxomycetes. In: *Handbook of the Protists*, second ed. Springer, pp. 1405–1432.
- Stephenson, S.L., Feest, A., 2012. Ecology of soil eumycetozoans. *Acta Protozool.* 51 (3), 201e208.
- Suweis, S., Bertuzzo, E., Mari, L., Rodríguez-Iturbe, I., Maritan, A., Rinaldo, A., 2012. On species persistence-time distributions. *J. Theor. Biol.* 303, 15–24.
- Tamayama, M., 2000. Nivicolous taxa of the myxomycetes in Japan. *Stapfia* 73, 121–129.
- Thapa, A., Wu, R., Hu, Y., Nie, Y., Singh, P.B., Khatriwada, J.R., et al., 2018. Predicting the potential distribution of the endangered red panda across its entire range using MaxEnt modeling. *Ecol. Evol.* 8 (21), 10542–10554.
- Townsend-Peterson, A., Papeš, M., Eaton, M., 2007. Transferability and model evaluation in ecological niche modeling: a comparison of GARP and Maxent. *Ecography* 30 (4), 550–560.
- Truong, T.T., Hardy, G.E.S.J., Andrew, M.E., 2017. Contemporary remotely sensed data products refine invasive plants risk mapping in data poor regions. *Front. Plant Sci.* 8, 770.
- Tryon, R., 1970. Development and evolution of fern floras of oceanic islands. *Biotropica* 2, 76–84.
- Venkataramani, R., Kalyanasundaram, I., 1986. Distribution and ecology of myxomycetes in India. *Plant Sci. (Limerick)* 96, 289–301.
- Wang, X.Y., Huang, X.L., Jiang, L.Y., Qiao, G.X., 2010. Predicting potential distribution of chestnut phyloxerid (Hemiptera: phyloxeridae) based on GARP and Maxent ecological niche models. *J. Appl. Entomol.* 134, 45e54.
- Williams, R.A., Owens, H.L., Clamp, J., Peterson, A.T., Warren, A., Martín-Cereceda, M., 2018. Endemicity and climatic niche differentiation in three marine ciliated protists. *Limnol. Oceanogr.* 63 (6), 2727–2736.
- Yamamoto, Y., Matsumoto, J., Santo, H., Takahashi, K., 1993. A list of myxomycetes collected in the Hida Mts., Central Japan. *HIKOBIA* 11, 249–260.
- Yang, X.Q., Kushwaha, S.P.S., Saran, S., Xu, J., Roy, P.S., 2013. Maxent modeling for predicting the potential distribution of medicinal plant, *Justicia adhatoda* L. in Lesser Himalayan foothills. *Ecol. Eng.* 51, 83–87.
- Yatsiuk, I., Leontyev, D., 2020. Two species of nivicolous myxomycetes that formed fruiting bodies during three spring seasons in the lowlands of the Eastern Ukraine. *Phytotaxa* 437 (3), 147–155.
- Yuan, H.-S., Wei, Y.-L., Wang, X.-G., 2015. Maxent modeling for predicting the potential distribution of Sanghuang, an important group of medicinal fungi in China. *Fungal Ecology* 17, 140–145.

3.3 A workflow for low-cost automated image analysis of myxomycete spore numbers, size and shape

Jan Woyzichovski¹, Oleg N. Shchepin^{1,2}, Nikki H.A. Dagamac^{1,3}, Martin Schnittler¹

¹Institute of Botany and Landscape Ecology, Greifswald University, Soldmannstr. 15, 17487 Greifswald, Germany

²Komarov Botanical Institute of the Russian Academy of Sciences, Laboratory of Systematics and Geography of Fungi, Prof. Popov Street 2, 197376 St. Petersburg, Russia

³Department of Biological Sciences and Research Center for the Natural and Applied Sciences, University of Santo Tomas, Manila, Philippines

Corresponding author:

Jan Woyzichovski, Soldmannstr. 15, 17489 Greifswald, Germany

Email address: jan.woyzichovski@uni-greifswald.de

Manuscript published 16 November 2021 in *PeerJ*.

A workflow for low-cost automated image analysis of myxomycete spore numbers, size and shape

Jan Woyzichovski¹, Oleg Shchepin^{1,2}, Nikki Heherson Dagamac^{1,3} and Martin Schnittler¹

¹Institute of Botany and Landscape Ecology, Greifswald University, Greifswald, Mecklenburg-Western Pomerania, Germany

²Laboratory of Systematics and Geography of Fungi, Komarov Botanical Institute of the Russian Academy of Sciences, St. Petersburg, Russia

³Department of Biological Sciences and Research Center for the Natural and Applied Sciences, University of Santo Tomas, Manila, Philippines

ABSTRACT

Measuring spore size is a standard method for the description of fungal taxa, but in manual microscopic analyses the number of spores that can be measured and information on their morphological traits are typically limited. To overcome this weakness we present a method to analyze the size and shape of large numbers of spherical bodies, such as spores or pollen, by using inexpensive equipment. A spore suspension mounted on a slide is treated with a low-cost, high-vibration device to distribute spores uniformly in a single layer without overlap. Subsequently, 10,000 to 50,000 objects per slide are measured by automated image analysis. The workflow involves (1) slide preparation, (2) automated image acquisition by light microscopy, (3) filtering to separate high-density clusters, (4) image segmentation by applying a machine learning software, Waikato Environment for Knowledge Analysis (WEKA), and (5) statistical evaluation of the results. The technique produced consistent results and compared favorably with manual measurements in terms of precision. Moreover, measuring spore size distribution yields information not obtained by manual microscopic analyses, as shown for the myxomycete *Physarum albescens*. The exact size distribution of spores revealed irregularities in spore formation resulting from the influence of environmental conditions on spore maturation. A comparison of the spore size distribution within and between sporocarp colonies showed large environmental and likely genetic variation. In addition, the comparison identified specimens with spores roughly twice the normal size. The successful implementation of the presented method for analyzing myxomycete spores also suggests potential for other applications.

Submitted 16 November 2020

Accepted 20 October 2021

Published 16 November 2021

Corresponding author

Jan Woyzichovski,
jan.woyzichovski@uni-greifswald.de

Academic editor

Mark Gessner

Additional Information and
Declarations can be found on
page 19

DOI 10.7717/peerj.12471

© Copyright

2021 Woyzichovski et al.

Distributed under
Creative Commons CC-BY 4.0

OPEN ACCESS

Subjects Biogeography, Ecology, Mycology, Data Science, Population Biology

Keywords Particle analysis, *Physarum albescens*, Size distribution, Spore diameter, Computer vision, Spore shape

INTRODUCTION

Spores and pollen have evolved to overcome the challenge of dispersal in terrestrial environments, because only very small particles can float in the air. Such propagules are often formed in huge amounts (Li, 2011), may be actively released into the air

(Ingold, 1965), assume diverse shapes (Woo et al., 2018), and occur in many unrelated groups of terrestrial organisms with limited mobility, both prokaryotes and eukaryotes (Huang & Hull, 2017). Spores are usually formed on or within fructifications, including in the prokaryotic Myxobacteria (Reichenbach, 1993) and most eukaryotes, such as myxomycetes and myxomycete-like organisms (MMLO, a group comprising various protists, but mainly Amoebozoa (Schnittler, Unterseher & Tesmer, 2006), many fungi (Wijayawardene et al., 2020), mosses, lycophytes, ferns, and seed plants forming pollen grains. The pollen of seed plants shows similar dispersal behavior as spores, but cannot germinate independently, only at the pistil of a receptor plant (Punt et al., 2007). The average size of these propagules is an important trait for species differentiation, even in taxa rich in morphological characters (Brown, 1960). However, only 20–50 propagules are measured in most taxonomic monographs and species descriptions, although a much greater sample size would be desirable for sound statistical analyses.

Spore size is conventionally determined by light microscopy. This is time-consuming and error-prone, depending crucially on the accurate use of the measuring device. Many microscope manufacturers now offer optional camera and software solutions that may be purchased at an estimated minimum price of US\$ 4,000. Some of these applications use machine learning algorithms that can be trained to recognize objects and measure them automatically. ZEN (blue edition) by Zeiss is an example. Furthermore, algorithms for range thresholding, simple filters, and edge detection based on intensity change are now widely used. However, these algorithms typically fall short of achieving a segmentation of objects with a complex shape or touching each other. Additional problems are that only a small fraction of the spores on a slide is in focus and that spore densities are too low to measure large numbers. Packing spores more densely leads to high overlap and thus poses problems for the software to separate individual spores optically.

A number of devices have been developed to overcome such limitations. These include the Beckman Coulter particle counter (Brea, CA, USA), which is based on resistive pulse sensing (approximately US\$ 38,000); systems based on laser diffraction spectroscopy developed by A. Paar GmbH (Graz, Austria); a system marketed by HORIBA (Kyoto, Japan) based on dynamic light scattering (approximately US\$ 45,000); and imaging flow cytometry (IFC) like the FlowCam (Buskey & Hyatt, 2006) as an automated flow-through microscopic device (approximately US\$ 65,000). All of these devices except for the FlowCam need to be adjusted for a given application, since the visual inspection of single particles is not possible. A major downside of all these instruments is that acquisition costs are high.

Affordable alternatives are the PlanktonScope (Pollina et al., 2020) and an IFC system described by Göröcs et al. (2018). However, limitations associated with the lower costs typically include the use of a rolling shutter system, which needs an extra algorithm to compensate for the image tearing effect. Moreover, for deep flow cells in particular, the use of entocentric lenses introduces measuring errors, distortion, astigmatism, as well as chromatic and spherical aberrations.

Alternative image analysis tools like scripts, plug-ins, or stand-alone applications based on brightfield microscopy of preserved samples have also been designed (Korsnes et al., 2016; Wagner & Macher, 2012; Vidal-Diez de Ulzurrun et al., 2019; Benyon et al., 1999) to

identify and count small particles as well as to determine their morphological features. These approaches enable reliable analyses when contrast between object and background within the field of depth is consistently high and objects are non-overlapping. However, they become unreliable when these conditions are not met.

Here we present a procedure that allows for the reliable low-cost image analysis of spores, pollen, or biological aerosols at high densities. Our procedure is independent of special equipment and proprietary software. Spores are evenly spread on a slide to measure up to 50,000 objects based on photographs taken with a conventional compound microscope. The images are subsequently processed with the open-source software Fiji ImageJ (version 1.52p; [Schindelin et al., 2012](#)), which facilitates incorporating plug-ins and machine learning scripts. The workflow allows the visual inspection of every particle. This is often important to ascertain the quality of measurements, since spores are usually mixed with other particles, like pieces of cell wall (anthers, fern sporangia), hyphal fragments (fungi), elaters (liverworts), or capillitia (myxomycetes). We illustrate possible applications on the example of the myxomycete *Physarum albescens* Ellis ex T. Macbr., which releases large numbers of airborne meiospores for long-distance dispersal ([Kamono et al., 2009](#)). Specifically, we assessed variation in shape and spore size distribution within a colony and depending on environmental conditions during sporocarp formation. Our goal was to develop a workflow that (1) is based on standard slide preparations routinely used for identification, (2) is independent of special equipment and proprietary software, and (3) measures spore quantities large enough to construct a size distribution graph for robust statistical evaluations.

MATERIALS AND METHODS

Physarum albescens is a typical member of the dark-spored clade of the Mycetozoa ([Leontyev et al., 2019](#)), the slime molds. This group belongs to the Amoebozoa and comprises more than 1,000 described species ([Lado, 2005–2020](#)). *Ph. albescens* was sampled throughout the Northern Hemisphere to cover a maximum of intraspecific variation (Rocky Mountains, German and French Alps, Khibine Mountains of the Kola Peninsula, Northern Caucasus, Spanish Sierra Nevada, Kamchatka, see [Supplement 1A](#) and [Supplement 1B](#)). The life cycle of *Ph. albescens* involves the formation of a colony of usually stalked sporocarps ([Schnittler et al., 2012](#); [Stephenson & Schnittler, 2017](#)), each containing between 0.5 to 2.5 million spores ([Schnittler & Tesmer, 2008](#)). For each colony, spores of five sporocarps were analyzed.

Slide preparation

[Figure 1](#) outlines the process of slide preparation. One mounted slide was prepared with Hoyer's medium for each sporocarp ([Neubert, Nowotny & Baumann, 1993](#)). The sporocarp was crushed and its spores suspended in 0.2 ml PCR tubes with 20 µl of 70% (v/v) ethanol. Since the spores of myxomycetes (and many other organisms) have hydrophobic ornamentations, ethanol was chosen to avoid spore aggregation. The spores were separated by repeatedly and carefully dipping the sporotheca (stalked fruit body) into the ethanol while holding the stalk with tweezers ([Fig. 1A](#)). Spore release was controlled by tilting the

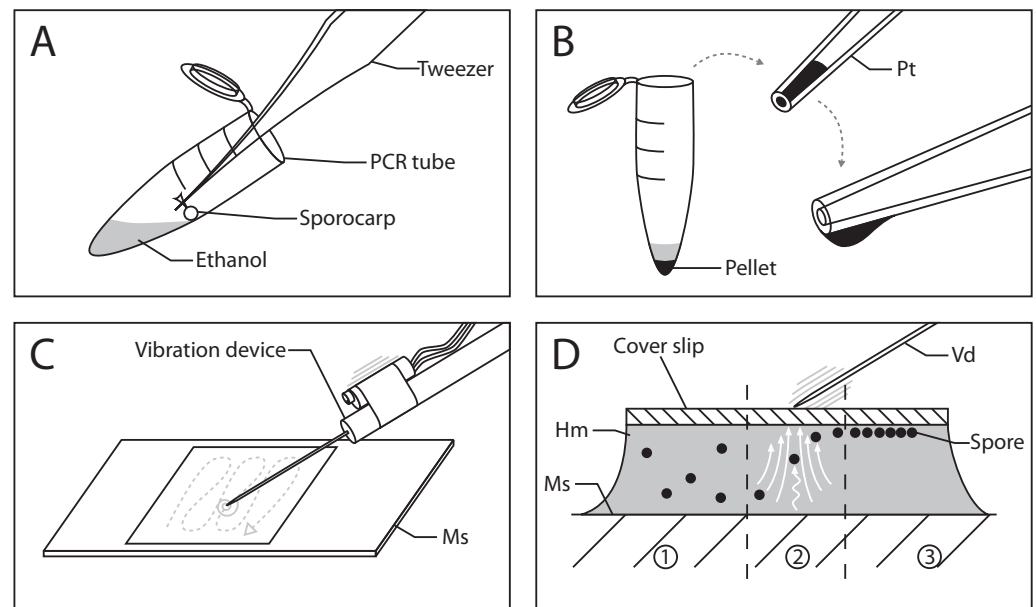


Figure 1 Workflow for spore preparations from *Physarum albescens* sporocarps for quantitative measurements. (A) Step 1: spores are suspended in 20 μ l ethanol and centrifuged. (B) Step 2: The pellet containing the spores is transferred to a slide using a pipette tip; the formation of a hanging drop facilitates the evaporation of ethanol to further concentrate the spore suspension before placing it on the slide. (C) Step 3: The spores are arranged in a single layer with an oscillating preparation needle connected to a vibration device. (D) Alignment of spores under the influence of granular convection induced by the vibration device: 1 - untreated spores, 2 - spores under granular convection (white arrows), 3 - spores arranged in a monolayer beneath the coverslip. Abbreviations: Hm, Hoyer's medium; Ms, microscope slide; Pellet, pellet containing spores; Pt, pipette tip; Vd, vibration device.

Full-size [DOI: 10.7717/peerj.12471/fig-1](https://doi.org/10.7717/peerj.12471/fig-1)

tube and dipping the sporotheca into the ethanol at the edge of the liquid. This reduced the risk of submerging and losing significant parts of the capillitium and peridium.

After brief centrifugation (1 min), the supernatant in the PCR tube was removed with a 20 μ l pipette tip by capillary forces until the ethanol barely covered the pellet, which was subsequently resuspended. The remaining volume of this concentrated spore suspension must be sufficiently large to be able to transfer it to a microscope slide with a pipette. Slow ejection from the pipette produces a hanging drop so that ethanol can evaporate, resulting in further concentration of the suspension (Fig. 1B). This step is crucial since the ethanol needs to evaporate to the point where no excess liquid is visible when transferring the spores to the slide next to a drop of Hoyer's medium. The spore mass should be moist, similar in consistence to mud. A spore droplet containing too much liquid will cause the suspension to spill out, rather than being mounted into the medium on the slide. Finally, a coverslip was carefully placed on the deposited droplet, which resulted in a dense spore cluster when the spore suspension and Hoyer's medium mix.

Vibration was used to disperse the spores in a monolayer. We used a device consisting of a preparation needle attached to a resonance speaker (impedance and power output: 4 Ω by 25 W, no specific manufacturer) connected to a 25 W amplifier (LEPY LP-VS3, Supplement 2).

The shaft of the preparation needle is fixed to the shock rod of the resonance speaker by hand or small 3D-printed clamp (Supplement 3). The amplifier is connected to a laptop over the headphone jack or auxiliary port. A frequency signal generator application on the laptop, accessed *via* an internet browser (e.g., <https://www.wavtones.com/functiongenerator.php>), can be used to generate and control the vibration frequency of the resonance speaker. We initially used 400–600 Hz (sinus wave type) for a pre-alignment of our spores and increased the frequency to 800–1,000 Hz for fine adjustment. Ideally, this sorts the spores into a single layer, thus arranging them at the same height in the z-plane. The pre-alignment and fine adjustment steps each took 1–2 min. The volume regulation on the amplifier and laptop can be used to increase the force of the vibrations. In our configuration, we used 60–80% of the amplifier’s volume and 100% on the laptop.

By applying vibrations generated by this device on the coverslip *via* the needle (Fig. 1C and Supplement 3), a granular convection is induced within the medium. As a result, the spores start to move upwards and align beneath the coverslip (Fig. 1D). Two fingers should hold the coverslip in place during the vibration treatment. Since the vibration only affects a small area around the needle, the vibrating needle is moved over the entire area of the coverslip in a tapping motion to align as many spores as possible (Fig. 1C, gray dashed line). This determines the number of spores that can later be analyzed. The entire process can be monitored under a dissecting microscope. In addition to frequency, vibrations can be adjusted by the pitch angle, roll angle of the device, and the pressure applied to the coverslip.

Image acquisition and ImageJ pipeline

Microscopic images (resolution $2,880 \times 2,048$ pixels) were acquired with a Nikon Eclipse 90i compound microscope in the brightfield mode under twentyfold magnification ($0.12 \mu\text{m}/\text{pixel}$ on the object plane). The camera system was a Nikon DS-Fi3 with a $1/1.8''$ CMOS-color sensor and a pixel size of $2.4 \mu\text{m}$. The pixel intensity of the background was set to 90% of the maximum for all three color channels to provide consistent images for the automated segmentation process. For the same reason, the deconvolution function was switched off. The “large-images”-mode of the microscope software (NIS-Elements AR, Version 5.02.03) was used to automatically acquire 144 (12×12) single unstitched images. The overlap was set to the lowest possible value to prevent repeated measurements of the same spores at the edges during the subsequent image analysis. The software was set to automatically refocus after every fourth image.

We used ImageJ (version 1.52p) to automate most image processing and analysis steps. ImageJ offers options to use various computer languages. We used mainly Python-based commands on a desktop system with 12 GB RAM and a 3.6 GHz Intel Core i7-7700 processor without GPU processing.

Several subsequent scripts were written to organize, process and later analyze the raw images (Table 1, <https://github.com/JanWoyzi/Sporesize-Measurement>). Spores were counted and sized in ImageJ using the built-in function “Analyze Particles” (Paana.py, Table 1) or the plug-in “Ellipse Split” (Elli.py, Table 1, version 0.4.0, Wagner & Eglinger, 2017). Both functions work by counting and measuring pixels on a binary image,

Table 1 Scripts used for image analysis. Underlining indicates scripts crucial for the analysis. The column D/S indicates whether calculations are performed on a desktop computer (D) or server (S).

Script name	D/S	Script function
<u>IScore.py</u> v1.0	D	Assesses background intensities (calculates a score for background intensity by mixing RGB values into a grayscale; figure must be comparable for all images)
<u>BScore.py</u> v2.0	D	Calculates a score for spore density from the brightness of the total area covered by spores
CreatingDir.py v2.0	S/D	A script designed to build directories for scripts (for instance, Elli.py) that cannot create them automatically
<u>Structurefilter.py</u> v3.0	S/D	Detects edges of and sharp angles between objects to separate them by a regional watershed line; the result is an image with overlaid separation lines between spores; necessary for handling images with high spore density
<u>Weka.py</u> v3.2.33	S/D	Machine Learning algorithm, works with a pre-trained model to recognize objects (as differently colored patches of pixels); the result is a classification probability of each pixel as spore or background (more than two classes can be defined as well); this is presented as a stacked image (one for each class)
Destacker.py v4.0	S/D	Separates the WEKA segmentation stack (here two classes, i.e., spores and background) and saves the respective results
<u>Paana.py</u> v6.0	S/D	Particle Analyzer, analyzes spore shapes, describes features like circularity, roundness, etc. (does not use a pre-defined shape, therefore more sensitive but requires precise segmentation)
<u>Elli.py</u> v2.0	D	Ellipse Split plugin (alternative algorithm to Paana.py), analyses the spore shapes according to a pre-defined ellipsoid shape (less sensitive to a particular shape, since measurements are based on approximated ellipses), more robust in case of segmentation errors
RGBROI.py v2.0	S/D	Extracts area-related object features (e.g., RGB values) by comparison with the raw image

characterizing clusters of pixels to provide detailed information about spore shape and size. In addition, Ellipse Split approximates for each pixel cluster the ellipse that fits best, which was then used to characterize the objects.

We employed a plug-in called “Trainable WEKA segmentation” (version 3.2.33, [Arganda-Carreras et al., 2017](#)) based on Waikato Environment for Knowledge Analysis (WEKA) toolsets with various machine-learning algorithms to perform functions like clustering, classification, regression, visualization, and segmentation. However, other open software for segmentation and classification (e.g., Ilastik, described in [Berg et al., 2019](#)) can be used as alternatives to WEKA. We chose WEKA because it could be easily implemented in our script workflow with ImageJ without using too many different software applications.

To train the tool, the user takes an example image and visually marks about 10 target objects (spores) and non-target objects (background) on an exemplary sample image. Additional classes of objects (e.g., branches of the capillitium or remains of hyphae) can be defined to delimit contaminations, but this approach will increase error rates when

separating the target objects from the background. For most applications, it will be more effective to exclude these objects at a later stage of the analysis. The best segmentation results in terms of processing time per image were achieved with small and straightforward models and fine-tuned filter sets. Not only can the number of segmentation classes and filter sets be adjusted, but the complexity of the decision tree can also be freely modified. Our model has only two segmentation classes and uses a minimum of filter sets (see Github repository). After a few iteration steps, after which the user can correct the decisions made by the algorithm, the result can be saved as a model to be applied to additional images in a batch process.

Figure 2 shows the entire segmentation process for a few spores. A consequence of high spore densities on the images (Fig. 2A shows a small section) is that segmentation with the WEKA plug-in generated spore clusters. These clusters could not be resolved by standard watershed methods (Soille & Vincent, 1990), which would falsely identify two adjacent spores as a single object. To prevent such false assignments, we created an overlay of each image where lines one-pixel wide and in background color separate the individual spores. The separating lines were computed by combining the plug-ins “FeatureJ” (version 3.0.0, Meijering, 2015) and “BioVoxxel” (version 12, Brocher, 2012). “FeatureJ structure” calculates for each pixel the eigenvalue of its structure tensor. For two spores that touch each other, the pixels in the two areas in the acute-angled corners have the highest eigenvalues. The function “Watershed Irregular Features” was used to connect only the center points of areas that are close enough to belong to adjacent spores, using a pre-defined maximum radius as a criterion. The resulting connected lines (Fig. 2B) were overlaid on the raw images, separating spores in high-density areas, and were successfully segmented by the WEKA plug-in (Fig. 2C). Figure 2D shows the result of the subsequent analysis with the Ellipse Split tool. The fitted shapes for each spore (green circles in Fig. 2D) are then subject to further analysis. The script can run in batch mode to process a series of images for just one or many specimens.

Initial tests and the segmentation problems encountered with images characterized by high spore densities revealed the need for a robust approach to estimate spore densities on the images. This approach was then used to exclude critical images where high spore densities would lead to erroneous measurements or, conversely, very low densities would lead to errors in some analysis functions in ImageJ. We established the proxy “BScore” to measure the overall brightness of the entire image. Due to the dark spores and white background under brightfield conditions, high spore densities lower the overall brightness. By delimiting the two extreme conditions, no spores *versus* spores filling (nearly) the entire field, the approximate boundaries can be set and used as filters both during the segmentation step and later during the statistical analysis.

Figure 3 shows a slide with a high spore density in the center, illustrating subsequent segmentation problems. To eliminate such cases, two scripts for image analysis were created (Github repository). The first, called IScore, uses the background intensity of an image as a proxy to ensure consistent image acquisition. The second, named BScore, generates a proxy value for spore density based on which images with extremely high spore densities are identified and discarded (Fig. 3). Critically low BScores result from massive spore clusters

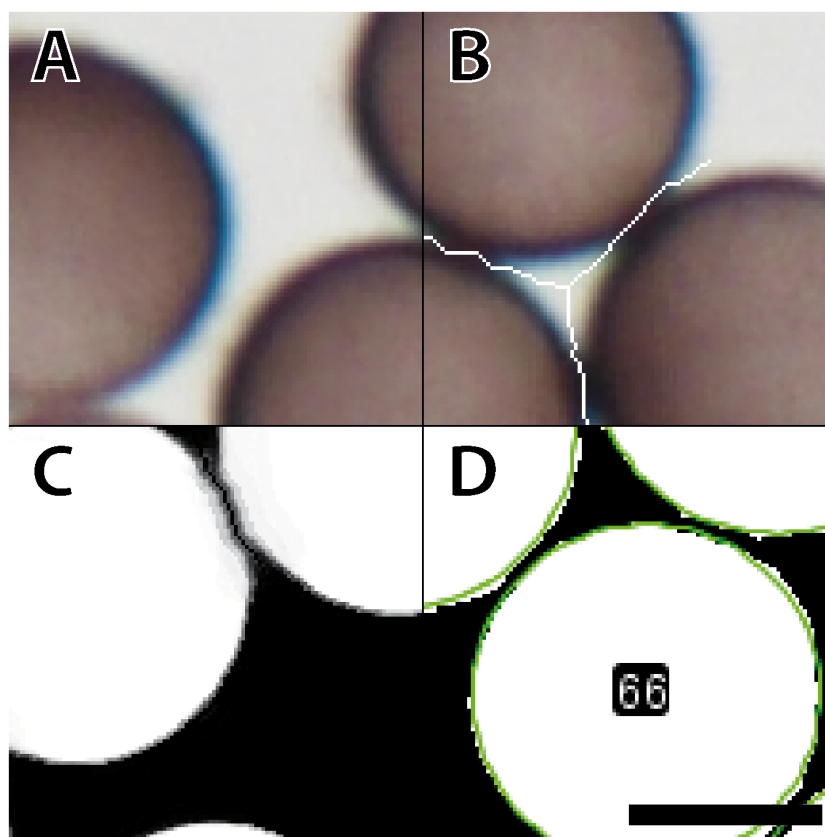


Figure 2 Workflow for image processing of *Physarum albescens* spores. (A) Raw image, (B) structure filter applied, (C) segmented image, and (D) spore shapes selected with the procedure “Ellipse Split”; at this stage an ID is given to every single spore (example: no. 66). These operations are carried out simultaneously on all spores of a given image. Bar = 6 μ m.

[Full-size](#) DOI: [10.7717/peerj.12471/fig-2](https://doi.org/10.7717/peerj.12471/fig-2)

or when spaces between densely packed spores are filled by fine amorphous particles. These situations can be avoided by reapplying the vibration device to spread the spores more evenly and thus limit the number of images to be excluded based on a low BScore (0–2 per slide). [Figure 4](#) and [Table 1](#) show the entire workflow and the respective scripts for the image analysis. The final result is an array of shape features for each object such as area, circularity, aspect ratio and maximum diameter ([Table 2](#)). In addition to determining spore size and shape based on this information, specific regions of interest can be selected for every single spore and be used with the raw images to measure RGB values as a proxy for spore coloration.

Calibration

A range of parameters can be adjusted (e.g., overall spore density, contrast, and homogeneity of background intensities) to distinguish spores from the background and from one another. The arrays summarizing the features of each captured object must be filtered to exclude non-target objects (capillitium, hyphal fragments, air bubbles and amorphous particles;

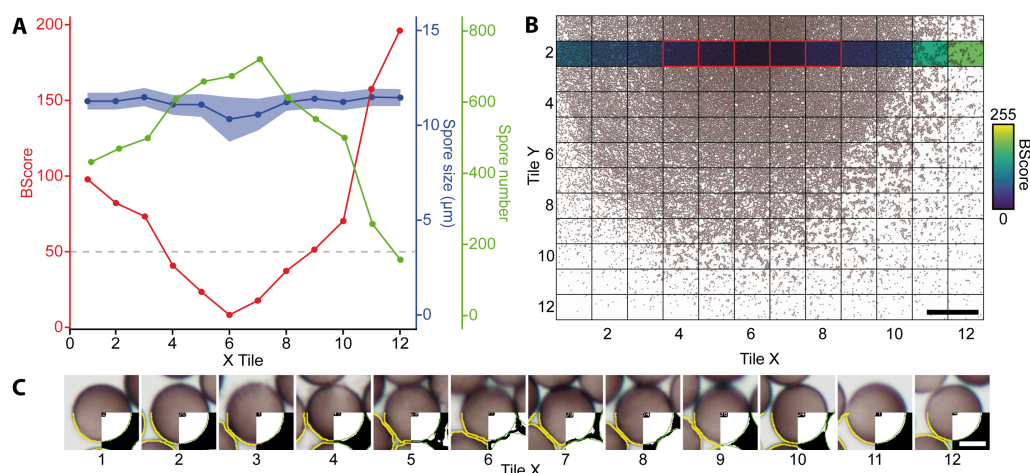


Figure 3 Analysis of a mounted slide shown are the parameters for a belt of 12 images (43,540 spores in total) taken from a slide with varying spore densities. (A) BScores (red line), spore numbers per image (green line), spore diameter (blue line with shaded standard deviation), and threshold for excluding an image based on the BScore (gray dotted line). (B) Overview of a slide showing spore densities on 144 stitched images (bar = 500 μm); the second row with the colored background was selected to generate the graph shown in A. Tiles framed in red have a low BScore and were thus excluded. (C) Examples for watershed-separated spores from 12 images (bar = 6 μm) differing in spore densities; the upper half of each image shows the raw image, the lower left quarter the final selection obtained with the particle analyzer (yellow line), and the lower right corner the final segmentation obtained with the Ellipse split function (green line).

[Full-size](#) DOI: 10.7717/peerj.12471/fig-3

Supplement 4). This can be checked at any stage, since each object can be retrieved with ImageJ by using its unique label or address given by the scripts.

These settings are species-specific and hence need to be adjusted for every new application.

This critically requires measuring many spores with sufficient precision instead of striving for the highest possible precision for just a few spores. Consequently, we used only 20 \times objectives (NA: 0.5, Nikon Plan Fluor), resulting in a resolution of 0.12 $\mu\text{m}/\text{pixel}$. However, higher magnification may have to be used for smaller objects. The most critical step in the process is the slide preparation since spores have to be densely distributed to allow many spores to be photographed at once, but the vibration treatment should aim to arrange all spores in a single plane.

The image acquisition and analysis can be automated, using the same settings for single species or a group of related species. For *Ph. albescens*, we used a light intensity of 225 of 255 scale units, resulting in an exposure time of 15–16 ms, 20 \times magnification, variation of the IScore between images $\leq 10\%$, and a BScore ≥ 50 . The removal of non-target particles can be optimized in an iterative process, based on the compiled array of object features. Useful criteria are particularly the minimum area to exclude small amorphous particles), the aspect ratio to exclude remnants of the capillitium and air bubbles, and circularity or roundness.

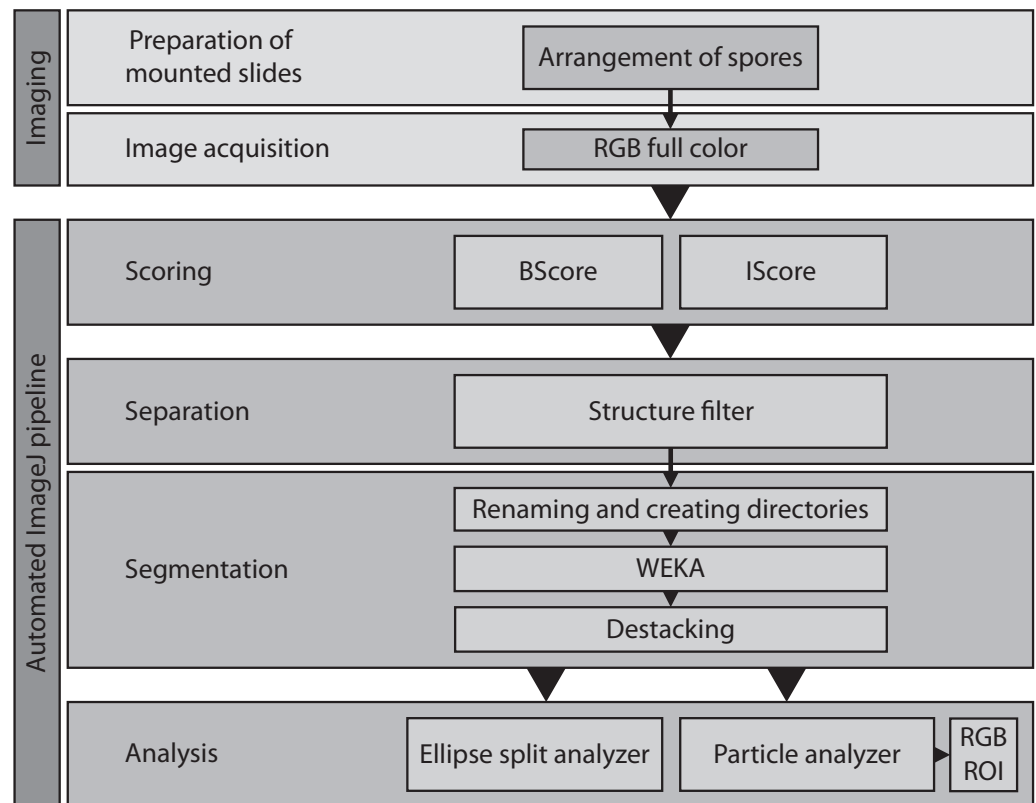


Figure 4 Overview of the entire workflow from sample preparation to data acquisition. See Table 1 for the respective scripts.

Full-size DOI: 10.7717/peerj.12471/fig-4

For *Ph. albescens*, we expected spore sizes between 8 and 15 μm . Therefore, we removed all particles exceeding 1,500 pixels (equivalent to a sphere diameter of 5.25 μm), or showing an aspect ratio >2 or a circularity <0.7 . These settings are likely to be species-specific.

Data analysis

The results of the image analysis (Table 1 and Fig. 4) are saved as csv-files for subsequent analysis with statistical software such as R (R Core Team, 2017). Between 10,000 and 50,000 spores per slide (Supplement 1) were measured and a frequency density plot was constructed. To compare specimens within a region, we calculated the mean absolute deviation (MAD) between specimens as:

$MAD = \frac{1}{n} \sum_{i=1}^n |x_i - \bar{x}|$, where n is the number of data points, \bar{x} the mean of the individual values x_i . To analyze the resulting distribution plots, we calculated a function for each sample with the built-in density function of R to automatically locate all local maxima and minima in the data set. Setting frequencies thresholds allowed us to exclude rare occurrences of non-target objects and classify different types of objects (e.g., amorphous particles, normal-sized spores, oversized spores, large amorphous particles). These object classes can also be fit to different distribution families, in our case the gamma distribution (Supplement 1C).

Table 2 Overview of all measured spore features included in the data set.

Column name	Description
Indiv	Sample name
Label	Complete identification name
Area	Area in pixel
Perim.	Perimeter in pixel
Major	Major axis in pixel
Minor	Minor axis in pixel
Circ.	Circularity = $4\pi \cdot \text{area} / \text{perimeter}^2$
AR	Aspect ratio between major and minor axis
Round	Roundness = $4 \cdot \text{area} / (\pi \cdot \text{major_axis}^2)$
Solidity	Area of a particle divided by its convex hull area
Mean_r	Mean intensity value*
StdDev_r	Standard deviation of the intensity value*
Mode_r	Mode intensity value*
Min_r	Minimum intensity value*
Max_r	Maximum intensity value*
X	Coordinate of the image on the x-axis
Y	Coordinate of the image on the y-axis
Index	Image number within a sample
BScore	Brightness score
Type	Object classification based on size

Notes.

*Recorded for all red, green and blue channels, but shown only for the red channel (r) to avoid repetition.

To compare the performance of our automated approach with that of standard manual measurements, we measured the diameter of 100 randomly selected spores from an image with 520 spores of *Ph. albescens*, specimen Sc29313. To test for the effect of sample size, we compared results obtained for 25, 50, or all 100 spores. A second treatment group with three levels was used to test for precision. These were (1) manual measurement at the standard magnification of 20x, (2) manual measurement at an additional 8x digital zoom, and (3) application of the automated measuring algorithm. For manual measurements, the manually selected vertical distance between spore margins (without ornaments) was measured as spore diameter. We repeated all measurements five times. Additionally, automated measurements of all 520 manually measured spores were compared with those of all 144 images acquired for this specimen (35,176 spores in total). However, the latter two data sets were not included in the statistical test. A linear mixed model was used to test for the main and interactive effects of digital magnification (zoom level), numbers of analyzed spores and repeated measurements (Table 3). A pairwise least-square means *post hoc* test (R package: Emmeans, version 1.6.2-1) with false discovery rate correction (Benjamini & Hochberg, 1995) was applied to identify significant main and interaction effects between pairs. The repeated measurements of spores were treated in the model as a random variable.

Table 3 Results of Type III Analysis of Variance with degrees of freedom calculated according to Satterthwaite's method. Effects of digital magnification (Zoom), spore numbers analyzed, and number of replicate counts and their interactions on spore diameters.

Source of variation	Sum of squares	Mean square	NumDF	DenDF	F	P-value
Zoom	6.10	3.05	2	2481.0	111.22	<0.001
Spore number	0.71	0.35	2	2494.2	12.92	<0.001
Replicate	0.11	0.03	4	2481.0	0.99	0.413
Zoom:Spore number	2.23	0.56	4	2481.0	20.38	<0.001
Zoom:Replicate	0.57	0.07	8	2481.0	2.59	0.008
Spore number:Replicate	0.82	0.10	8	2481.0	3.72	<0.001
Zoom:Spore number:Replicate	1.59	0.10	16	2481.0	3.67	<0.001

Furthermore, we analyzed the spatial distribution of different spore sizes with 25,000 Monte–Carlo simulations of spore position within the 12 by 12 image matrix of sample Sc24902, and calculated Moran's I to assess the spatial displacement effectiveness of the vibration device on different spore sizes.

RESULTS

Spore size distribution

The large number of counted objects made it possible to define extremely narrow size classes, resulting in quasi-continuous distributions for spore size (Fig. 5). The spore size distributions can be approximated by a Gamma function (Figs. 5A–5D, Supplement 1A, Supplement 1C). Altogether we processed 7.5 million spores, on average 31,000 per sporocarp. Diameters ranged between 10.1 (Sc29307, Rocky Mts.) and 13.6 μm (Sc29276, Rocky Mts.) with an overall mean of 11.9 μm . The average standard deviation within a sample (sporocarp level) was 0.48 μm (range 0.33–0.90 μm). The skewness of the approximated Gamma function is a measure of overall spore size uniformity. High positive values indicate the frequent occurrence of oversized spores, as evident in specimen Sc24902 (Caucasus Mts.) with a skewness >0.5 and a bimodal spore size distribution (Type 1: normal-sized spores, Type 2: oversized spores). Colonies from the Kamchatka Peninsula and the Caucasus showed highly uniform and narrow distributions (mean absolute deviation between specimens of 0.35 and 0.32 μm , respectively; Supplement 1D). Colonies from the Rocky Mountains were less uniform (mean absolute deviation of 0.99 μm) and included both the smallest and largest spores of all analyzed strains.

The distribution of spore sizes was asymmetric in many specimens, especially in spores that appeared not to be fully mature (Figs. 5B, 5D). Therefore, the best measure of average spore size was the peak of the fitted Gamma-distribution, rather than the mean diameter (Supplement 1C), which coincides with, or is close to, the modal value, *i.e.*, the size class containing the largest number of objects. Figure 5C shows a case of two co-occurring individuals sampled in a mixed colony of sporocarps, where the spore size distribution of two sporocarps differs from that of the other three.

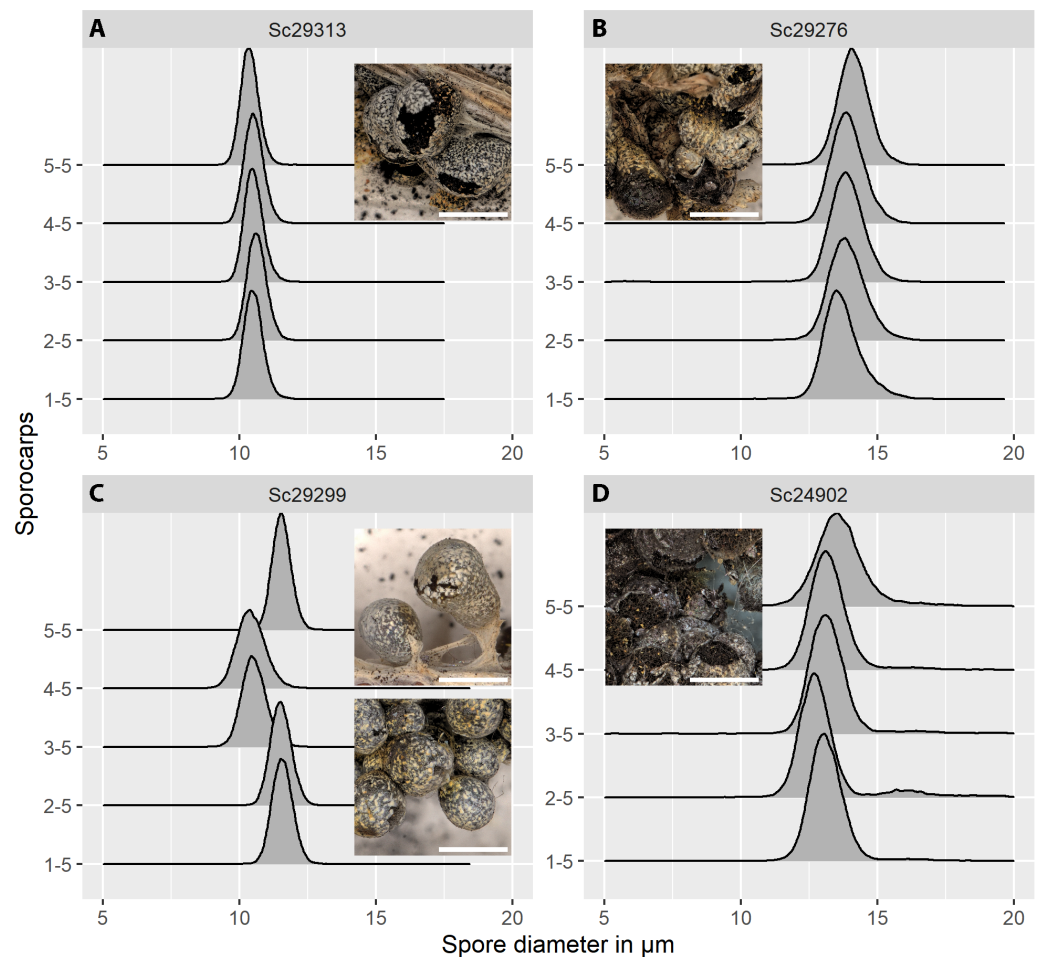


Figure 5 Spore size distributions (black line: density function) for five sporocarps from each of four strains of *Physarum albescens*. (A) Sample Sc29313, well-matured sporocarps. (B) Sample Sc29276, sporocarps nearly mature. (C) Sample Sc29299, a mixed colony with sporocarps belonging to two genetically different individuals (sporocarps 1, 2, and 5 vs. 3 and 4). (D) Sample Sc24902, including a noticeable fraction of oversized spores. Images show the appearance of the respective specimens, note the densely crowded sporocarps with poor calcification in sample Sc24902. Bar = 1 mm (magnification = 20x).

[Full-size !\[\]\(dfbd6b3763a6d1d9afaa974f64e2e4b5_img.jpg\) DOI: 10.7717/peerj.12471/fig-5](https://doi.org/10.7717/peerj.12471/fig-5)

Spore size distributions of some sporocarps, for example, sporocarp 2–5 shown in [Fig. 5D](#) could be fitted to two overlapping gamma functions ([Fig. 6](#)) with two peaks, one for normal-sized and one for oversized spores. The total spore volumes corresponding to the two peaks ($1,013$ and $1,959 \mu\text{m}^3$) were equivalent to a ratio of 1:1.93. A Monte Carlo simulation of Moran's I (25,000 simulations) showed the I-value to be significant (0.69, $p < 0.001$) for normal-sized spores ($12.9 \pm 0.6 \mu\text{m}$ diameter) in the total scanned area (12×12 images covering 12.2 mm^2), indicating clustering. For oversized spores ($15.9 \pm 0.5 \mu\text{m}$ diameter), the I-value was not significant (-0.10 , $p = 0.99$), indicating a random distribution of spores for this size class.

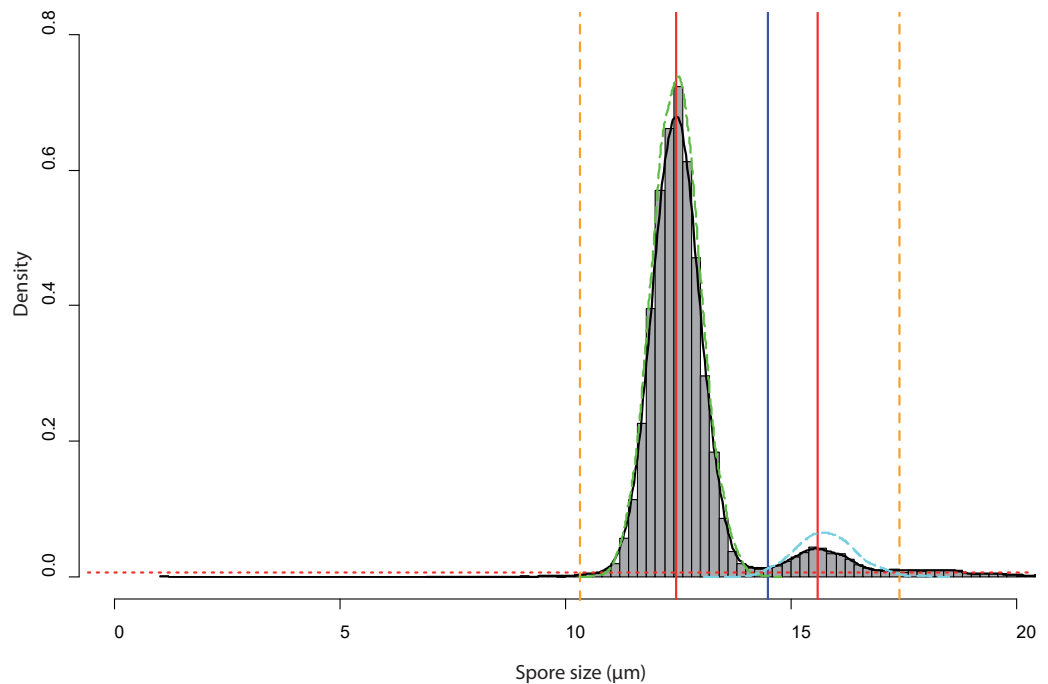


Figure 6 Analysis of the bimodal spore size distribution for Sporocarps 2–5 of *Physarum albescens* specimen Sc24902. The histogram in grey (bin width ca. 0.10 μm) and the density function (black line) displays the spore size distribution. The red dotted horizontal line depicts the threshold at 0.000004 frequency density units and works as a high-pass filter. The vertical blue line shows the minimal local frequency between the two peaks. The red vertical line is the position of the highest frequency. The orange dashed vertical lines indicate the left and right limits of the analyzed interval, which were set as intersects between the thresholds for particle detection and the density function. The green and cyan dashed lines are the density functions of the fitted spore size distribution of the normal-sized and oversized spores, respectively.

Full-size DOI: [10.7717/peerj.12471/fig-6](https://doi.org/10.7717/peerj.12471/fig-6)

Accuracy of the method

Figure 7 shows the results of different manual and automatic measurements of spore size from the same sample. For automated measurements including all images, 95% confidence interval of the means were very small (10.62–10.63 μm , in Fig. 7, last bar), which was consistent with the spore size measurements of various samples (Supplement 1B). This low variation is a direct effect of the large number of objects measured, which also increases the number of extreme outliers (Fig. 7, compare results from 520 spores with those from a total of 35,176 spores sized on 144 images).

A linear mixed model (Table 3) revealed a significant three-way interaction among zoom level, the number of analyzed spores, and repeated measurements ($F(16, 2,481) = 3.63, p < 0.0001$) for spore diameter, indicating that all factors influenced each other, including effects of human error in delineating spore margins. All two-factor interactions were also statistically significant, indicating that the factors in all pairwise combinations influenced each other as well. Differences among zoom levels ($F(2, 2,481) = 111.2, p < 0.0001$) and number of spores analyzed ($F(2, 2,494.2) = 12.9, p < 0.0001$) were highly significant, but not among repeated measurements ($F(4, 2,481) = 0.99, p = 0.41$). The *post*

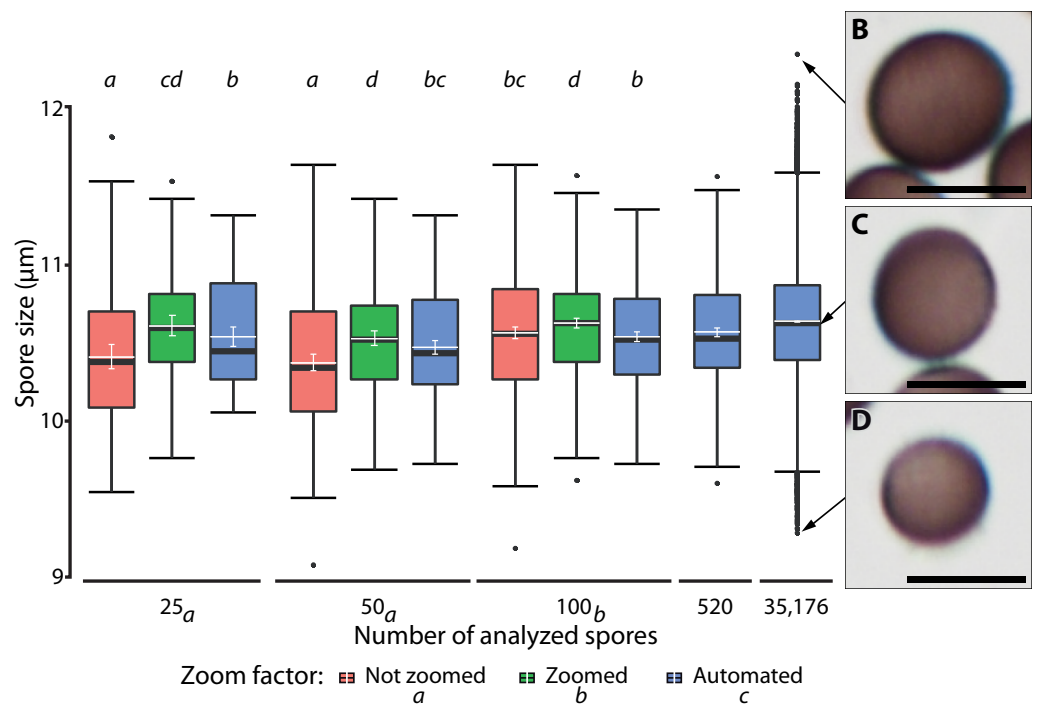


Figure 7 Ranges of spore size for manual and automated measurements. (A) Box plots of spore size in *Physarum albescens* determined by manual and automated measurements (box: 25th to 75th empirical quartiles, black whiskers: 1.5 times the interquartile range, black thick horizontal line: median, dots: single outliers, white horizontal line: mean, white whiskers: 95% CI). Varying numbers of spores were measured on single images (all up to 520 spores) and 144 images (last box, 35,176 spores). Different lower-case letters in the legend indicate significant differences in spore size in pairwise *post hoc* tests between zoom levels. Lower case letters on the upper facet level represent a grouping results of pairwise *post hoc* test according to the numbers of spores measured. Letters on the lower facet level refer to post hoc grouping results for zoom levels grouped by amount levels. (B–D) Examples of individual spores representing (B) upper outliers (oversized spores), (C) average-sized, and (D) lower outliers (unusually small spores), with the arrows pointing to the respective diameter in (A). Bars = 10 μm.

Full-size [DOI: 10.7717/peerj.12471/fig-7](https://doi.org/10.7717/peerj.12471/fig-7)

hoc analysis showed that the measured spore diameter fell into two groups, depending on the number of measured spores. Results for 25 and 50 measured spores were similar and resulted in significantly ($p < 0.001$) smaller spore diameters than for 100 measured spores. Differences among zoom levels were as well significant ($p < 0.0001$). Manual measurements without magnifying the spores with a digital zoom resulted in the smallest mean spore diameters, whereas additional digital magnification produced the largest spore diameters. Automatic measurements resulted in intermediate values. The *post hoc* analysis of significant interaction effects between zoom levels and number of analyzed spores showed that manual measurement without the digital zoom and low spores numbers led to significantly smaller average spore sizes ($p < 0.001$). Regardless of the number of measured spores, all automated measurements grouped with 100 manually measured spores (without zoom) and resulted in intermediate spore sizes (Fig. 7).

DISCUSSION

Spore size is an important taxonomic character in many organisms. Myxomycetes are no exception. Their spores are mostly spherical, rarely ovoid, and ornamented. According to the descriptions given in standard monographs, size varies little within species ($<1\ \mu\text{m}$ in diameter, except for oversized spores) but greatly among species, with sizes ranging from $4\text{--}22\ \mu\text{m}$, although for $>80\%$ of all species the range is narrowed to $7\text{--}12\ \mu\text{m}$ (Schnittler & Tesmer, 2008). This small variation indicates that spore size is under strong evolutionary constraints. The smaller a particle, the greater its dispersal potential (Norros et al., 2014), since its terminal velocity is inversely related to the power of its radius according to Stoke's law. The workflow outlined here assigns a shape to each photographed spore, which allows analyzing subtle differences not only in spore diameter, but also in spore characteristics such as area, perimeter, circularity, and coloration (Table 2).

Accuracy of the method

Manual measurements of small particles such as spores are tedious, even when assisted by an image analysis tool. Proprietary software marketed with expensive high-end microscopes offer suitable working environments to analyze such particles, with many possibilities offered to integrate different machine learning approaches (e.g., ZEN, blue edition of Celldiscoverer 7 from Zeiss, <https://www.zeiss.de/mikroskopie/produkte/mikroskopsoftware/zen.html>; Apeer, also from Zeiss, <https://www.appeer.com/home>; or Leica imaging software, <https://www.leica-microsystems.com/products/microscope-software>). Nevertheless, it remains challenging with manual measurements to correctly determine the major and minor axis of non-spherical spores, like those of most ascomycetes.

Here we present an alternative to manual measurements, aiming primarily to maximize the number of objects measured rather than focusing on high-precision measurements of spore dimensions. The reason for this choice is that variation induced by the biological processes leading to spore formation, such as mitosis or meiosis that influence spore cleavage, is always much greater than measurement errors. Therefore, we used only a 20-fold objective for magnification, although the method would work equally well for higher magnifications. Greater magnification would slightly improve precision but cover significantly fewer spores per image. Thus, the accuracy of our method exceeds that of careful manual measurements and maximizes the number of analyzed spores.

The main qualitative difference of our method compared to manual measurements is that the shape (and color) of each object can be determined separately. This may be achieved by fitting the analyzed objects to a pre-determined shape like an ellipsoid (script Elli.py, Table 1), or by a more flexible procedure (Paana.py) that approximates the real shape of an object. Accuracy of the measurements is critically influenced by the watershed process separating objects that touch each other. This requires spores to be arranged in a monolayer on the slides because overlapping spores cannot be adequately separated. The script BScore.py we used has been designed to ensure this condition is met. Overlapping spores introduce systematic errors by underestimating mean particle size and inflating variation (Fig. 3A, x-tiles 4–8). Consequently, a balance must be found between spore

densities low enough to ensure high accuracy (at the expense of effectiveness) and high enough to increase efficiency (but risking high spore overlap).

Spores of different sizes respond slightly differently to the vibration device we used. The resulting sorting effect leads to a better random distribution of the oversized (Moran's $I = -0.1$, $p = 0.99$) compared to the smaller spores. Larger spores appear to be more susceptible to the applied vibration and move further than the smaller spores (compare Figs. 7B–7D). The high and highly significant I-value (0.69, $p < 0.001$) for normal-sized spores can be explained by the interaction between the highly concentrated spore suspension and Hoyer's medium when placing the cover slip on the suspension. It is thus recommended to analyze numerous images (144 in our case) at different positions of the spore cloud (Fig. 3) to avoid biased sampling. However, the sorting effect is certainly much smaller than the range of biological variation, as also suggested by the similar number of outliers (*i.e.*, extremely small or extremely large objects) in all images analyzed in Fig. 3A.

A third challenge is the exclusion of non-target objects, like capillitium parts in myxomycetes or hyphae in true fungi. This is achieved by defining thresholds for object features such as shape, size, or volume. A big advantage of a microscope-based workflow, such as ours, compared to the use of particle counters is that every single object can be manually inspected. Therefore, the respective filtering procedures can be refined on stored images in several iterative rounds of analysis to improved data reproducibility, independent from any human biases.

Automatic recognition of objects by machine learning

Machine learning algorithms allow fast and reliable object recognition (*i.e.*, separation from a background) in different biological systems such as cell growth in plants (Galotto, Bibeau & Vidali, 2019) or moth species identification (Feng, Bhanu & Heraty, 2016; Feng *et al.*, 2016). The model we trained and integrated into a batch workflow in WEKA is exceptionally fast and can be used with a few single images only. The only strict requirement is that the image acquisition setup (*i.e.*, exposure time, light intensity, etc.) is highly standardized. However, complex tasks like identifying single spores in a tight cluster (touching or overlaying each other) require more elaborate machine learning approaches and cannot be done by WEKA segmentation. As a solution, we developed a vibration-based sample preparation procedure to arrange the objects on a single plane and applied a separation filter by combining the plug-ins “FeatureJ” and “BioVoxel” in ImageJ (see Materials and Methods). The generated segmented objects revealed a number of distinguishing features such as area, circularity, aspect ratio and maximum diameter (see Table 2) for every object and ensured large sample sizes and extremely small confidence intervals (see above). As a result, the estimated median spore sizes in large samples approached the true mean of the entire spore population (Fig. 7A).

Possible applications

Spore size is an important criterion in taxonomy. Therefore, exact measurements may help to identify cryptic biological species (*i.e.*, reproductively isolated sympatric populations), for example in myxomycetes, as found in a number of molecular studies (Feng & Schnittler,

2015; Feng, Bhanu & Heraty, 2016; Feng et al., 2016; Shchepin, Novozhilov & Schnittler, 2016; Dagamac et al., 2017; Janik, Lado & Ronikier, 2020). Figure 5C shows such a case, where colonies of two different phylogroups (i.e., putative biological species) growing together differ in spore size distribution. Furthermore, where fructifications develop rapidly, such as in myxomycetes (often within 1–5 days, Schnittler, 2001), weather conditions may strongly influence spore size. For example, snowbank (nivicolous) myxomycetes like *Ph. albescens* (Ronikier & Ronikier, 2009) develop fructifications under the edges of melting snowbanks where temperatures notably increase within hours (Schnittler et al., 2015). Figure 5B shows less regular size distributions of spores as a possible consequences of such unsuitable environmental conditions, which could be due to impacts on spore cleavage.

Quantitative methods like ours are also suitable to estimate the proportion of oversized spores (“macrospores”). Samples with a significant fraction of oversized spores are fairly common in nivicolous myxomycetes and are often described as forms on their own. Poulain, Meyer & Bozonnet (2011) list macrosporous forms within the genera *Lamproderma* (4 of 22 nivicolous species, plus the enigmatic *L. acanthosporum* with extremely large spores) and *Meriderma* (4 of 8 species with macrosporous forms). Such a case is shown in Figs. 5D and 6, where a population of spores with the roughly twofold volume of normal spores can be distinguished. Quantitative investigations are needed to prove if these macrosporous varieties represent indeed separate taxa. Even more interesting, what is the genetic constitution of such spores? Are they multinucleated (as shown for myxomycetes, Novozhilov et al., 2013), or do they represent restitutional diploid nuclei after an aberrant meiosis? There is evidence that in myxomycetes, meiosis usually occurs after spore cleavage inside the young spores (Clark & Haskins, 2013). If the second hypothesis can be proven, would such nuclei give rise to diploid amoebae and initiate an asexual life cycle, resulting in homothallic clones (Collins, 1979; Collins, 1981)? Apparently, asexual (non-heterothallic) strains (see discussion in Feng, Bhanu & Heraty, 2016; Feng et al., 2016; Walker & Stephenson, 2016) were found in many cultivable myxomycetes (Clark & Haskins, 2010).

Our method can also be used to answer an old question: does genome size influence spore size? For flowering plants, ploidy level (and thus DNA content) is often positively correlated with pollen grain size in polyploid evolutionary lineages of related species (e.g., Katsiotis & Forsberg, 1995; Marinho et al., 2013; Möller, 2018). Although we are not aware of similar studies for myxomycetes, chromosome numbers appear to vary as well, at least within larger groups (Hoppe & Kutschera, 2014), suggesting that such a positive relationship could also exist in myxomycetes.

Our first results on myxomycetes demonstrate that quantitative analyses of spore size and shape may help to answer this and many similar biological questions. Large amounts of spores are often easy to obtain, like crushed sporocarps of myxomycetes, spore prints in mushrooms and ferns, spore bearings in plant parts infected by smuts and rusts, or anthers in flowering plants, which facilitates such investigations.

Limitations of the method

Myxomycetes have nearly spherical spores, unlike many asco- and basidiomycetes. Structures protruding from spores or pollen grains, like bulged germination pores or a hilus where basidiomycete spores were attached to the sterigma, may also cause difficulties. Only for a small fraction of spores, these structures will be situated in the optical plane, and the apparent spore size will hence vary. Fitting objects to a pre-defined structure, like an ellipsoid, may help overcome such problems, because such structures will be ignored when they are situated in the optical plane. A major challenge that remains, however, is to estimate the shape of irregular objects from only one 2D projection.

The analysis of spores with conspicuous ornamentation such as spines (e.g., *Meriderma spinulisporum*) or a reticulum of elevated ridges (e.g., *M. cribrarioides*, Poulain, Meyer & Bozonnet, 2011) requires a more sophisticated machine learning algorithm. In our example, the outer limit of a spore is simply defined as the steepest gradient in contrast. To measure the size of spores with ornamentations being ignored, a mathematical correction for the average extension of the ornaments could be applied. A lack of optical contrast may also be a problem. However, very pale objects can be stained or analyzed by using phase or differential interference contrast. Commonly applied dyes, such as Melzer's reagent for fungi, can solve the problem of poor contrast but may introduce other uncertainties, such as inflated objects (e.g., McKnight, 1968) or altered shapes.

CONCLUSIONS

The quantitative method presented herein allows analyzing a large number of spores that can usually be quantified and sized only by employing expensive equipment. The method is based on the image analysis of monolayered spores in simple slide preparations. It proved highly reliable compared to manual measurements, which enabled us to demonstrate intraspecific variation in the average spore size of different individuals of *Ph. albensens*. A cohort of spores having twice the volume of normal spores could be precisely quantified. Various applications of the method are conceivable, particularly with other spore-bearing organisms.

ADDITIONAL INFORMATION AND DECLARATIONS

Funding

Oleg Shchepin received support from the state task of BIN RAS 'Biodiversity, ecology, structural and functional features of fungi and fungus-like protists' (AAAA-A19-119020890079-6). Funding for this study was provided in the frame of a Ph.D. position for Jan Woyzichowski within the Research Training Group RESPONSE (RTG 2010), supported by the Deutsche Forschungsgemeinschaft (DFG). The funders had no role in study design, data collection and analysis, decision to publish, or preparation of the manuscript.

Grant Disclosures

The following grant information was disclosed by the authors:

The state task of BIN RAS ‘Biodiversity, ecology, structural and functional features of fungi and fungus-like protists’: AAAA-A19-119020890079-6.

The Research Training Group RESPONSE (RTG 2010), supported by the Deutsche Forschungsgemeinschaft (DFG).

Competing Interests

The authors declare there are no competing interests.

Author Contributions

- Jan Woyzichowski conceived and designed the experiments, performed the experiments, analyzed the data, prepared figures and/or tables, authored or reviewed drafts of the paper, and approved the final draft.
- Oleg Shchepin analyzed the data, authored or reviewed drafts of the paper, and approved the final draft.
- Nikki Heherson Dagamac performed the experiments, authored or reviewed drafts of the paper, and approved the final draft.
- Martin Schnittler conceived and designed the experiments, authored or reviewed drafts of the paper, and approved the final draft.

Data Availability

The following information was supplied regarding data availability:

Further and detailed measurements are available in the [Supplemental File](#).

The scripts or data are available at GitHub: <https://github.com/JanWoyzi/Sporesize-Measurement>.

Supplemental Information

Supplemental information for this article can be found online at <http://dx.doi.org/10.7717/peerj.12471#supplemental-information>.

REFERENCES

- Arganda-Carreras I, Kaynig V, Rueden C, Eliceiri KW, Schindelin J, Cardona A, Seung HS. 2017. Trainable Weka Segmentation: a machine learning tool for microscopy pixel classification. *Bioinformatics* 33(15):2424–2426 DOI 10.1093/bioinformatics/btx180.
- Benjamini Y, Hochberg Y. 1995. Controlling the false discovery rate: a practical and powerful approach to multiple testing. *Journal of the Royal Statistical Society, Series B* 57(1):289–300 DOI 10.1111/j.2517-6161.1995.tb02031.x.
- Benyon FH, Jones AS, Tovey ER, Stone G. 1999. Differentiation of allergenic fungal spores by image analysis, with application to aerobiological counts. *Aerobiologia* 15:211–223 DOI 10.1023/A:1007501401024.
- Berg S, Kutra D, Kroeger T, Straehle CN, Kausler BX, Haubold C, Schiegg M, Ales J, Beier T, Rudy M, Eren K, Cervantes JI, Xu B, Beuttenmueller F, Wolny A, Zhang C, Koethe U, Hamprecht FA, Kreshuk A. 2019. Ilastik: interactive machine learning for (bio)image analysis. *Nature Methods* 16:1226–1232 DOI 10.1038/s41592-019-0582-9.

- Brocher J. 2012. BioVoxxel. Available at <http://www.biovoxxel.com/> (accessed on 01 August 2020).
- Brown C. 1960. What is the role of spores in fern taxonomy? *American Fern Journal* 50(1):6–14 DOI 10.2307/1545238.
- Buskey EJ, Hyatt CJ. 2006. Use of the FlowCAM for semi-automated recognition and enumeration of red tide cells (*Karenia Brevis*) in natural plankton samples. *Harmful Algae* 5(6):685–692 DOI 10.1016/j.hal.2006.02.003.
- Clark J, Haskins EF. 2010. Reproductive systems in the myxomycetes: a review. *Mycosphere* 1(4):337–353.
- Clark J, Haskins EF. 2013. The nuclear reproductive cycle in the myxomycetes: a review. *Mycosphere* 4(2):233–248 DOI 10.5943/mycosphere/4/2/6.
- Collins ONR. 1979. Myxomycete biosystematics: some recent developments and future research opportunities. *Botanical Review* 45:145–201 DOI 10.1007/BF02860855.
- Collins ONR. 1981. Myxomycete genetics, 1960–1981. *Journal of the Elisha Mitchell Scientific Society* 97:101–125.
- Dagamac NHA, Rojas C, Novozhilov YK, Moreno GH, Schlueter R, Schnittler M. 2017. Speciation in progress? A phylogeographic study among populations of *Hemitrichia serpula* (Myxomycetes). *PLOS ONE* 12(4):1–22 DOI 10.1371/journal.pone.0174825.
- Feng L, Bhanu B, Heraty J. 2016. A software system for automated identification and retrieval of moth images based on wing attributes. *Pattern Recognition* 51:225–241 DOI 10.1016/j.patcog.2015.09.012.
- Feng Y, Klahr A, Janik P, Ronikier A, Hoppe T, Novozhilov YK, Schnittler M. 2016. What an intron may tell: several sexual biospecies coexist in *Meriderma* spp. (Myxomycetes). *Protist* 167(3):234–253 DOI 10.1016/j.protis.2016.03.003.
- Feng Y, Schnittler M. 2015. Sex or no sex? Group I introns and independent marker genes reveal the existence of three sexual but reproductively isolated biospecies in *Trichia varia* (Myxomycetes). *Organisms Diversity & Evolution* 15:631–650 DOI 10.1007/s13127-015-0230-x.
- Galotto G, Bibeau JP, Vidali L. 2019. Automated image acquisition and morphological analysis of cell growth mutants in *Physcomitrella patens*. In: Cvrčková F, Žárský V, eds. *Plant cell morphogenesis. Methods in molecular biology*. vol. 1992. 307–322 DOI 10.1007/978-1-4939-9469-4_20.
- Göröcs Z, Tamamitsu M, Bianco V, Wolf P, Roy S, Shindo K, Yanny K, Wu Y, Koydemir HC, Rivenson Y, Ozcan A. 2018. A deep learning-enabled portable imaging flow cytometer for cost-effective, high-throughput, and label-free analysis of natural water samples. *Light: Science & Applications* 7(1):1–12 DOI 10.1038/s41377-018-0067-0.
- Hoppe T, Kutschera U. 2014. Chromosome numbers in representative myxomycetes –a cytogenetic study. *Mycological Progress* 13:189–192 DOI 10.1007/s11557-013-0934-2.
- Huang M, Hull CM. 2017. Sporulation: how to survive on planet Earth (and beyond). *Current Genetics* 63:831–838 DOI 10.1007/s00294-017-0694-7.
- Ingold CT. 1965. *Spore Liberation*. Oxford: Clarendon Press, 210 pp.

- Janik P, Lado C, Ronikier A. 2020. Phylogeography of a nivicolous protist *Didymium nivicola* Meyl, (Myxomycetes, Amoebozoa): striking contrasts between the Northern and the Southern Hemisphere. *Protist* 171(6):1–39 DOI 10.1016/j.protis.2020.125771.
- Kamono A, Kojima H, Matsumoto J, Kawamura K, Fukui M. 2009. Airborne myxomycete spores: detection using molecular techniques. *Naturwissenschaften* 96:147–151 DOI 10.1007/s00114-008-0454-0.
- Katsiotis A, Forsberg RA. 1995. Pollen grain size in four ploidy levels of the genus *Avena*. *Euphytica* 83:103–108 DOI 10.1007/BF01678036.
- Korsnes R, Westrum K, Fløistad E, Klinge I. 2016. Computer-assisted image processing to detect spores from the fungus *Pandora neoaphidis*. *Methods* 3:231–241 DOI 10.1016/j.mex.2016.03.011.
- Lado C. 2005–2020. An on line nomenclatural information system of Eumycetozoa. Available at <http://www.nomen.eumycetozoa.com> (accessed on 01 September 2020).
- Leontyev DL, Schnittler M, Stephenson SL, Shadwick LL, Novozhilov YK, Shchepin ON. 2019. Towards a phylogenetic classification of the myxomycetes. *Phytotaxa* 399(3):209–238 DOI 10.11646/phytotaxa.399.3.5.
- Li D-W. 2011. –Five trillion basidiospores in a fruiting body of *Calvatia gigantea*. *Mycosphere* 2(4):457–462.
- Marinho RC, Mendes-Rodrigues C, Bonetti AM, Oliveira PE. 2013. Pollen and stomata morphometrics and polyploidy in *Eriotheca* (Malvaceae-Bombacoideae). *Plant Biology* 16(2):508–511 DOI 10.1111/plb.12135.
- McKnight KH. 1968. Artifacts on spores of Discineae induced by common reagents. *Mycologia* 60(3):723–727 DOI 10.2307/3757447.
- Meijering E. 2015. FeatureJ: an ImageJ plugin suite for image feature extraction. Available at <http://imagescience.org/meijering/software/featurej/> (accessed on 01 September 2020).
- Möller M. 2018. Nuclear DNA C-values are correlated with pollen size at tetraploid but not diploid level and linked to phylogenetic descent in *Streptocarpus* (Gesneriaceae). *South African Journal of Botany* 114:323–344 DOI 10.1016/j.sajb.2017.11.017.
- Neubert H, Nowotny W, Baumann K. 1993. *Die Myxomyceten Deutschlands und des angrenzenden Alpenraumes unter besonderer Berücksichtigung Österreichs. Band 1 Ceratiomyxales, Echinosteliales, Liceales, Trichiales*. Gomaringen, Germany: K. Baumann Verlag DOI 10.1002/biuz.19940240622.
- Norros V, Rannik Ü, Hussein T, Petäja T, Vesala T, Ovaskainen O. 2014. Do small spores disperse further than large spores? *Ecology* 95(6):1612–1621 DOI 10.1890/13-0877.1.
- Novozhilov YK, Okun MV, Erastova DA, Shchepin ON, Zemlyanskaya IV, García-Carvajal E, Schnittler M. 2013. –Description, culture and phylogenetic position of a new xerotolerant species of *Physarum*. *Mycologia* 105:1535–1546 DOI 10.3852/12-284.
- Pollina T, Larson AG, Lombard F, Li H, Colin S, de Vargas C, Prakash M. 2020. PlanktonScope: affordable modular imaging platform for citizen oceanography. *BioRxiv*. DOI 10.1101/2020.04.23.056978.

- Poulain M, Meyer M, Bozonnet J. 2011.** *Les Myxomycètes*. Sevrier: federation mycologique et botanique Dauphiné-Savoie. Sevrier, France: Federation mycologique et botanique Dauphiné-Savoie, 556 pp.
- Punt W, Hoen PP, Blackmore S, Nilsson S, Thomas ALe. 2007.** Glossary of pollen and spore terminology. *Review of Palaeobotany and Palynology* **143**(1–2):1–81 DOI [10.1016/j.revpalbo.2006.06.008](https://doi.org/10.1016/j.revpalbo.2006.06.008).
- Reichenbach H. 1993.** Biology of the Myxobacteria: ecology and Taxonomy. In: Dworkin M, Kaiser D, eds. *Myxobacteria II*. Washington, DC, USA: American Society for Microbiology, 13–62.
- Ronikier A, Ronikier M. 2009.** How ‘alpine’ are nivicolous myxomycetes? A worldwide assessment of altitudinal distribution. *Mycologia* **101**:1–16 DOI [10.3852/08-090](https://doi.org/10.3852/08-090).
- Schindelin J, Arganda-Carreras I, Frise E, Kaynig V, Longair M, Pietzsch T, Preibisch S, Rueden C, Saalfeld S, Schmid B, Tinevez J-Y, White DJ, Hartenstein V, Eliceiri K, Tomancak P, Cardona A. 2012.** Fiji: an open-source platform for biological-image analysis. *Nature Methods* **9**(7):676–682 DOI [10.1038/nmeth.2019](https://doi.org/10.1038/nmeth.2019).
- Schnittler M. 2001.** Ecology of Myxomycetes from a winter-cold desert in western Kazakhstan. *Mycologia* **93**:653–669 DOI [10.1080/00275514.2001.12063197](https://doi.org/10.1080/00275514.2001.12063197).
- Schnittler M, Erastova DA, Shchepin ON, Heinrich E, Novozhilov YK. 2015.** Four years in the Caucasus –observations on the ecology of nivicolous myxomycetes. *Fungal Ecology* **14**:105–115 DOI [10.1016/j.funeco.2015.01.003](https://doi.org/10.1016/j.funeco.2015.01.003).
- Schnittler M, Novozhilov YK, Romeralo M, Brown M. 2012.** Myxomycetes and Myxomycete-like organisms. In: Frey W, ed. *Engler’s syllabus of plant families*. Vol. 4. Stuttgart, Germany: Bornträger, 40–88.
- Schnittler M, Tesmer J. 2008.** A habitat colonisation model for spore-dispersed organisms –does it work with eumycetozoans? *Mycological Research* **112**:697–707 DOI [10.1016/j.mycres.2008.01.012](https://doi.org/10.1016/j.mycres.2008.01.012).
- Schnittler M, Unterseher M, Tesmer J. 2006.** Species richness and ecological characterization of myxomycetes and myxomycete-like organisms in the canopy of a temperate deciduous forest. *Mycologia* **98**:223–232 DOI [10.1080/15572536.2006.11832694](https://doi.org/10.1080/15572536.2006.11832694).
- Shchepin ON, Novozhilov YK, Schnittler M. 2016.** Disentangling the taxonomic structure of the *Lepidoderma chailletii-carestianum* species complex (Myxogastria, Amoebozoa): genetic and morphological aspects. *Protistology* **10**(4):117–129 DOI [10.21685/1680-0826-2016-10-4-1](https://doi.org/10.21685/1680-0826-2016-10-4-1).
- Soille P, Vincent LM. 1990.** Determining watersheds in digital pictures via flooding simulations. In: Kunt M, ed. *Proceedings SPIE 1360, visual communications and image processing ’90: fifth in a series, (1 1990)*. DOI [10.1117/12.24211](https://doi.org/10.1117/12.24211).
- Stephenson SL, Schnittler M. 2017.** Myxomycetes. In: Archibald JM, Simpson AGB, Slamovits CH, Margulis L, Melkonian M, Chapman DJ, Corliss JO, eds. *Handbook of the protists*. 2nd edition. Springer International Publishing: Cham, Germany, 1405–1432.
- R Core Team. 2017.** R: a language and environment for statistical computing. R Foundation for Statistical Computing, Vienna, Austria. Available at <https://www.R-project.org/>.

- Vidal-Diez de Ulzurrun G, Huang TY, Chang CW, Lin HC, Hsueh YP. 2019. Fungal feature tracker (FFT): a tool for quantitatively characterizing the morphology and growth of filamentous fungi. *PLOS Computational Biology* 15(10):1–20 DOI 10.1371/journal.pcbi.1007428.
- Wagner T, Eglinger J. 2017. thorstenwagner/ij-ellipsesplit: ellipseSplit 0.6.0 SNAPSHOT. Zenodo. Available at <http://doi.org/10.5281/zenodo.834339> (accessed on 01 September 2020).
- Wagner J, Macher J. 2012. Automated spore measurements using microscopy, image analysis, and peak recognition of near-monodisperse aerosols. *Aerosol Science and Technology* 46(8):862–873 DOI 10.1080/02786826.2012.674232.
- Walker LM, Stephenson SL. 2016. The species problem in Myxomycetes revisited. *Protist* 167(4):319–338 DOI 10.1016/j.protis.2016.05.003.
- Wijayawardene NN, Hyde KD, Al-Ani LKT, Tedersoo L, Haelewaters D, Rajeshkumar KC, Zhao RL, Aptroot A, Leontyev VD, Saxena RK, Tokarev YS, Dai DQ, Letcher PM, Stephenson SL, Ertz D, Lumbsch HT, Kukwa M, Issi VI, Madrid H, Phillips AJL, Selbmann L, Pfliegler WP, Horvath E, Bensch K, Kirk PM, Kolarikova K, Raja HA, Radek R, Papp V, Dima B, Ma J, Malosso E, Takamatsu S, Rambold G, Gannibal PB, Triebel D, Gautam AK, Avasthi S, Suetrong S, Timdal E, Fryar SC, Delgado G, Reblova M, Doilom M, Dolatabadi S, Pawlowska JZ, Humber RA, Kodsueb R, Sanchez-Castro I, Goto BT, Silva DKA, De Souza FA, Oehl FR, Silva GAd, Silva IR, Blaszkowski J, Jobim K, Maia LC, Barbosa FR, Fiuza PO, Divakar PK, Shenoy BD, Castaneda-Ruiz RF, Somrithipol S, Lateef AA, Karunarathna SC, Tibpromma S, Mortimer PE, Wanasinghe DN, Phookamsak R, Xu J, Wang Y, Tian F, Alvarado P, Li DW, Kusan I, Matocec N, Masic A, Tkalec Z, Maharachchikumbura SSN, Papizadeh M, Heredia G, Wartchow F, Bakhshi M, Boehm E, Youssef N, Hustad VP, Lawrey JD, Santiago ALCMA, Bezerra JDP, Souza-Motta CM, Firmino AL, Tian Q, Houbraken J, Hongsan S, Tanaka K, Dissanayake AJ, Monteiro JS, Grossart HP, Suija A, Weerakoon G, Etayo J, Tsurykau A, Vazquez V, Mungai P, Damm U, Li QR, Zhang H, Boonmee S, Lu YZ, Becerra AG, Kendrick B, Brearley FQ, Motiejunaite J, Sharma B, Khare R, Gaikwad S, Wijesundara DSA, Tang LZ, He MQ, Flakus A, Rodriguez-Flakus P, Zhurbenko MP, McKenzie EHC, Stadler M, Bhat DJ, Liu JK, Raza M, Jeewon R, Nassonova ES, Prieto M, Jayalal RGU, Erdogdu M, Yurkov A, Schnittler M, Shchepin ON, Novozhilov YK, Silva-Filho AGS, Gentekaki E, Liu P, Cavender JC, Kang Y, Mohammad S, Zhang LF, Xu RF, Li YM, Dayarathne MC, Ekanayaka AH, Wen TC, Deng CY, Pereira OL, Navathe S, Hawksworth DL, Fan XL, Dissanayake LS, Kuhnert E, Thines M. 2020. Outline of fungi and fungus-like taxa. *Mycosphere* 11(1):1060–1456 DOI 10.5943/mycosphere/11/1/8.
- Woo C, An C, Xu S, Yi S-M, Yamamoto N. 2018. Taxonomic diversity of fungi deposited from the atmosphere. *International Society for Microbial Ecology Journal* 12:2051–2060.

3.4 High environmental induced plasticity in spore size and numbers of nuclei per spore in *Physarum albescens* (Myxomycetes)

Jan Woyzichovski^{a1}, Oleg N. Shchepin^{a,b}, Martin Schnittler^a

^aInstitute of Botany and Landscape Ecology, Greifswald University, Soldmannstr. 15, 17487 Greifswald, Germany

^bKomarov Botanical Institute of the Russian Academy of Sciences, Laboratory of Systematics and Geography of Fungi, Prof. Popov Street 2, 197376 St. Petersburg, Russia

Corresponding author:

Jan Woyzichovski, Soldmannstr. 15, 17489 Greifswald, Germany

Email address: jan.woyzichovski@uni-greifswald.de

Manuscript submitted 19 February 2022 in *Protist*.

High environmentally induced plasticity in spore size and numbers of nuclei per spore in *Physarum albescens* (Myxomycetes)

Jan Woyzichovski^{a1}, Oleg N. Shchepin^{a,b}, Martin Schnittler^a

^aInstitute of Botany and Landscape Ecology, Greifswald University, Soldmannstr. 15, 17487 Greifswald, Germany

^bKomarov Botanical Institute of the Russian Academy of Sciences, Laboratory of Systematics and Geography of Fungi, Prof. Popov Street 2, 197376 St. Petersburg, Russia

¹Corresponding author.

email jan.woyzichovski@uni-greifswald.de (J. Woyzichovski)

Abstract

Plasmodial slime molds (Myxomycetes) belong to the spore-dispersed groups within protists, and spore size is an important taxonomic character. By analyzing brightfield and fluorescent images of DAPI-stained spores with machine learning-based algorithms, we recorded the size and the number of nuclei for several thousand spores in multiple accessions of the nivicolous myxomycete *Physarum albescens*. Several biological species from different mountain ranges of the Northern Hemisphere were included. Spore size was constant within the sporocarps of one colony (mean variation 0.4 μm , 1.5%), but highly variable between accessions (10.6–13.5 μm , 10%) even within clonal groups of specimens (8%). ANOVA revealed most of this variation to be explained by the locality (accession: 32.7%; region: 21.4%), less by biospecies (13.5%), whereas the contribution of intra-colony variation was negligible (<0.1%). Spore size shows high phenotypic plasticity, and differences of 1 μm in spore diameter, as claimed to be decisive in determination keys for myxomycetes, appear to be of limited taxonomic value. Spore size distribution showed narrow peaks, and spores were mostly uninucleate. Two rare aberrations occur: 1) multinucleate spores and 2) oversized spores with a double or triple volume of normal spores. Both aberrations are not related to each other or limited to certain biospecies.

Keywords DAPI staining; particle analysis; spore diameter; spore size distribution; wind dispersal

Introduction

Besides the Arcellinida (Thecamoebae) with their intricately structured husks (Lahr 2021) the plasmodial slime molds (Myxomycetes, Stephenson & Schnittler 2017) are one of the few protist groups with a well-developed morphological species concept, used even in recent monographs (Neubert et al. 1993, 1995, 2000; Poulain et al. 2011). More than 1000 species have been described up to date (Lado et al. 2005–2022). As a result of ca. 200 years of research based on records of the fructifications, which can be stored as herbarium specimens, a solid body of data on their worldwide distribution at the level of morphological species is available (Stephenson et al. 2008). The main vegetation zones on earth, different continents (Dagamac et al. 2017a), but even more microhabitats (like litter, decaying wood, or tree bark) show clearly different species assemblages (Schnittler et al. 2021).

Molecular investigations within the last decade revealed that most of these morphologically defined species seem to be complexes of cryptic species, and now a number of case studies are available (*Badhamia melanospora*, Aguilar et al. 2014; *Trichia varia*, Feng & Schnittler 2015; *Meriderma* spp., Feng et al. 2016; *Tubifera ferruginosa*, Leontyev et al. 2015; *Hemitrichia serpula*, Dagamac et al. 2017b). In each case, the respective species shows an unexpected diversity in ribosomal 18SrRNA sequences, used as the primary barcode marker in myxomycetes (Schnittler et al. 2017, Borg Dahl et al. 2018). If a second marker was studied, recombination was restricted within groups of specimens which can thus be called putative biological species. In some cases, they do not show morphological differences (*Trichia varia*), in others they slightly (*Hemitrichia serpula*) or more pronouncedly (*Tubifera ferruginosa*) differ in morphological features and are sometimes, but not always (Aguilar et al. 2014, Janik et al. 2020, 2021), geographically separated. This has led to a renewed interest in classical morphology-based taxonomy. In all monographs, spore size is consistently given as one of the most important characters to distinguish species. Given the fact that the terminal velocity of spores (Tesmer & Schnittler 2007) is heavily influenced by spore size as to expect according to Stoke's Law, this should be a character under strong selective pressure.

In addition, the number of nuclei per spore might influence spore size, their terminal velocity and thus colonization ability, as explained in a model (Schnittler & Tesmer 2008). This is governed by the mating types of myxomycetes, which were detected already in classical experiments with the few easily cultivable species, like *Physarum polycephalum* or *Didymium iridis*, in the 1970s (Collins 1979, 1981). The rule in myxomycetes is heterothallism: only amoebae that are not

descendants from the same clone will mate (Clark & Haskins 2010), which leads according to the "textbook life cycle" (Stephenson & Schnittler 2017) to a diploid plasmodium. A second precondition for successful mating seems to be a certain density of amoebae, making them sexually competent (Clark & Haskins 2016). The diploid plasmodium gives rise to fruitbodies developing wind- or animal-dispersed spores (Alexopoulos, 1963; Gray et al. 1968; Ing, 1994; Kamono *et al.*, 2009), and this process is connected with a meiosis. Older literature includes numerous studies about meiosis based on light-microscopical observations, and these often report synaptonemal complexes in young spores (Clark & Haskins 2013). After meiosis, all but one of the four nuclei degenerate, as found for *Physarum polycephalum* (Laane & Haugli 1976), leading to haploid uninuclear spores. Restitutional fusion may exceptionally restore diploid nuclei and enable automictic lineages, which explains the existence of homothallic strains often found in culture studies (reviewed in Clark & Haskins 2013). For heterothallic strains, spores in this "post-cleavage" model initially include diploid nuclei, with both mating types. As to expect for the always heterozygous loci carrying the mating types, one sporocarp should have spores of complementary mating types in a 50:50 ratio if random survival of post meiotic nuclei is assumed. Spores that accidentally include two haploid nuclei of different mating types should have a colonization advantage, since a single spore entering a new habitat island could germinate with two amoebae which later can mate (Schnittler & Tesmer 2008). The disadvantage of binucleate spores would be that they are heavier and perhaps larger, if we assume a correlation between the number of nuclei and the amount of cytoplasm included in a spore. This results in a higher terminal velocity and a lower dispersal ability (Tesmer & Schnittler 2007). In addition, descendants from such a binucleate spore should suffer from inbreeding, essentially rendering the mating types non-functional. Although most studies based on electron-microscopy support the "post-cleavage model", Clark & Haskins (2013) review as well light-microscopic support for a "pre-cleavage" model. Here, meiosis takes place in the plasmodium, and each of the resulting haploid nuclei forms a spore. This would again result in a haploid uninuclear spore. However, here as well, two nuclei may accidentally be included in a spore, with similar consequences as in the post-cleavage model. Regardless of the meiosis model, first mitotic divisions may take part already before a spore germinates. If spores become multinucleated this way, they would give rise to genetically identical amoebae and would thus not enjoy a colonization advantage. In this case, however, multinucleate spores with post-mitotic nuclei should not be larger than uninucleate ones.

But how stable is spore size and the number of nuclei included in "wild" populations of myxomycetes? To answer this question, we studied spores of different accessions of the nivicolous myxomycete *Physarum albescens* Ellis ex T. Macbr. quantitatively. It is a typical member of the dark-spored clade of the Mycetozoa (Leontyev et al. 2019) and occurs predominantly in humid mountain ranges of the Northern Hemisphere (Dagamac et al. 2021). The guild of nivicolous myxomycetes, discovered first by Meylan (1908), forms fruit bodies under the melting snow, which often emerge with snowmelt. Members of the guild fruit most commonly but not exclusively in mountains (Roniker & Ronikier 2009). Fructifications mature during the snow melt, and environmental conditions change rapidly over a short time (Schnittler et al. 2015). *Ph. albescens* is genetically diverse and includes numerous putative biological species that are probably reproductively isolated (Shchepin et al. 2021). Perhaps due to spore dispersal, only some but not all of these biospecies show a clear-cut geographical pattern, as found for non-sporulating testate amoebae (Singer et al. 2019) and occur often sympatric. Genetic patterns, as resolved with Sanger sequencing of three different markers and genotyping by sequencing, revealed a predominance of sexual reproduction, although geographically isolated putative clones were as well found.

We used the accessions of *Ph. albescens* investigated in Shchepin et al. (2021) to answer three questions: 1) How constant is the spore size (i) within a colony of sporocarps, (ii) within a group of colonies constituting a clone and (iii) within a biological species? 2) Is there a relation between the number of nuclei and the spore size? 3) How common are multinucleate spores, and does their occurrence follow a recognizable pattern?

Results

Spore size and nucleus counts

Altogether, 103 sporocarps of *Ph. albescens* from 39 accessions (Supplementary Material Table S1) were measured for spore size (Supplementary Material Table S2), with 27 accessions analyzed for three or more sporocarps. The number of spores successfully counted reached from 892 to 43,353 per sporocarp (mean value 14,857). In addition, 21 sporocarps from 15 accessions could be analyzed as well for the number of nuclei per spore (Fig. 1). If discernible spore populations exist, recognizable by multimodal distribution patterns, only the one with the smallest (and always most numerous) spores was considered for mean spore size.

Fig. 1 shows examples for the two corresponding images used for the measurement process, visualizing spores of slightly different sizes and different numbers of nuclei occurring within one specimen.

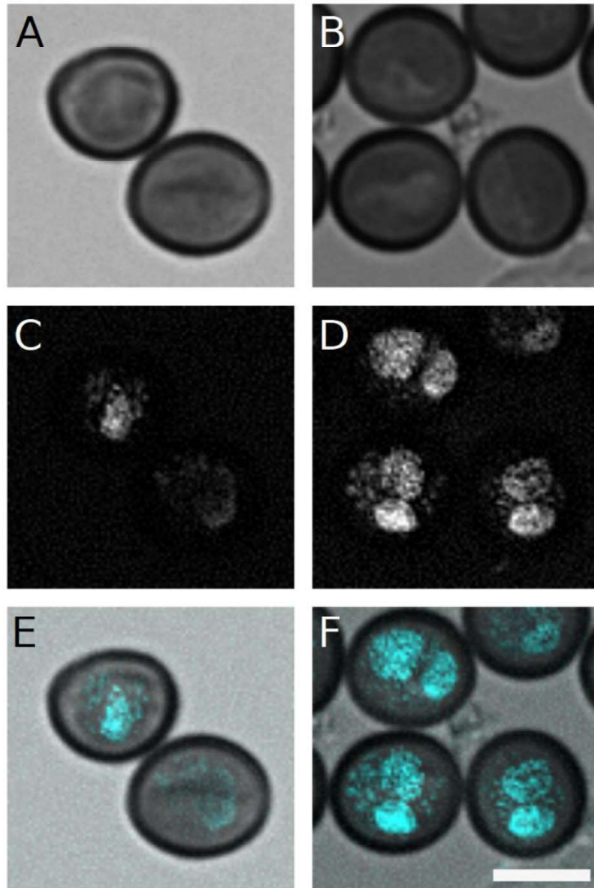


Figure 1. Example for sections of pairs of corresponding images for simultaneous assessment of spore diameter and number of nuclei per spore in accession Sc30211: **A, B** bright field, **C, D** fluorescent light (DAPI) and **E, F** digitally merged images indicating DAPI fluorescence in cyan. In **C** and **D**, examples of diffuse (background) fluorescence can be seen, but as well sharply delimited fluorescence, indicating the presence of a nucleus. Images **A, C, E** shows examples of uninucleate spores, images **B, D, F** depict binucleate spores. Bar: 10 μ m.

On average, 84,4% of all spores captured in an image were measured (spores that were not too close to the margin). For selected specimens, this number was lower when spores were measured

and counted for nuclei simultaneously (68.9%). The obtained figures (see Supplementary Material Table S2) were used for all following analyses.

Performance of the machine-learning algorithm

Two different models trained for their specific tasks were applied: the one trained for the recognition of spores (bright field, spore model) and the other for the recognition of nuclei (fluorescent images, nucleus model). Both models performed rather stably over a wide range of intersection over union (IoU) thresholds (Supplementary Material Figure S3). For the spore model, an IoU threshold of 0.5 was used with a non-maximum suppression threshold of 0.3. The nucleus model ran under 0.5 and 0.4 IoU, respectively. A stable and high performance could be reached for the spore model over a range of 0.1 to 0.8 IoU, while for the nucleus model the performance began to visibly decrease above an IoU of 0.5. With IoU = 0.5, the spore model reached a precision of 99%, a recall of 91%, and an F1-score of 0.94; the nucleus model performed best at IoU = 0.3 with figures of 90%, 90%, and 0.91, respectively.

The spore model performed nearly instantly well and could separate a single spore in a densely packed environment in most cases without a problem. The nucleus model had to be improved by increasing the training dataset further and expanding the different training cases drastically, like haziness, different low intensities, damaged and degraded nuclei, including cases with different concentrations of mitochondrial (background) DNA in spores. Even though the StarDist algorithm uses semantic segmentation, false segmentation of overlapping spores was almost completely avoided due to the mounting procedure spreading the spores evenly under the cover slip.

Fluctuations in spore size

If we look only at the average spore size (based on all objects identified by the spore model as spores), the range of average spore size reaches from 10.64 μm (sporocarp 1, Sc26413, Ile Alatau, Kazakhstan) to 13.54 μm (sporocarp 1, Sc29276, Rocky Mountains, USA) in the morphospecies *Ph. albenscens*. Range of mean spore size within the three sporocarps measured for the same specimen is between 0.07 and 1.42 μm , with a mean range of 0.40 μm (27 accessions analyzed for three or more sporocarps). If expressed as percent of the mean size, the intra-colony variation ranges from ± 1 to $\pm 5\%$ (average $\pm 1.5\%$). Fig. 2 visualizes mean spore size for all measured accessions.

The average width of the spore size distributions, expressed as multiples of σ , ranges between 0.22 μm and 1.68 μm , with an average of 0.42 μm . A correlation test between the mean spore size of each accession and their standard deviation showed a significant correlation ($r = 0.45$, $p = 0.004$).

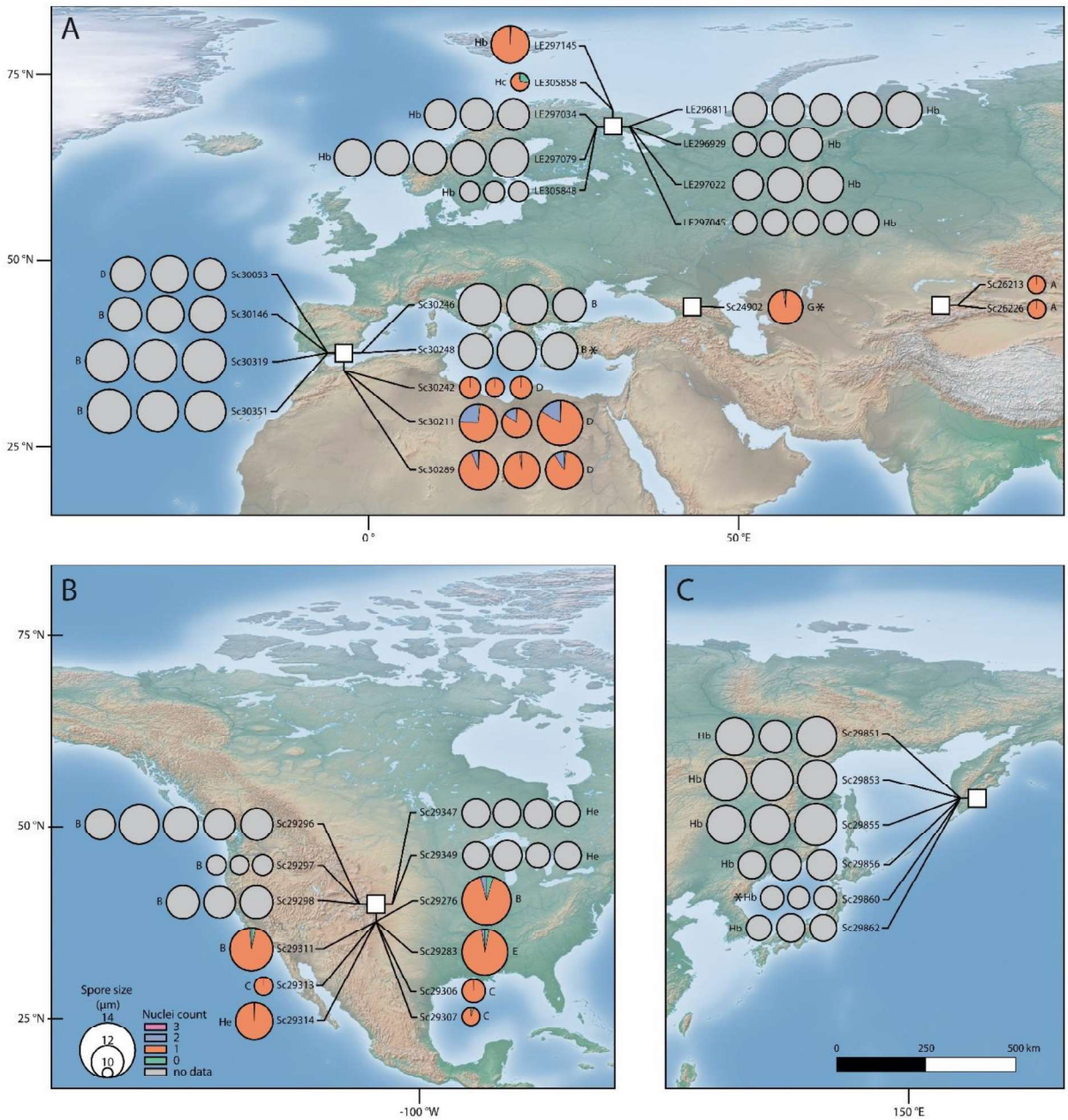


Figure 2. Map of the Northern Hemisphere showing the origin of all accessions analyzed for spore size (grey circles) and the number of nuclei (colored pie diagrams). Vertical rows of circles / pie diagrams show the accessions analyzed from one region, and horizontal rows show sporocarps for a certain accession. The size of a pie diagram indicates spore size according to the scale given in

the lower-left corner; colored pies indicate the proportion of spores with 0, 1, 2, or 3 nuclei. Rectangles indicate the investigated regions. The letter symbols for each accession correspond to the putative biospecies, according to Shchepin et al. (2021). An asterisk denotes samples with multiple spore populations.

Although some patterns are recognizable, there is a considerable fluctuation within the members of different biospecies. For example, biospecies A (Kazakhstan, Shchepin et al. 2021), as well the most deviating in other morphological characters, has the smallest spores (mean 10.66 μm , two accessions); biospecies E (Rocky Mts.) has the largest (13.38 μm , two accessions). Biospecies C, also from the Rocky Mts., has again small spores than E (10.83 μm , three accessions). Table 1 shows mean figures and variation for the more commonly encountered biospecies: spore size varies 8–10% within a biospecies.

Table 1. Variation in spore size within a biospecies of *Physarum albescens*, shown are results for four biospecies represented by three or more accessions.

Biospecies	Hb	He	B	D
Number of sporocarps				
measured	46	9	30	9
Number of accessions				
measured	14	3	10	3
Spore size				
Min	10.92	11.30	10.73	10.74
Max	12.87	12.43	13.14	13.25
Mean	11.94	11.62	12.31	12.01
SD	0.58	0.34	0.65	0.90
% variation from mean	91–108	97–107	87–107	89–110

To explain variation in spore size of the first spore population, an ANOVA was performed with the factors region, biospecies, accession, and sporocarp (Table 2).

Table 2. Results of an ANOVA for variation in spore size over different mountain ranges, biospecies, accessions and sporocarps. Shown are degrees of freedom (Df), sum of squares and their proportion on total variation, mean squares, F and p-values.

Source of variation	Df	Sum of squares	Mean squares	F	p-value
Region	6	15,934.3 (21.40%)	2,655.71	11,375.66	<0.00001
Biospecies	5	10,048.7 (13.50%)	2,009.74	8,608.65	<0.00001
Accession	27	24,367.7 (32.73%)	902.51	3,865.85	<0.00001
Sporocarp	4	57.5 (0.08%)	14.38	61.60	<0.00001
Residuals	102,957	24,035.9 (32.29%)	0.23		

The respective accession turned out to be the main source for spore size variation, explaining 32.73% of the total observable variation. Another 21.40% were attributed to region, 13.50% to biospecies, and only 0.08% of the total variation was explained by the different sporocarps measured for one accession. About one third (32.29%) of the variation in spore size could not be explained by the four factors. All factors were significantly different ($p < 0.00001$). A *post hoc* analysis (not shown; computed as Tukey's honestly significant difference test) verifies that between each factor, every level of combinations is significantly different, which is caused by the large sample sizes (1000 randomly selected spores were considered). Only much smaller sample sizes (below 50 spores sampled, data not shown) would produce p-values exceeding 0.05.

Spore size varies as well considerably between different accessions belonging to the same clone (Fig. 3). A clone from Kamchatka (collected in 2017, six collections made within a distance of 25 m, biospecies Hb, identical in three genetic markers and GBS profiles, Shchepin et al. 2021) showed a variation of nearly 2 μm in mean spore size, well comparable to the variation in the entire, worldwide data set. Except for accession Sc29851, different sporocarps from the same colony of sporocarps are rather similar in spore size (mean SD 0.14 μm). A type III analysis of variance reveals that the respective accession is the main source of variation in clonal accessions (Table 3), similar to the results for the whole data set (Table 2). After that, additional spatial factors contribute only marginally to explain further the variation in spore size. These spatial factors were assigned to sporocarps regardless of possible order or affiliation to each other within the same accession/colony and should provide additional information for size differentiation on a micro

spatial level. The factor “twig” (the assignment of sporocarps to different twigs of one shrub, regardless of possible order or affiliation to each other within the same accession) provides more variation than the exact position (lower, middle, upper) of the sporocarps on the twig itself. An effect size calculation for these two factors with interpretation rules from Cohen (1992) was performed and showed that for the factor “twig” effect size is rather small ($\eta^2 = 0.07$, CI95: 0.06–0.08), but for the factor “twig position” it is one order of magnitude smaller ($\eta^2 = 0.002$, CI95: 0.002–0.002).

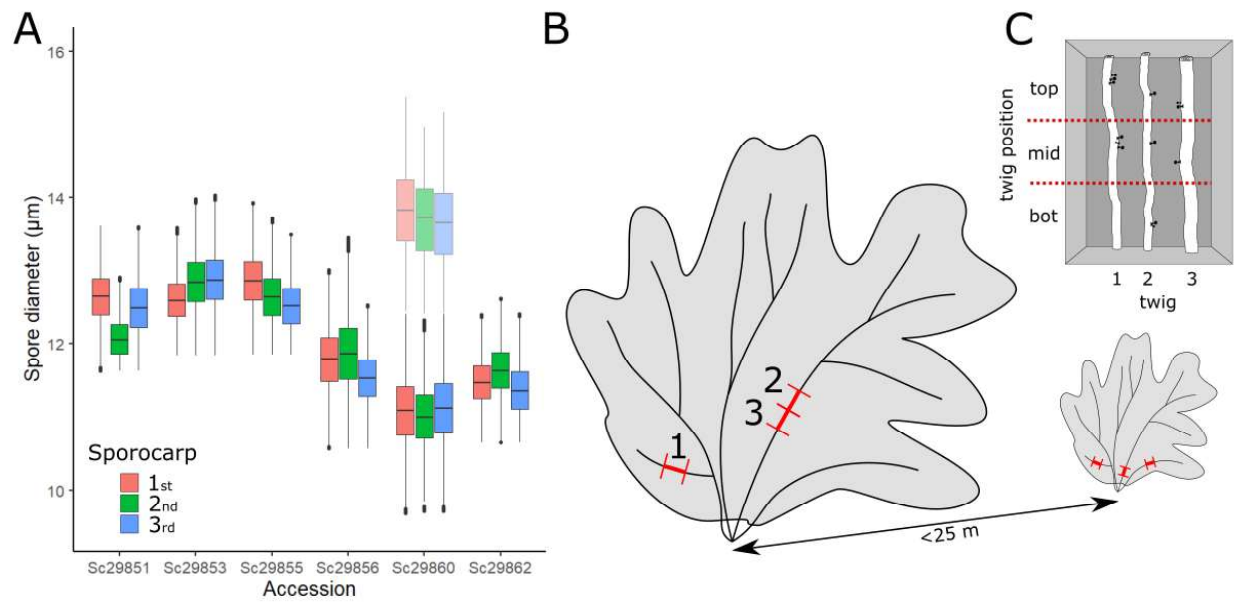


Figure 3. **A** Spore sizes of six accessions from the same clone of biospecies Hb (Kamchatka, June 2017) collected from different twigs of shrubs within 25 m distance. Means of spore size (ranging from 11.01 µm to 12.88 µm) per sporocarp for the first (most abundant) spore population are shown. For accession Sc29860, a second discernible population of spores is shown in semitransparent mode. **B** Collecting scheme showing multiple twigs (red) with fruiting colonies sampled from shrubs at the margin of a snowfield, used as variable “twig” in statistical analyses (see text). **C** Position of sporocarps within a colony on twigs sampled in boxes (bottom, middle, top) used as variable “twig position”.

Table 3. Results of Type III Analysis of Variance with degrees of freedom calculated according to Satterthwaite's method in spore size over a group of clones with additional microspatial information

(twig = different twigs of shrubs where the colonies fruited; position = upper, mid, lower position of the measured sporocarp on a twig). Abbreviations are as in Table 2.

Source of Variation	Df	Sum of squares	Mean squares	F	p-value
Position	2	5.05	2.52 (0.79%)	15.38	<0.00001
Twig	2	220.19	110.09 (34.46%)	671.12	<0.00001
Random effects	Variance	Standard deviation			
Accession	0.48	0.70			
Residuals	0.16	0.41			

Mantel tests

We used Mantel tests to test for a correlation of spore size with biospecies and with accession. For the data set as a whole, spore size was neither significantly correlated with biospecies ($r = 0.09$, $p = 0.09$) nor with accession ($r = 0.04$, $p = 0.12$).

Within the clonal accessions, we had three clonal groups where at least one accession was found significantly further away than the others. The first group came from the Spanish Sierra Nevada (four accessions, Sc30353 and Sc30319 with 230 m distance, Sc30146 and Sc30053 over 2 km apart); here we found a significant spatial correlation ($r = 0.68$, $p = 0.001$) between differences in mean spore size and the distance between collections. The second group from the Khibine Mts. in Russian (four accessions along a valley; LE296811 with 4 km distance to the closest LE296929, ca. 1 km to LE297022, and 1 km to LE297045) showed as well a significant spatial correlation ($r = 0.23$, $p = 0.027$). Similar results were found for the third group (Khibine Mts., three accessions, LE297034 and LE297079 were 70 m apart, but LE305848 found 44.6 km further in a second valley and two years later; $r = 0.92$, $p = 0.001$).

Occurrence of different spore populations

Spore size distributions in most specimens were uniform and rather narrow (Supplementary Material Table S2), but three specimens had two (Sc24902, Caucasus; Sc30248, Sierra Nevada) or even three (Sc29860, Kamchatka) discernible spore populations (Table 4). If the volumes of these spore populations are derived from the mean diameter, roughly a relation of 1:2:3 appears. Fig. 4 shows examples of the spore size distribution curves.

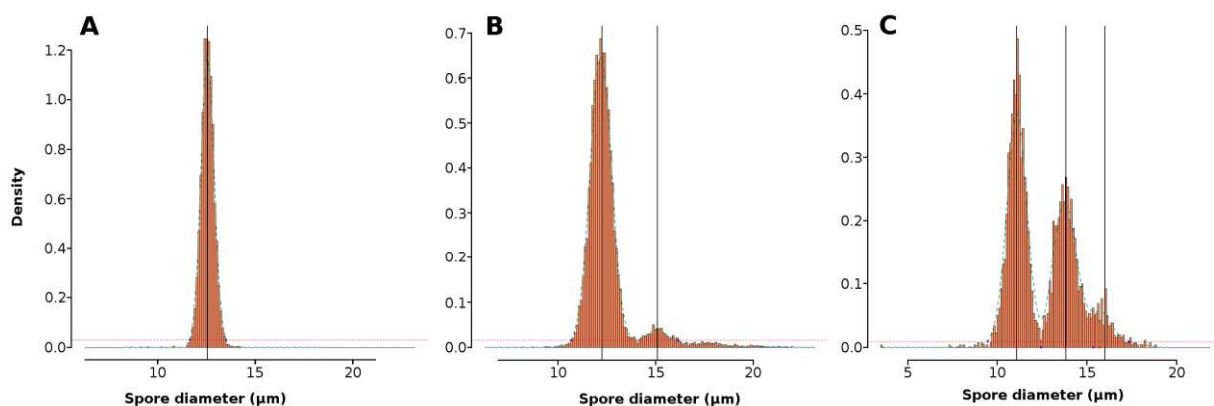


Fig. 4. Three examples of spore size distribution within one sporocarp, showing one, two, and three discernible spore populations. **A** Specimen Sc30289 with a narrow size distribution (the normal case). **B** Specimen Sc24902 with two populations, this accession shows a significant proportion of binucleate spores. **C** Specimen Sc29860 with three discernible spore populations, their volumes follow roughly a relation of 1:2:3 (see text).

Table 4. Specimens with more than one discernible spore population (compare Fig. 3). For each sporocarp (coded with accession/sporocarp) the following figures are listed: numbers of spores measured (n), spore diameters (mean $\bar{x} \pm$ standard deviation σ), mean spore volume (\bar{V}) derived from it, and the respective ratios (r).

Acc	Spore Population 1				Spore Population 2				Spore Population 3			
	Spore size		Spore volume		Spore size		Spore volume		Spore size		Spore volume	
	(μm)		(μm^3)		(μm)		(μm^3)		(μm)		(μm^3)	
	n	$\bar{x} \pm \sigma$	\bar{V}	r	n	$\bar{x} \pm \sigma$	\bar{V}	r	n	$\bar{x} \pm \sigma$	\bar{V}	r
Sc24902	15427	12.20	951	1	1005	15.10	1802	1.90				
/1		± 0.54				± 0.52						
Sc30248	4330	13.06	1167	1								
/1		± 1.68										
Sc30248	13823	12.87	1116	1	5998	15.68	2019	1.81				
/2		± 0.65				± 0.30						

Sc30248	499	12.15	940	1								
/3		±0.43										
Sc29860	1360	11.09	714	1	1024	13.82	1383	1.94	182	16.00	2143	3.00
/1		±0.48				±0.61				±0.44		
Sc29860	2385	11.00	697	1	1366	13.72	1353	1.94	486	15.85	2083	2.99
/2		±0.45				±0.59				±0.64		
Sc29860	3016	11.12	720	1	1674	13.65	1332	1.85	271	15.87	2094	2.91
/3		±0.49				±0.59				±0.44		

Nuclei per spore

For a total of 21 sporocarps from 15 accessions, the number of nuclei per spore was assessed additionally to their size. For a small fraction of spores, usually below 1%, no nucleus was detected (from the 21 analyzed sporocarps, five had between 2 and 5% of spores without a nucleus, but one specimen had 27%, LE305858, Supplementary Material Table S2). Most spores (72–99%), including spores without a nucleus, were uninucleated. The fraction of binucleate spores was very small (usually below 1%). However, a single specimen (sc30211, Spanish Sierra Nevada) had 15–25% binucleate spores in all three analyzed sporocarps, but the spore size distributions were unimodal. Fig. 2 shows the proportions of the respective fractions of spores with 0, 1, and 2 nuclei as pie diagrams.

Only one of the 21 sporocarps analyzed for the number of nuclei (sc24902, Caucasus) displayed a well-separated second spore population (Fig. 3B, 6.5% of 16432 analyzed spores). The relation of spores with 0, 1 and 2 nuclei were 0.01:0.98:0.01 for the first spore population, but 0.08:0.64:0.28 for the second. This second spore population had roughly two times the volume of the first one (1.895).

Discussion

This study combined two quantitative, image-based methods to measure spore size and the number of nuclei per spore simultaneously. It allows for the first time in myxomycetes to (i) derive very reliable measurements for spore size without any human bias and (ii) to look at the number of nuclei included in these spores. The respective procedures are time-consuming but rather accurate: even subtle differences in spore size can be revealed. With sample sizes exceeding 10,000 spores

per sporocarp the effect size necessary to produce a significant difference between two samples is ca. 0.03 μm . Thus, reaching significance in comparisons between accessions is not the goal but the large number of spores measured provides more precise confidence intervals. Therefore, we focus on how much variation in spore size can be explained by given covariates like clone assignment (genetic identity), biospecies (genetic relationship), or spatial information (as a proxy for variation in environmental conditions). With the rapid temperature differences typically occurring during spore formation in nivicolous myxomycetes (Schnittler et al. 2015) and the rugged relief in mountains, environmental conditions can be expected to vary strongly in distances of meters and times of a few days. If we consider such factors as exposure to the sun, microenvironmental conditions can vary even at the scale of centimeters, providing different conditions for the development of sporocarps within one colony. Looking at the importance of spores for dispersal and colonization, our null hypothesis was nevertheless that this trait is under a strict genetic control.

Measurement errors

Measurements errors for spore size are within the ranges explained in Woyzichovski et al. (2021), even with the slight method modifications described in material and method. For nuclei counts, recognition of fluorescence from DAPI staining requires gentle bleaching of spore walls, and this is the crucial step in this procedure. Exposing spores too long to the bleaching reagent may destroy the spore wall and reveal the autofluorescent protoplast. The autofluorescence overpowers any DAPI signal and thus renders nuclei non-recognizable. We tried to find an optimum for the bleaching time, which worked: except for one specimen (LE305858), the proportion of spores where no nucleus could be detected was always below 5%. Establishing a relationship between the different images, bright-field and fluorescence, to assign the number of nuclei to a measured spore is an automatic process and virtually free of errors.

More difficult is the accurate detection of the number of nuclei for a spore. First, mitochondria, containing DNA as well, and other cell structures might cause background fluorescence. Second, even if the spores in our mounts are precisely arranged in a plane (see Woyzichovski et al. 2021), their nuclei may overlap each other. Due to the sheer mass of possible observations, we sample, such overlaid nuclei constitute a minor fraction, but we should be aware that the number of binucleated spores may be rather under- than overestimated. Here, we did not further investigate this issue, but the use of a confocal microscope should allow it to acquire information along the z-

axis in high resolution and identify DAPI signals on multiple layers. An additional step would be needed to separate nuclei signals in the 3D space.

Our model for segmenting single spores on grayscale images worked with precision and recall values of 99% and 91%, respectively. A visual inspection revealed that in most samples only a few (typically 1–3 of 150–200) spores in every image were not registered or falsely segmented. In most cases, this was related to dense spore clusters or fragments from destroyed spores. Most spores were excluded due to the limits we set to avoid overlap between images: they were too close to the margin.

For our nucleus model, the lower performance was caused by the underestimated variety of DAPI-signal in spores of myxomycetes. We could not train the nucleus model to recognize all different appearances of nuclei, which in part might be caused by deformation of nuclei in the 4–8 yrs old samples kept as herbarium specimens. Therefore, damaged nuclei may occur and escape detection. Furthermore, the melanin concentration differed slightly between accessions, but the same bleaching protocol was always applied. A different intensity in the DAPI signal could be the consequence, and here the nucleus model begins to underperform, resulting in wrong predictions. We thus run this model with different IoU thresholds (not shown) and inspected the results visually. At higher IoU thresholds, performance decreases considerably, since the model starts to detect false nuclei in the noisy fluorescence background, which would overestimate the proportion of multinucleated spores. Hence we decided to choose a lower IoU threshold and non-maximum suppression value, which again might lead to an underestimation of the proportion of multinucleated spores.

Intraspecific variation in spore size

First, our results are of interest for a basic question: how changeable is spore size in myxomycetes at all? Virtually all of the monographs in the group present spore measurements, usually from 25–50 spores and with a precision of $\pm 0.5 \mu\text{m}$, as inferred from the measures given (Rostafiński 1873; Lister 1894, 1911, 1925; Martin & Alexopoulos 1969; Nannenga-Bremekamp 1973; Neubert et al. 1993, 1995, 2000; Poulain et al. 2011). For a spore of $10 \mu\text{m}$ diameter, as typical for many species (Schnittler & Tesmer 2008), this would translate into a variation of 5%. Since we are not aware of any study looking at the natural variation in spore size, our results are the first large-scale measurements for myxomycetes.

Spore diameter seems to be fairly constant for different sporocarps of a colony, usually stemming from the partition of one plasmodium into fruit bodies ($\pm 1.5\%$ on average). This would mean that spore size for a certain accession (a voucher specimen) can be more precisely measured than it is given in many monographs. However, variations between specimens are much larger (Fig. 2). Variations are in the range of $\pm 10\%$ within a biospecies (Table 1) and $\pm 8\%$ even within the members of a single clone (Fig. 3). Looking at the whole data set, about 1/3 of the variation in spore size is explained by accession (Table 2), which can be seen as a proxy for small-scale fluctuations in environmental conditions. Instead, biospecies affiliation explained only 1/8 of the variation. This is confirmed by the fact that most of this variation is still explained by accession when we exclude genetic variation and large-scale spatial variation (Fig. 3, Table 3). In this clonal group of accessions, the median spore size varies by $1.73\ \mu\text{m}$ (between 11.07 and $12.80\ \mu\text{m}$), but the width of the average spore size distribution reaches $2.72\ \mu\text{m}$ ($\pm 2 \times \text{SD}$). We, therefore, conclude that spore size seems to be much more plastic than commonly assumed and likely to be shaped by microenvironmental differences: there is a lot of variation between members of a clone, and even between different twigs of a shrub sampled for one accession (Fig. 3). Exposition and weather conditions during spore formation, which lasts 48–96 hrs, may play a decisive role. Therefore, differences in mean spore size of $1\ \mu\text{m}$, as often applied in keys, may not be sufficient to delimit species from each other.

The chosen model species *Physarum albescens* is probably at the upper end of variation in myxomycetes. First, it is genetically very diverse: 85 multilocus genotypes of three independent markers were found in 182 accessions over the Northern Hemisphere, combined into 18 reproductively isolated groups (Shchepin et al. 2021) half of which were investigated in this study. Second, nivicolous myxomycetes experience extreme fluctuations in temperature when the snow melts rapidly during fructification (Schnittler et al. 2015). Third, nivicolous myxomycetes tend to have slightly larger spores than non-nivicolous forms (Stephenson & Stempen 1994; Poulain et al. 2011) and have a higher proportion of so-called "macrosporous" varieties (Poulain et al. 2011).

Spore diameter, volume, and number of nuclei

A minor fraction of all specimens (3 of 39 accessions, 8%) showed multiple peaks in the spore size distribution (Fig. 4). These spores are not part of the normal variation: specimen 29860 of the clonal group pictured in Fig. 3 displayed a second spore population with 13.65 – $13.85\ \mu\text{m}$ size which is clearly out of the variation range of this clone (11.07 – $12.80\ \mu\text{m}$). The appearance of a second spore

population is not linked to the occurrence of two nuclei in a spore: from the 15 specimens with nuclei counted, only one shows a second spore population (Sc24902), and the specimen with a significant proportion of binucleated spores (Sc30211, 15-25% binucleate spores) possesses a single spore population only.

The nuclei counts are laborious and thus too limited for detailed statistical analyses but allow for several conclusions. First, uninucleate spores seem to be the normal case, at least in *Ph. albescens*: all 15 investigated specimens had >70% uninucleate spores, and two specimens had even >90% (Supplementary Material Table S2). Second, spore size is not correlated with the number of nuclei: most of the rare non-nucleate or binucleate spores fall within the first (and mostly the only) spore population and do not differ in diameter from uninucleate spores. But mean spore size is positively correlated with the spore size standard deviation and therefore with the width of the distribution. Leading to the conclusion that the formation of larger spores is performed under a less regular mode. The accession Sc30211 (Spanish Sierra Nevada) has a higher proportion of binucleate spores in all sporocarps of a colony. A small proportion of binucleate spores seems to occur in most or all accessions, and a visual inspection of the respective images under fluorescence microscopy confirmed this.

As such, uninucleate spores of a rather uniform size, like for specimen Sc30289 pictured in Fig. 3A, are the normal case. Two kinds of aberrations in spore formation were found: first, "macro" spores of two- or three-fold volume may occur (Figs. 3 B, C). Unrelated is the second case: spores with none or more than one nucleus (Fig. 2). These cases seem as well not to be linked to certain biospecies.

Implications for spore ontogenesis and meiosis

The rare occurrence of spores with the double and triple volume of normal ones and the missing correlation of spore size with the number of nuclei may be explained best by the post-cleavage model of meiosis. Initially, one diploid nucleus with two different mating types from the fruiting plasmodium is included in a spore. With regular meiosis progressing in young and initially uninucleate spores, one haploid nucleus carrying one of the two mating types survives.

If the spore cleavage mechanism is occasionally disturbed by detrimental environmental conditions, two or even more diploid nuclei may be included in a spore, and these end up with the double or triple volume of normal spores. If meiosis takes place in parallel, only a single haploid nucleus may survive. If accidentally more than one nucleus survives, regardless of the initial

number of diploid nuclei, this results in a binucleate spore. Such a binucleate spore should have a colonization advantage if it carries nuclei with opposite mating types, but its descendants would potentially suffer from inbreeding depression. In addition, the additional nucleus might increase the density of the spore cytoplasm.

If we assume a pre-cleavage model of meiosis and a spore volume correlated with the number of nuclei enclosed, only macrospores (the second spore population) should include two post-meiotic haploid nuclei. The smaller and less dense a particle is, the greater its dispersal potential (Norros et al. 2014). For spores, terminal velocity is inversely related to the power of its radius according to Stoke's law, which was shown for myxomycetes (Tesmer & Schnittler 2007). Thus macrospores should have a disadvantage, but counterselection against aberrant spores may not be as strong as expected from Stoke's Law. But this assumption of correlation between spore volume and number of nuclei seems not to be the case, as found for specimen Sc30211 which has 15-25% binucleate spores but only a single spore population. If studies like this one can be combined with single-spore sequencing for the mating-type locus, it would be possible to reveal the exact meiotic mechanism. For now, the spore counts revealed two important results. First, a uninucleate spore seems to be the normal state at least for *Ph. albescens*, but probably for all myxomycetes. Second, deviations occur, at least in nivicolous myxomycetes, although there are reports of binucleate spores as well for *Physarum pseudonotabile*, a species of Central Asian steppes and deserts (Novozhilov et al. 2013), in several species of *Arcyria* and *Badhamia affinis* (Smith 1929, Gray & Alexopoulos 1968), for *Arcyria cinerea* (Alexopoulos 1966, Mims & Rogers 1975, Mims 1971) and for *Didymium iridis* (Sherman & Mims 1985). In both environments, rapid temperature changes may occur during the 48–96 hrs. of fruit body development: in *Ph. albescens* caused by rapid snowmelt (Schnittler et al. 2015), in *Ph. pseudonotabile* by day/night differences under the continental climate. The interesting question is about the consequences of such deviations: do they have consequences for the reproductive mode or the colonization ability of a species?

Conclusions

Spore size in myxomycetes is somewhat more variable than assumed by the often narrow differences declared to be decisive in keys for species determination: even in accessions from the same clone, it may vary by eight percent. In spite of strong selection for an optimum size to be expected from Stoke's Law and the derived terminal velocities, the trait is rather plastic and seems

to be heavily influenced by microenvironmental conditions. Nevertheless, the relative constancy in spore size within the sporocarps of one colony calls for a strong genetic background of this trait. Two aberrations, seemingly not linked, may occur in myxomycete spores: multinucleate spores and “macrospores”, the latter often have the double or triple volume of normal-sized spores. These deviations are likely to be caused by environmental factors; we did not find a regular pattern with respect to the biospecies occurring in *Ph. albescens*.

Methods

Study material: *Physarum albescens* was sampled throughout the Northern Hemisphere to cover a maximum of intraspecific variation (Rocky Mountains, CO, USA; German and French Alps; Khibine Mountains, Northern Caucasus and mountains of the Kamchatka Peninsula, Russia; Spanish Sierra Nevada, Kamchatka, see Supplementary Material Table S1). Sampling was done in an opportunistic way, with a new colony found more than 0.5 m apart from the last one defined as a new accession. Geographic coordinates were recorded with a hand-held GPS device (accuracy 3–10 m). From each accession, we typically analyzed three sporocarps.

Preparation of spore mounts: Using the light-microscopic method described in Woyzichovski et al. (2021), between 10,000 and 20,000 spores per sporocarp were analyzed. For 39 accessions from 6 mountain ranges, up to 5 sporocarps were analyzed (Supplementary Material Table S2). Spores from an entire sporocarp were arranged in a single plane in a mounted slide (Woyzichovski et al. 2021), and from the resulting images, a number of parameters among this spore diameter can be inferred. The result is a spore-size distribution, which precisely determines the median and average spore size. Since the shape of spores in *Ph. albescens* approaches a sphere tightly, spore volume can be easily inferred. The big advantage of overflow-cytometric methods to determine particle size in a quantitative manner is its comprehensibility: at the images, the position of every spore is known. This allows to count as well the number of nuclei per spore (see below).

In comparison to Woyzichovski et al. (2021), the slide preparation was slightly improved to speed up the process. The spore mass was placed on the slide with a small removable polydimethylsiloxane (PDMS) frame. It has a rectangular form with an outer dimension of approximately 6 x 10 mm, a height of 1–2 mm, and a rectangular 2 x 6 mm sized hole. The spore-ethanol mixture was transferred into the pocket and observed until the ethanol was nearly evaporated as described in Woyzichovski et al. (2021). During this step, the embedding medium

was placed adjacent to one of the longer sides of the frame. After evaporation of the ethanol, the PDMS frame was removed, and after placing a coverslip, the medium and the spore mass were mixed.

Spore staining and nuclei counts: In dark-spored myxomycetes as *Ph. albescens*, spore size can be measured without further staining. To detect the nuclei, their DNA was stained with the fluorescent dye DAPI (4',6-Diamidin-2-phenylindol) in a selection of 15 samples. Since spore walls contain a high concentration of melanin (Rakoczy & Panz 1994), the effect of fluorescent staining is not directly visible. Therefore, an initial step including hydrogen peroxide was used to bleach the melanin. The duration of this step depends on the concentration of melanin in the spore wall. Preliminary experiments showed that suitable bleaching of *Ph. albescens* spores was reached with incubation in 30% hydrogen peroxide (H₂O₂) for 3 hours at room temperature. To preserve the fragile nuclear membranes, spores were first fixated with Carnoy's fixative (6 parts 96% ethanol, 3 parts 96% chloroform, and 1 part 96% glacier acetic acid) for 40 min, then bleached with 30% H₂O₂ for three hours, and subsequently stained with 0.1 µg DAPI in 1 ml EtOH. Additionally, 5 µl of each Tween20 and Triton X-100 were added to the staining solution. Between these three steps, the spore samples were washed three times for 10 min each with 70% EtOH to break the hydrophobicity of the spore wall (Hoppe, 2014). After fixation, bleaching, and staining, the slides were prepared as mentioned above and simultaneously analyzed in fluorescent light (detection of nuclei) and bright-field (recording of spore diameters).

Image acquisition: We used a Nikon Eclipse 90i compound microscope with a monochrome digital camera from Nikon (DS-2MBWc, 2.11-megapixel, 1,600 x 1,200 pixel, 4.4 µm pixel size) to acquire images at 20× magnification (NA: 0.5, Plan Fluor DIC, Nikon, 0.31 µm/pixel on the object plane). For spore size measurement, images were taken in bright-field. For nuclei detection, the same section of the slide was photographed under fluorescent light with a filter optimized for DAPI (Fig. 1).

Bright-field images of slides with mounted spores were used to record the diameter and position of all spores. In the second step, single spores were isolated from corresponding fluorescence images using the spatial information from the previous step. The obtained DAPI signatures were then used to identify the number of nuclei per spore.

Object recognition: For these procedures, we used the deep learning algorithm StarDist (Schmidt *et al.*, 2018; Weigert *et al.*, 2020) for semantic segmentation on our image dataset with two different

models trained for their specific tasks. The first model (called spore model) was trained on bright-field images for finding and segmenting the spores on an image frame densely packed with spores. Dirt particles of varying sizes and shapes, ranging from filamentous contaminants (capillitium) to small air bubbles, were trained to be excluded. The second model (called nucleus model) was trained on fluorescence images to recognize DAPI signals of certain intensity and arrangement – we defined a nucleus as a dense cluster of DAPI signals with a distinct round shape; scattered single signals, perhaps arising from mitochondrial DNA, were ignored. The performance of the models was inspected via plotting a standard metric based on the intersection over union (IoU) thresholds. The IoU represents the shared pixel amount of the ground truth mask (GT, images annotated for training) and the prediction mask (outcome of the algorithm) divided by the total pixel amount of both mentioned masks. For the GT mask, in 1300/1250 images (spore model/nucleus model) all spores were manually marked. Four classes are consequently generated. For the true-positive (TP) class, predicted pixels and target pixels from the GT mask are matched for each group of pixels comprising an object. Their IoU values exceed the set threshold (typical at 0.5) for those objects. Hence a true-negative (TN) classification describes objects that fail the IoU threshold. Usually, these are background pixels or pixels describing non-target objects. False-positive (FP) class pixels are type I errors that falsely get the classification as a target. Finally, the False-negative (FN) class defines the type II error when target pixels fail to exceed the IoU threshold. With these classes, the following performance metrics can be formulated:

$$\text{Precision: } \frac{TP}{TP+FP}$$

$$\text{Recall: } \frac{TP}{TP+FN}$$

$$\text{Accuracy: } \frac{TP+TN}{TP+TN+FP+FN}$$

$$\text{F1-score: } 2 \times \frac{\text{precision} \times \text{recall}}{\text{precision} + \text{recall}}$$

The figure for precision gives the percentage of correct positive predictions and tells us how well the model selects only the relevant target objects. The recall gives the percentage of how well the model could find all target objects. The accuracy reflects the percentage of correctly classified pixels from the model classes (in our case target objects, i.e., spores or nuclei, and background). The F1-score is an alternative figure for describing the model's accuracy to select the target objects correctly.

To avoid analyzing spores cut by the margin of the images, we excluded all spores closer to the margin than the size of an average spore (12 μm or 40 pixels).

Data analysis: This procedure resulted in a table with spore size and a table with numbers of nuclei for sized spores, which was further analyzed with R (R Core Team, 2021). Before any statistical test, the dataset was checked for errors created by the segmenting process or overlapping spores. Outliers and background noise were excluded by cutting off the density function of the spore size distribution at its intersection points with a horizontal line equivalent to the height of 1/40 of the maximum of the spore size distribution. The height was chosen based on a good separation effect from noise in the data. After visual inspection, these defined ranges were wider or equal to three times the standard deviation point for the spore size distribution, including at least 99% of the data points around the median. For multimodal spore size distributions, a parameter “spore population” was introduced to assign spores to their respective distribution. These multimodal distributions were visually detected. Defining the interval points on these distributions were done via finding maxima and minima within the total distributions.

We applied multiple Mantel tests to analyze the relationship between spore size and spatial distribution in different specimens found to represent a clone with Genotyping by Sequencing (Shchepin et al. 2021). Distances between specimens of a clone ranged from 25 m up to 44 km. The Mantel tests were performed with 10,000 permutations and the Pearson product-moment correlation coefficient (R package: *vegan*, version 2.5-7). Differences in spore size between regions or samples were further analyzed by ANOVA tests (R package: *stats*, version 4.1.1). For the ANOVA, we randomly sampled size values for 1,000 spores from each measured sporocarp (which includes resampling for the few samples including less than 1,000 spores).

To test for possible influences of small-scale fluctuations in environmental parameters on spore features (which cannot be meaningfully measured during the collection procedure), we used the position of colonies on the collected plant parts (grass culms, twigs of shrubs) as a proxy. A factor “twig” was defined to denote colonies from different plant parts of one accession. The position of investigated sporocarps on this twig (lower, mid, upper end) was described by a factor “twig position”. For these tests, the factor “accession” was set as a random blocking factor.

Declaration of interests

The authors declare that they have no conflict of interest.

572

573 **CRedit authorship contribution statement**

574 Jan Woyzichowski: Methodology, Image acquisition, data analysis, writing – original draft. Oleg
575 Shchepin: Molecular investigations. Martin Schnittler: Conceptualization, Supervision. All
576 authors: Specimen collecting, writing, and editing of further drafts.

577

578 **Acknowledgements**

579 JW acknowledges a scholarship from the German Research Council (RTG 2010 RESPONSE). The
580 work of OS was carried out within the framework of the project no. AAAA-A18-118022090078-
581 2 of the Komarov Botanical Institute of the Russian Academy of Sciences. All authors are grateful
582 to Ángela López-Villalba, Anna Ronikier, Daria Erastova, Gabriel Moreno, Marianne Meyer,
583 Paulina Janik, Renato Cainelli, and other researchers for sharing specimens.

584

585 **Appendix A. Supplementary Data**

586 Supplementary data to this article can be found online at ...

587

588 **References**

589 **Aguilar M, Fiore-Donno AM, Lado C, Cavalier-Smith T** (2013) Using environmental niche
590 models to test the ‘everything is everywhere’ hypothesis for *Badhamia*. The ISME Journal **8**:737–
591 745

592 **Alexopoulos CJ** (1963) The Myxomycetes. II Bot Rev **29**:1–78

593 **Alexopoulos CJ** (1966) Chapter 8 Morphogenesis in the Myxomycetes. In Ainsworth and Sussman
594 (Eds) Fungi, Vol 2, Academic Press Co., New York, pp 211 – 234

595 **Borg Dahl M, Brejnrod AD, Unterseher M, Hoppe T, Feng Y, Novozhilov YK, Sørensen SJ,**
596 **Schnittler M** (2018) Genetic barcoding of dark-spored myxomycetes (Amoebozoa) –
597 identification, evaluation and application of a sequence similarity threshold for species
598 differentiation in NGS studies. Molecular Ecology Resources **18**:306–318
599 <https://doi.org/10.1111/1755-0998.12725>

600 **Clark J, Haskins EF** (2010) Reproductive systems in the myxomycetes: a review. *Mycosphere*
601 **1**:337–353

602 **Clark J, Haskins EF** (2013) The nuclear reproductive cycle in the myxomycetes: a review.
603 *Mycosphere* **4**:233–248 <https://doi.org/10.5943/mycosphere/4/2/6>

604 **Clark J, Haskins EF** (2016) *Mycosphere Essays* 3. Myxomycete spore and amoeboflagellate
605 biology: a review. *Mycosphere* **7**:86–101 <https://doi.org/10.5943/mycosphere/7/2/1>

606 **Cohen, J** (1992) Statistical Power Analysis. *Curr Dir Psychol Sci* **1**:98–101

607 **Collins ONR** (1979) Myxomycete biosystematics: some recent developments and future research
608 opportunities. *Bot Rev* **45**:145–201

609 **Collins ONR** (1981) Myxomycete genetics 1960–1981. *J Elisha Mitch Sci Soc* **97**:101–125

610 **Dagamac NHA, Novozhilov YK, Stephenson LS, Rojas C, dela Cruz TEE, Unterseher M,**
611 **Schnittler M** (2017a) Biogeographical assessment of myxomycete assemblages across the
612 Tropics. *J Biogeogr* **44**:1524–1536 <https://doi.org/10.1111/jbi12985>

613 **Dagamac NHA, Rojas C, Novozhilov YK, Moreno GH, Schlueter R, Schnittler M** (2017b)
614 Speciation in progress? A phylogeographic study among populations of *Hemitrichia serpula*
615 (Myxomycetes). *PloS One* **12**:e0174825 <https://doi.org/10.1371/journal.pone0174825>

616 **Dagamac NHA, Bauer B, Woyzichovski J, Shchepin ON, Novozhilov YK, Schnittler M** (2020)
617 Where do nivicolous myxomycetes occur? – Modelling the potential worldwide distribution of
618 *Physarum albescens*. *Fungal Ecology* **53**:101079 <https://doi.org/10.1016/j.funeco.2021.101079>

619 **Feng Y, Klahr A, Janik P, Ronikier A, Hoppe T, Novozhilov YK, Schnittler M** (2016) What
620 an intron may tell: several sexual biospecies coexist in *Meriderma* spp. (Myxomycetes). *Protist*
621 **167**:234–253 <https://doi.org/10.1016/j.jprotis201603003>

622 **Feng Y, Schnittler M** (2015) Sex or no sex? Group I introns and independent marker genes reveal
623 the existence of three sexual but reproductively isolated biospecies in *Trichia varia*
624 (Myxomycetes). *Org Divers Evol* **15**:631–650 <https://doi.org/10.1007/s13127-015-0230-x>

625 **Gray WD, Alexopoulos CJ** (1968) Biology of the myxomycetes. Ronald Press Co, New York

- 626 **Hoppe T** (2014) Hydrophobicity of myxomycete spores: An undescribed aspect of spore
627 ornamentation. *Mycosphere* **5**:601–606
- 628 **Ing B** (1994) Tansley Review No 62 The phytosociology of myxomycetes. *New Phytologist*
629 **126**:175–201
- 630 **Janik P, Lado C, Ronikier A** (2020) Phylogeography of a nivicolous protist *Didymium nivicola*
631 Meyl (Myxomycetes, Amoebozoa): striking contrasts between the Northern and the Southern
632 Hemisphere. *Protist* **171**:125771 <https://doi.org/101016/jprotis2020125771>
- 633 **Janik P, Szczepaniak M, Lado C, Ronikier A** (2021) *Didymium pseudonivicola*: A new
634 myxomycete from the austral Andes emerges from broad-scale morphological and molecular
635 analyses of *D. nivicola* collections, *Mycologia*, DOI: 10.1080/00275514.2021.1961068
- 636 **Kamono A, Kojima H, Matsumoto J, Kawamura K, Fukui M** (2009) Airborne myxomycete
637 spores: detection using molecular techniques. *Naturwissenschaften* **96**:147–151
638 <https://doi.org/101007/s00114-008-0454-0>
- 639 **Laane MM, Haugli FB** (1976) Nuclear behavior during meiosis in the myxomycete *Physarum*
640 *polycephalum*. *Norwegian Journal of Botany* **23**:7–21
- 641 **Lado C** (2005–2022) An online nomenclatural information system of Eumycetozoa.
642 <https://www.eumycetozoa.com> (accessed 05 January 2022)
- 643 **Lahr DJ** (2021) An emerging paradigm for the origin and evolution of shelled amoebae,
644 integrating advances from molecular phylogenetics, morphology and paleontology. *Memorias do*
645 *Instituto Oswaldo Cruz* **116**:e200620 <https://doi.org/10.1590%2F0074-02760200620>
- 646 **Leontyev D, Schnittler M, Stephenson SL** (2015) A critical revision of the *Tubifera ferruginosa*-
647 complex. *Mycologia* **107**:959–985 <https://doi.org/103852/14-271>
- 648 **Leontyev DL, Schnittler M, Stephenson SL, Shadwick LL, Novozhilov YK, Shchepin ON**
649 (2019) Towards a phylogenetic classification of the myxomycetes. *Phytotaxa* **399**:209–238
650 <https://doi.org/1011646/phytotaxa39935>
- 651 **Lister A** (1894) A monograph of the Mycetozoa. Brit Museum, London, 224 p

- 652 **Lister A** (1911) A monograph of the Mycetozoa Ed 2. (revised by G Lister) Brit Museum, London,
653 304 p
- 654 **Lister A** (1925) A monograph of the Mycetozoa Ed 3. (revised by G Lister) Brit Museum, London,
655 296 p
- 656 **Martin GW, Alexopoulos CJ** (1969) The Myxomycetes. Iowa Univ Press, Iowa City, 576 p
- 657 **Meylan C** (1908) Contributions a la connaissance des myxomycetes du Jura. Bulletin de la Societe
658 Vaudoise des Sciences Naturelles **44**:285–302
- 659 **Mims CW** (1971) An Ultrastructural Study of Spore Germination in the Myxomycete *Arcyria*
660 *Cinerea*. Mycologia **63**:586 – 601 <https://doi.org/10.1080/00275514.1971.12019138>
- 661 **Mims CW and Rogers MA** (1975) A Light and Electron Microscopic Study of Stalk Formation
662 in the Myxomycete *Arcyria Cinerea*. Mycologia **67**:638 – 649 <https://doi.org/10.1080/00275514>
- 663 **Nannenga–Bremekamp NE** (1991) A guide to temperate Myxomycetes. Biopress Ltd, Bristol,
664 410 p
- 665 **Neubert H, Nowotny W, Baumann K** (1993) Die Myxomyceten Deutschlands und des
666 angrenzenden Alpenraumes unter besonderer Berücksichtigung Österreichs 1 Ceratiomyxales,
667 Echinosteliales, Liceales, Trichiales. Karlheinz Baumann Verlag, Gomaringen, 340 p
- 668 **Neubert H, Nowotny W, Baumann K** (1995) Die Myxomyceten Deutschlands und des
669 angrenzenden Alpenraumes unter besonderer Berücksichtigung Österreichs 2 Physarales.
670 Karlheinz Baumann Verlag, Gomaringen, 365 p
- 671 **Neubert H, Nowotny W, Baumann K, Marx H** (2000) Die Myxomyceten Deutschlands und des
672 angrenzenden Alpenraumes unter besonderer Berücksichtigung Österreichs 3 Stemonitales.
673 Karlheinz Baumann Verlag, Gomaringen, 391 p
- 674 **Norros V, Rannik Ü, Hussein T, Petäja T, Vesala T, Ovaskainen O** (2014) Do small spores
675 disperse further than large spores? Ecology **95**:1612–1621 <https://www.jstor.org/stable/43493764>

676 **Novozhilov YK, Okun MV, Erastova DA, Shchepin ON, Zemlyanskaya IV, García-Carvajal**
677 **E, Schnittler M** (2013) Description, culture and phylogenetic position of a new xerotolerant
678 species of *Physarum*. *Mycologia* **105**:1535–1546 <https://doi.org/103852/12-284>

679 **Poulain M, Meyer M, Bozonnet J** (2011) *Les Myxomycètes*. Federation mycologique et
680 botanique Dauphiné-Savoie, Sevrier, 556 pp

681 **R Core Team** (2021) R – A language and environment for statistical computing. R Foundation for
682 Statistical, Vienna, Austria <https://www.R-project.org/>

683 **Rakoczy L, Panz T** (1994) Melanin revealed in spores of the true slime moulds using the electron
684 spin resonance method. *Acta Protozoologica* **33**:227–231

685 **Ronikier A, Ronikier M** (2009) How ‘alpine’ are nivicolous myxomycetes? A worldwide
686 assessment of altitudinal distribution. *Mycologia* **101**:1–16 <https://doi.org/103852/08-090>

687 **Rostafiński J** (1873) *Versuch eines Systems der Mycetozoen*. Inaugural dissertation, Univ Press,
688 Strassburg, 115 p

689 **Schmidt U, Weigert M, Broaddus C, Myers G** (2018) In *Medical Image Computing and*
690 *Computer Assisted Intervention – MICCAI 2018*, Vol 11071, Frangi, AF, Schnabel, JA,
691 Davatzikos, C, Alberola-López, C and Fichtinger, G (Eds), Springer International Publishing,
692 Cham, pp 265–273

693 **Schnittler M, Erastova DA, Shchepin ON, Heinrich E, Novozhilov YK** (2015) Four years in
694 the Caucasus – observations on the ecology of nivicolous myxomycetes. *Fungal Ecology* **14**:105–
695 115 <https://doi.org/101016/jfuneco201501003>

696 **Schnittler M, Tesmer J** (2008) A habitat colonisation model for spore-dispersed organisms – does
697 it work with eumycetozoans? *Mycological Research* **112**:697–707
698 <https://doi.org/101016/jmycres200801012>

699 **Schnittler M, Dagamac NHA, Novozhilov YK** (2021) Chapter 10 Biogeographical patterns in
700 myxomycetes. In Stephenson SL, Rojas C, (Eds), *Myxomycetes – Biology, Systematics,*
701 *Biogeography and Ecology* 2nd ed Elsevier, Academic press, pp 377–416

702 **Schnittler M, Shchepin O, Dagamac NHA, Borg Dahl M, Novozhilov YK** (2017) Barcoding
 703 myxomycetes with molecular markers: challenges and opportunities. *Nova Hedwigia* **104**:323–341
 704 https://doi.org/10.1127/nova_hedwigia/2017/0397

705 **Shchepin O, Novozhilov Y, Woyzichovski J, Bog M, Prikhodko I, Fedorova N, Gmoshinskiy**
 706 **V, Borg Dahl M, Dagamac NHA, Yajima Y, Schnittler M** (2021) Genetic structure of the protist
 707 *Physarum albescens* (Amoebozoa) revealed by multiple markers and genotyping by sequencing.
 708 *Molecular Ecology* **31**:372–390 <https://doi.org/10.1111/mec.16239>

709 **Sherman JD and Mims CW** (1985) Ultrastructural Evidence for Meiosis in a Nonheterothallic
 710 Isolate of the Myxomycete *Didymium Iridis*. *Mycologia* **77**:328 – 332
 711 <https://doi.org/10.1080/00275514>

712 **Singer D, Mitchell EAD, Payne RJ, Blandenier Q, Duckert C, Fernández LD, Fournier B,**
 713 **Hernandez CE, Granath G, Rydin H, Bragazza L, Koronatova NG, Goia I, Harris LI,**
 714 **Kajukalo K, Kosakyan A, Lamentowicz M, Kosykh NP, Vellak K, Lara E** (2019) Dispersal
 715 limitations and historical factors determine the biogeography of specialized terrestrial protists. *Mol*
 716 *Ecol* **28**:3089–3100 <https://doi.org/10.1111/mec.15117>

717 **Smith EC** (1929) Some phases of spore germination in myxomycetes. *Am. Jour. Bot.* **16**:645 - 650

718 **Stephenson SL, Schnittler M** (2017) Myxomycetes. In Archibald JM, Simpson AGB, Slamovits
 719 CH, Margulis L, Melkonian M, Chapman DJ, Corliss JO (eds) *Handbook of the Protists* 2nd ed,
 720 Springer, pp 1405–1432

721 **Stephenson SL, Stempen H** (1994) *Myxomycetes – A handbook of slime molds*. Timber Press,
 722 Portland, 183 pp

723 **Stephenson SL, Schnittler M, Novozhilov YK** (2008) Myxomycete diversity and distribution
 724 from the fossil record to the present. *Biodivers Conserv* **17**:285–301 [http://dxdoiorg/101007/978-](http://dxdoiorg/101007/978-90-481-2801-3_5)
 725 [90-481-2801-3_5](http://dxdoiorg/101007/978-90-481-2801-3_5)

726 **Tesmer J, Schnittler M** (2007) Sedimentation velocity of myxomycete spores. *Mycological*
 727 *Progress* **6**:229–234 <https://doi.org/101007/s11557-007-0539-8>

Weigert M, Schmidt U, Haase R, Sugawara K, Myers G, eds (2020) Star-convex Polyhedra for 3D Object Detection and Segmentation in Microscopy. IEEE

Woyzichowski J, Shchepin ON, Dagamac NHA, Schnittler M (2021) A workflow for low-cost automated image analysis of myxomycete spore numbers, size and shape. PeerJ **9**:e12471 <https://doi.org/10.7717/peerj.12471>

Tables and Figures

Figure 1. Example for sections of corresponding images for simultaneous assessment of spore diameter and number of nuclei per spore in accession Sc30211: **A, B** bright field, **C, D** fluorescent light (DAPI) and **E, F** digitally merged images indicating DAPI fluorescence in cyan. In **C** and **D**, examples of diffuse (background) fluorescence but as well sharply delimited fluorescence, indicating the presence of a nucleus, can be seen. Images **A, C, E** shows examples of uninucleate spores, images **B, D, F** depict binucleate spores. Bar: 10 μ m.

Figure 2. Map of the northern hemisphere showing the origin of all accessions analyzed for spore size (grey circles) and the number of nuclei (colored pie diagrams with a diameter corresponding to mean spore size). Vertical rows of circles / pie diagrams show the accessions analyzed from one region, and horizontal rows show sporocarps for a certain accession. The size of a pie diagram indicates spore size according to the scale given in the lower-left corner; colored pies indicate the proportion of spores with 0, 1, 2, or 3 nuclei. Rectangles indicate the investigated regions. The letter symbols for each row of diagrams depict the putative biospecies, according to Shchepin et al. (2021). An asterisk denotes samples with multiple spore populations.

Figure 3. A Spore sizes of six accessions from the same clone of biospecies Hb in (Kamchatka, June 2017, colonies on different twigs of shrubs collected within 25 m distance). Means of spore size (ranging from 11.01 μ m to 12.88 μ m) per sporocarp for the first (and largest) spore population are shown. For accession Sc29860 a second discernible population of spores is shown in semitransparent mode. **B** Collecting scheme showing multiple twigs (red) with fruiting colonies sampled from shrubs at the margin of a snowfield, used as variable "twig" in statistical analyses

(see text). **C** Position of sporocarps within a colony on twigs sampled in boxes (bottom, middle, top, used as variable "twig position".

Fig. 4. Three examples of spore size distributions of one sporocarp, showing one, two, and three discernible spore populations. **A** Specimen Sc30289 with a narrow size distribution (the normal case). **B** Specimen Sc24902 with two population, this accession shows a significant proportion of binucleate spores. **C** Specimen Sc29860 with three discernible spore populations, their volumes follow roughly a relation of 1:2:3 (see text).

Table 1. Variations in spore size within a biospecies of *Physarum albescens*, shown are results for four biospecies represented by three or more accessions.

Table 2. Results of an ANOVA for variation in spore size over different mountain ranges, biospecies, accessions and sporocarps. Shown are degrees of freedom (Df), sum of squares and their proportion on total variation, mean squares, F and P values.

Table 3. Results of Type III Analysis of Variance with degrees of freedom calculated according to Satterthwaite's method in spore size over a group of clones with additional microspatial information (twig = different twigs of shrubs where the colonies fruited; position = upper, mid, lower position of the measured sporocarp on the twig). Abbreviations are as in Table 2.

Table 4. Specimens with more than one discernible spore population (compare Fig. 3). For each sporocarp (coded with Accession/sporocarp) are listed: numbers of spores measured (n), spore diameters (mean $\bar{x} \pm$ standard deviation σ), mean spore volume (\bar{V}) derived from it, and the respective ratios (r).

Supplementary Material

Table S.1. Locations and biospecies affiliation (see Shchepin et al. 2021) for all investigated accessions of *Physarum albescens*. File in Microsoft Excel 2013.

Table S.2. Average values for all measured sporocarps. Shown are total averages for spore size and the proportions of spores where 0, 1, 3, ≥ 4 nuclei were detected (columns indicated by "Total"), and the respective values if discernible spore populations are detected. Shown are used accessions, represented by 1 to 5 sporocarps (Spc), affiliation to phylogroup (Clade) measured number of spores (Count) in dependency to spore population (s1 to s4) and nuclei count (n0 to n3), median spore diameter (Median), the respective standard deviation (SD), lower and upper confidence interval of the median (lower-CI-95/upper-CI-95), kurtosis value, and skewness for the respective size distribution. First column shows the index of all accessions separated by used measurement protocol (n = nucleus measurements, s = only spore size measurements). File in Microsoft Excel 2013

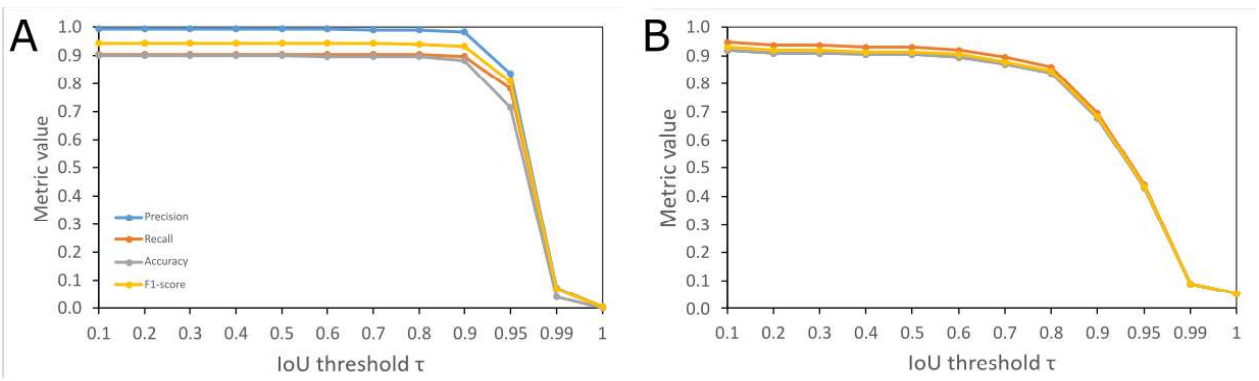


Figure S.3. Performance metrics (range 0–1) for both segmentation models. **A** Spore model (Recognition of spores in brightfield images). **B** Nucleus model (recognition of Nuclei in fluorescent light after staining with DAPI). In both models, an IoU threshold of 0.5 was used. Precision is the percentage of correct positive prediction and tells us how well the model selects only the relevant target objects. Recall is the percentage of target objects found. Accuracy reflects the percentage of correctly classified pixels from the model classes (in our case target objects, i.e., spores or nuclei, and background). The F1-score is an alternative figure for describing the model's accuracy to select the target objects correctly.

4 Conclusion and perspective

4.1 Main findings

This work focused on genetic and morphological differences (spore traits) of the myxomycetes *Physarum albescens*. Article 1 deals with the population genetics of the species. Three independent genetic markers, a test for reproductive isolation and additionally Genotyping by Sequencing (GbS) cryptic biospecies could be identified within the morphologically defined species *Ph. albescens*. Usually, two or more of these biospecies co-occur in a given mountain range, often sharing the same habitats (as defined by macroecological conditions), but some may be regional endemics. The existence of groups of clonal specimens and an overall high genotypic diversity within the biospecies indicate co-existence of sexual and asexual reproduction in natural populations. In detail:

- An investigation of 324 accessions collected over several mountain ranges of the northern hemisphere resulted in at least 18 cryptic biospecies (phylogroups), reproductively isolated for three independent genetic markers (SSU, EF1A, COI). This was confirmed by a phylogeny based on ca. 10,000 parsimony-informative SNP's generated via GBS.
- In a given mountain range several phylogroups can coexist, some may form regionally endemic populations, but only more intense surveys can ultimately proof the degree of endemism.
- The discovery of clonal samples separated by spatial distances in the m to km range, but as well time (repeated collections between years) indicates asexual reproduction not mediated by cellular fission of amoebae. Possible mechanisms may include automixis, repeated mating of the same two amoebal strains, or active movement/dispersal of plasmodium fragments.

Article 2 presents a species distribution model (SDM) based on updated world-wide occurrence data and a specially designed snow cover prediction layer to reveal the potential fundamental niche of *Ph. albescens*. In detail:

- As to expect, the range of the species is spatially fragmented by the mountain ranges investigated; fruiting in lowlands is predicted with a much a lower incidence and only beyond ca. 45° northern latitude.
- Snow cover and elevation are the decisive factors for the occurrence of fruitbodies, but especially elevation alone does not predict reliably occurrence in northern lowland areas or absence in arid mountain ranges, especially in Central Asia.

However, metabarcoding studies undertaken in a parallel project (data not shown) indicate that the SDM predicts the occurrence of fruit bodies only – areas surrounding mountain ranges may harbor non-fruiting amoebal populations that consist of sink populations.

Article 3 describes a new method for quantifying spore size. It can be used as well to analyze spore shape and color in any microscopically small spherical bodies (e.g., pollen grains). Two robust machine learning models were created to analyze spore images, which are capable to segment and separate spherical bodies consistently and measure as well fluorescence signals per identified object. In detail:

- Classical mounted slides can be analyzed, since a high-frequency vibration device build with low-cost materials was invented to arrange them in a plane.
- This allows to analyze thousands of spores simultaneously and enables (in contrast to the cost-intensive flow-cytometric methods) a visual inspection and verification of the results at any time.
- The method results in spore size distribution, which can be analyzed for width and skewness to reveal irregularities in spore formation.
- Additional information can be recorded, like shape or color. The method can be combined with DAPI fluorescent staining, thus simultaneously giving information on the number of nuclei included in a spore.

These methods are used (article 4) to analyze spore traits and intraspecific variation in selected biospecies of *Ph. albens*. This is the first quantitative analysis of spore size in myxomycetes. It revealed clear indications for a genetical control of spore size in the species (as expected) but at the same time, an overwhelming influence of (micro)environmental factors, i.e., an unexpected degree of phenotypic plasticity. If possible, three sporocarps per accession were separately investigated, revealing the following details:

- Spore size is fairly constant ($\pm 1.5\%$) within the sporocarps of a colony (exposed to the same microenvironmental conditions), indicating tight genetic control of this trait.
- Spore size varies considerably ($\pm 10\%$) within accessions, providing evidence that differences of 1 μm , as sometimes claimed as decisive in species keys, are in the range of intraspecific variation.
- This variation was explained best by accession (i.e., origin) as a factor, but to a lesser extent by Biospecies and to a negligible extent by intra-colony variation.

- A very similar range of variation ($\pm 8\%$) showed a clonal group of six accessions collected within 25 m distance, revealing that microenvironmental conditions, caused by the different position of the respective colonies, account for virtually all of the variation in spore size.
- Spore size distributions are usually narrow and symmetric, but mean spore size and standard deviation correlate significantly and positively ($R=0.45$, $p = 0.004$) – the larger the spores, the less regular their mode of formation.
- Whereas most sporocarps show uninuclear spores, two kinds of aberrations appear that seem not to be linked to each other: Some accessions displayed multimodal distributions with discernible populations, and the larger ones had on average the twofold (in one case: the threefold) volume of the basic spore population. Other accessions had a significant proportion of binucleate spores, mostly of normal size.

Contrary to our expectations, spore size, although it seems to be under initial genetic control, seems to be a highly plastic trait. The observed aberrations do not allow a decisive conclusion about the time of meiosis (before or after spore cleavage) but provide a new tool to shed light on these processes in combination with molecular methods. Through this investigation, multimodal distributions in spore size were the first time recorded in detail, and the distribution of multinucleated spores was related to their spore sizes.

Our study confirms the theoretical conclusion made through the detection of meiosis-related genes, that all eukaryotes, including Amoebozoa, are capable of sexual reproduction (Lahr et al. 2011; Brandeis 2021; Havird et al. 2015; Hofstatter and Lahr 2019; Hörandl et al. 2020; Feng et al. 2016; Speijer 2016) holds true as well for "wild" populations of myxomycetes. In accordance with (Kamono et al. 2009), dispersal capability is high, and does not explain evolutive radiation into biospecies. Evidence for this mode of evolution was found not only in *Physarum albescens*, but as well in recent studies with *Trichia varia* (Feng and Schnittler 2015), *Tubifera ferruginosa* (Leontyev et al. 2015), *Meriderma* spp. (Feng et al. 2016), *Hemitrichia serpula* (Dagamac et al. 2017) and *Didymium nivicola/pseudonivicola* (Janik et al. 2020; 2021), all taxa not closely related to our study species. The question is about the advantage of this evolutive radiation. We hypothesize that unlimited dispersal is a disadvantage since it favors outbreeding depression – but the proof is difficult to obtain.

This may as well explain why spore size, although the decisive factor for dispersal abilities, is undoubtedly genetically determined but not tightly controlled: there would be no need for it; the species seems to live well with a considerable amount of phenotypic plasticity in this trait.

The often sympatric occurrence of several biospecies in the same habitat, but as well in different mountain ranges lets it appear likely that nivicolous myxomycetes are capable to adapt to changing conditions (warming causes belts of stable snow cover to move upwards), a question to be investigated in a follow-up project (SCHN 1080-6). As this relative of the protists demonstrates, the evolutionary mechanisms to achieve this may be different in different groups of organisms, posing a major challenge to unified and non-static species distribution models aiming to account for such processes.

4.2 Outlook: Challenges and limitations

The major challenge in this study was the impossibility to cultivate *Ph. albescens* in the lab; respective trials (Shchepin et al. 2014) led only to amoebal strains which did not form plasmodia. On addition, growth in nivicolous myxomycetes is extremely slow – the formation of fruiting bodies may be triggered by a kind of quorum-sensing effect: only a critical density of amoebae may lead to the formation of plasmodia, and this process may take most of the winter. Experiments with data loggers (Schnittler et al. 2015; Dahl et al. 2018) showed that >4 month contiguous snow cover is the minimum for stable formation of fruit bodies. From these reasons, experiments to study the response characteristics of spore formation dependent on changing environmental parameters were not possible to perform on *Ph. albescens*. The challenge will be to find an easily cultivable species to perform the respective manipulative experiments – strains of the model species *Ph. polycephalum*, which is extremely rare in the wild, do not any more reliable form fruiting bodies.

For our species, multiple factors like age of spores, germination conditions, the medium's acidity, contamination of harmful fungi, the right food supply in co-culture (which microorganisms) are still unknown. A correlation study based on metabarcoding of alpine soil samples, analyzing simultaneously myxomycetes (18SrDNA as a marker), bacteria (16SrDNA) and fungi (ITS2) failed to reveal correlations due to the sheer diversity of operational taxonomic units (OTUs) obtained for these groups of organisms (Borg Dahl et al. 2019). Relations in the soil food web, which is to a certain extent controlled by myxomycetes (Urich et al. 2008) are simply too complex to be unraveled for all species involved.

Although the comparison of spore size between clonal and non-clonal groups of accessions would allow to calculate a broad sense heritability as demonstrated for the clonal duckweeds (*Lemna* spp.) in Fischer et al. (2021), it would only show the overwhelming effect of (micro) environmental conditions. Only a model species that is (1) cultivable and (2) common enough to investigate multiple native accessions would allow to estimate narrow-sense heritability via an F1 generation raised strictly under controlled conditions ("common garden"). However, a long-term study on a taxonomically

related nivicolous myxomycete, *Diderma meyeræ*, where accessions from multiple years from a transect in the German Alps will be genotyped, may allow somewhat deeper conclusions, if multiple generations can be tracked in nature.

A major challenge that we solved during this study was the quantitative analysis of spore traits. By applying high-frequency vibration treatment, rearrangement of spores to a common two-dimensional plane was achieved. This avoided overlaying spores arranged in different focus planes, which would require additional steps like z-stacking and the selection against spores not in full focus. In contrast, spores touching each other, but as well non-target objects like capillitial remnants do not could be overcome by creating special filters and setting up / training machine learning models to accurately and reliably identify and separate spores from each other.

Extracting additional environmental information from prediction maps, global environmental maps, or via remote sensing techniques, like spectrum scans from satellites, a currently not be useful applied due to the low spatial resolution of these sources. Correlations produced with such information may lead to wrong conclusions due to missing spatial resolution. This may be overcome by installing data loggers on places known for regular fruiting of nivicolous myxomycetes, an information now available for the transect in the German Alps mentioned above. However, the outbreak of covid-19 sadly restricted us from installing such devices – only in 2021 we could briefly visit the site.

The research presented herein enlarges the toolkit for the studying the ecology of protists like myxomycetes by at least three instruments. These are (1) true genotyping, achieved with GbS or (now under preparation, MIG-Seq (Suyama and Matsuki 2015); (2) quantitative analysis of spore size distributions (and, if desirable color and shape); and finally (3) the analysis of nuclei numbers enclosed in these propagules. We look forward to apply these approaches in a planned comparative study in Polish and German lowlands (SCHN 1080/6-1), middle and high mountains to investigate the consequences of climate change for microscopic eukaryotes like the myxomycetes targeted in this study.

4.3 Literature

Borg DM; Brejnrod AD; Russel J; Sørensen SJ; Schnittler M (2019): Different Degrees of Niche Differentiation for Bacteria, Fungi, and Myxomycetes Within an Elevational Transect in the German Alps. In *Microbial ecology* 78 (3), pp. 764–780. DOI: 10.1007/s00248-019-01347-1.

Brandeis M (2021): Were eukaryotes made by sex?: Sex might have been vital for merging endosymbiont and host genomes giving rise to eukaryotes. In *BioEssays : news and reviews in molecular, cellular and developmental biology* 43 (6), e2000256. DOI: 10.1002/bies.202000256.

Dagamac NHA; Rojas C; Novozhilov YK; Moreno GH; Schlueter R; Schnittler M (2017): Speciation in progress? A phylogeographic study among populations of *Hemitrichia serpula* (Myxomycetes). In *PloS one* 12 (4), e0174825. DOI: 10.1371/journal.pone.0174825.

Dahl MB; Shchepin O; Schunk C; Menzel A; Novozhilov YK; Schnittler M (2018): A four year survey reveals a coherent pattern between occurrence of fruit bodies and soil amoebae populations for niviculous myxomycetes. In *Scientific reports* 8 (1), p. 11662. DOI: 10.1038/s41598-018-30131-3.

Feng Y; Klahr A; Janik P; Ronikier A; Hoppe T; Novozhilov YK; Schnittler M (2016): What an Intron May Tell: Several Sexual Biospecies Coexist in *Meriderma* spp. (Myxomycetes). In *Protist* 167 (3), pp. 234–253. DOI: 10.1016/j.protis.2016.03.003.

Feng Y; Schnittler M (2015): Sex or no sex? Group I introns and independent marker genes reveal the existence of three sexual but reproductively isolated biospecies in *Trichia varia* (Myxomycetes). In *Org Divers Evol* 15 (4), pp. 631–650. DOI: 10.1007/s13127-015-0230-x.

Fischer K; Kreyling J; Beaulieu M; Beil I; Bog M; Bonte D et al. (2021): Species-specific effects of thermal stress on the expression of genetic variation across a diverse group of plant and animal taxa under experimental conditions. In *Heredity* 126 (1), pp. 23–37. DOI: 10.1038/s41437-020-0338-4.

Havird JC; Hall MD; Dowling DK (2015): The evolution of sex: A new hypothesis based on mitochondrial mutational erosion: Mitochondrial mutational erosion in ancestral eukaryotes would favor the evolution of sex, harnessing nuclear recombination to optimize compensatory nuclear coadaptation. In *BioEssays : news and reviews in molecular, cellular and developmental biology* 37 (9), pp. 951–958. DOI: 10.1002/bies.201500057.

Hofstatter PG; Lahr DJG (2019): All Eukaryotes Are Sexual, unless Proven Otherwise: Many So-Called Asexuals Present Meiotic Machinery and Might Be Able to Have Sex. In *BioEssays : news and reviews in molecular, cellular and developmental biology* 41 (6), e1800246. DOI: 10.1002/bies.201800246.

- Hörandl E; Bast J; Brandt A; Scheu S; Bleidorn C; Cordellier M et al. (2020): Genome Evolution of Asexual Organisms and the Paradox of Sex in Eukaryotes. In Pierre Pontarotti (Ed.): *Evolutionary Biology—A Transdisciplinary Approach*. Cham: Springer International Publishing, pp. 133–167.
- Janik P; Lado C; Ronikier A (2020): Range-wide Phylogeography of a Nivicolous Protist *Didymium nivicola* Meyl. (Myxomycetes, Amoebozoa): Striking Contrasts Between the Northern and the Southern Hemisphere. In *Protist* 171 (6), p. 125771. DOI: 10.1016/j.protis.2020.125771.
- Janik P; Szczepaniak M; Lado C; Ronikier A (2021): *Didymium pseudonivicola*: A new myxomycete from the austral Andes emerges from broad-scale morphological and molecular analyses of *D. nivicola* collections. In *Mycologia* 113 (6), pp. 1327–1342. DOI: 10.1080/00275514.2021.1961068.
- Kamono A; Kojima H; Matsumoto J; Kawamura K; Fukui M (2009): Airborne myxomycete spores: detection using molecular techniques. In *Die Naturwissenschaften* 96 (1), pp. 147–151. DOI: 10.1007/s00114-008-0454-0.
- Lahr DJG; Parfrey LW; Mitchell EAD; Katz LA; Lara E (2011): The chastity of amoebae: re-evaluating evidence for sex in amoeboid organisms. In *Proceedings. Biological sciences* 278 (1715), pp. 2081–2090. DOI: 10.1098/rspb.2011.0289.
- Leontyev DV; Schnittler M; Stephenson SL (2015): A critical revision of the *Tubifera ferruginosa* complex. In *Mycologia* 107 (5), pp. 959–985. DOI: 10.3852/14-271.
- Schnittler M; Erastova DA; Shchepin ON; Heinrich E; Novozhilov YK (2015): Four years in the Caucasus – observations on the ecology of nivicolous myxomycetes. In *Fungal Ecology* 14, pp. 105–115. DOI: 10.1016/j.funeco.2015.01.003.
- Shchepin ON; Novozhilov YK; Schnittler M (2014): Nivicolous myxomycetes in agar culture: some results and open problems 8 (2), pp. 53–61.
- Speijer D (2016): What can we infer about the origin of sex in early eukaryotes? In *Philosophical transactions of the Royal Society of London. Series B, Biological sciences* 371 (1706). DOI: 10.1098/rstb.2015.0530.
- Suyama Y; Matsuki Y (2015): MIG-seq: an effective PCR-based method for genome-wide single-nucleotide polymorphism genotyping using the next-generation sequencing platform. In *Scientific reports* 5, p. 16963. DOI: 10.1038/srep16963.
- Urich T; Lanzén A; Qi J; Huson DH; Schleper C; Schuster SC (2008): Simultaneous assessment of soil microbial community structure and function through analysis of the meta-transcriptome. In *PLOS ONE* 3 (6), e2527. DOI: 10.1371/journal.pone.0002527.

5 Affidavits

5.1 Eidesstattliche Erklärung / statutory declaration

Hiermit erkläre ich, dass diese Arbeit bisher von mir weder an der Mathematisch-Naturwissenschaftlichen Fakultät der Universität Greifswald noch einer anderen wissenschaftlichen Einrichtung zum Zwecke der Promotion eingereicht wurde. Ferner erkläre ich, dass ich diese Arbeit selbstständig verfasst und keine anderen als die darin angegebenen Hilfsmittel und Hilfen benutzt und keine Textabschnitte eines Dritten ohne Kennzeichnung übernommen habe.

Greifswald 22 February 2022

Jan Woyzichowski

5.2 Erklärung bei Gemeinschaftsarbeiten selbständig

Hiermit erkläre ich, dass die in der folgenden Inhaltsübersicht mit meinem Namen gekennzeichneten Kapitel von mir selbständig verfasst worden sind:

1 Abstract	Jan Woyzichovski
2 Introduction	Jan Woyzichovski
3 Publications	-
3.1 Genetic structure of the protist <i>Physarum albescens</i> (Amoebozoa) revealed by multiple markers and genotyping by sequencing	Shchepin, Oleg; Novozhilov, Yuri; Woyzichovski, Jan ; Bog, Manuela; Prikhodko, Ilya; Fedorova, Nadezhda; Gmoshinskiy, Vladimir; Borg Dahl, Mathilde; Dagamac, Nikki H. A.; Yajima, Yuka; Schnittler, Martin
3.2 Where do niviculous myxomycetes occur? – Modeling the potential worldwide distribution of <i>Physarum albescens</i>	Dagamac, Nikki Heherson A.; Bauer, Barbara; Woyzichovski, Jan ; Shchepin, Oleg N.; Novozhilov, Yuri K.; Schnittler, Martin
3.3 A workflow for low-cost automated image analysis of myxomycete spore numbers, size and shape	Woyzichovski, Jan ; Shchepin, Oleg; Dagamac, Nikki Heherson; Schnittler, Martin
3.4 High environmental induced plasticity in spore size and numbers of nuclei per spore in <i>Physarum albescens</i> (Myxomycetes)	Woyzichovski, Jan ; Shchepin, Oleg; Schnittler, Martin
4 Conclusion & Perspectives	Jan Woyzichovski

Ich erkläre weiterhin, das ich die im folgenden beschriebenen Teile derjenigen Kapitel, bei denen ich nicht Alleinautor bin, selbstständig verfasst habe:

I hereby declare that I have independently written the following parts of chapters where I was not the sole author.

Chapter 3.1 Genetic structure of the protist *Physarum albescens* (Amoebozoa) revealed by multiple markers and genotyping by sequencing.

I contributed to this manuscript with sample preparations and field collecting, and assisted with the genetic investigations and data analyses. In a later step I helped to finalize the data for publication and took part in manuscript writing.

Chapter 3.2 Where do nivicolous myxomycetes occur? – Modeling the potential worldwide distribution of *Physarum albescens*.

I improved the species distribution models with scripts written in R, streamlined database management and edited the figures for the final incidence map. In the final stages of manuscript submission I took over the lead from the first author in final manuscript edition and submission.

Chapter 3.3 A workflow for low-cost automated image analysis of myxomycete spore numbers, size and shape.

In collaboration with Prof. M. Schnittler I designed the new method, defined the software requirements, wrote and tested the software scripts for the image analysis. All necessary field work was carried out by me, with Prof. Schnittler, Dr. Dagamac and Dr. Shchepin assisting in some of the surveys. I conducted all the laboratory work (sample preparation) and subsequent automated data analysis. Interpretation of data were done with the assistance of Prof. Schnittler. Prof. Kreyling assisted me with solving statistical problems; Prof. Harzsch provided the microscopy facilities and scientific supervision for these instruments. I wrote the manuscript as the first author, corresponding authors help with specific parts, proofreading and contributed useful literature.

Chapter 3.4 High environmental induced plasticity in spore size and numbers of nuclei per spore in *Physarum albescens* (Myxomycetes)

For this manuscript I designed the analysis and all methods applied. Dr. Shchepin provided phylogenetic information for all used samples, which were collected mainly by Prof. Schnittler; Prof. Novozhilov and partially by Dr. Borg Dahl, Dr. Shchepin and Dr. Dagamac (all former PhD students in or associated with RESPONSE). Data analysis, and interpretation were conducted by me with the assistance from Prof. Schnittler. I wrote the manuscript as the first author with the help of the two, corresponding authors, and carried out the submission process.

Greifswald 22nd February 2022

Jan Woyzichowski

Prof. Dr. Martin Schnittler
(Wissenschaftlicher Betreuer)

6 Acknowledgement

In this part of my thesis, I would like to take the opportunity to express my deepest gratitude to people that turned during these 3+ years into friends and more. Without them, this entire thesis would have never happened or finished.

Firstly, I would like to thank my supervisor Prof. Martin Schnittler for trusting me and giving me a chance to carry out this work. I enjoyed all the small and lengthy meeting-ups and discussions with him about possibilities for studying myxomycetes. Particularly, field trips with him were always eye-opening events for my body and mind. Never have I experienced going so many times on my physical limits for collecting specimens than on the field works with him.

I am very grateful to my co-supervisor and friend Nikki Dagamac for supporting and helping me in many situations and giving guidance for my work and life. Your perspective on life and people is marvelous. Special thanks go as well to my friend Oleg Shchepin his work and effort helped my thesis a lot and gave it the basis that it needed.

I would like to give my heartfelt thanks to the whole working group AG Schnittler. Thank you for creating such a friendly, cheerful, and full of support atmosphere.

I don't want to forget to appreciate the time with Prof. Yuri Novozhilov it was a great experience to go on a field trip and conference with him.

I would like to thank my fellow PhD students from RESPONSE for their great scientific discussions but also for all the fun and laughter we shared in between meetings.

I'm particularly grateful to Prof. Gerald Kerth and Dr. Susann R  th for all the effort and work they put into the organization of our meetings.

Furthermore, I would like to thank my dearest friends and family. I am deeply grateful that I was able to get to know you and share part of our time together.

I don't want to forget my brother, thank you for being there when I needed you for talks or just being with me. You helped me a lot going through some tough times knowingly or not.

Finally, an unimaginable "thank you" that can't be described with words goes to my love Kasia. Thank you so much to bear with me during the writing process of this thesis and the other manuscripts. Your appearance in my life is the biggest and happiest encounter that I experienced so far, and I hope that many more will follow with you.